國 立 交 通 大 學

機械工程學系研究所

博 士 論 文

電漿處理對奈米碳管合成及奈米碳管表面特性之影響

The Effect of Plasma Treatment on the Synthesis and Surface Characteristics of Carbon Nanotubes

研 究 生：溫華強

指導教授：周長彬　教授

　　　　　吳文發　博士

中 華 民 國 九 十 六 年 六 月

電漿處理對奈米碳管合成及奈米碳管表面特性之影響

The Effect of Plasma Treatment on the Synthesis and Surface Characteristics of Carbon Nanotubes

研 究 生：溫華強　　　　　Student：Hua-Chiang Wen

指導教授：周長彬　　　　　Advisor：Prof. Chang-Pin Chou

　　　　　吳文發　　　　　Advisor：Dr. Wen-Fa Wu

國 立 交 通 大 學

機械工程學系

博 士 論 文

A Thesis

Submitted to Institute and Department of Mechanical Engineering

National Chiao Tung University

in partial Fulfillment of the Requirements

for the Degree of

Ph.D

in

2007

Hsinchu, Taiwan, Republic of China

中華民國九十六年六月

國 立 交 通 大 學

論 文 口 試 委 員 會 審 定 書

本校＿＿機 械 工 程＿＿學系博士班＿＿溫華強＿君

所提論文（中文）電漿處理對奈米碳管合成及奈米碳管表面特性之影響

（英文）The Effect of Plasma Treatment on the Synthesis and
Surface Characteristics of Carbon Nanotubes

合於博士資格水準、業經本委員會評審認可。

口試委員：

指導教授：

系 主 任：　　　　　　　　　　　教授

中 華 民 國　　　　年　　　　月　　　　日

電漿處理對奈米碳管合成及奈米碳管表面特性之影響

學生：溫華強　　　　　　　　指導教授：周長彬 教授

吳文發 博士

國立交通大學工學院 機械工程系（研究所）博士班

摘要

　　近年來，在矽元件尺寸微小化的趨勢下，奈米碳管特別被期待應用在奈米電子元件上，此乃因奈米碳管具有極佳的特性。本論文試圖提出電漿處理運用於奈米碳管的研究，將實驗結果中包括前處理與成長特性、表面特性、電子傳輸能力、與機械特性作連貫性的探討。

　　在前處理與成長特性部分，氫電漿前處理，可促使微小顆粒產生聚集，依據對鎳層觸媒前處理產生之效應，證明週期時間、氫氣流量對於顆粒化有其對應的趨勢。經由拉曼光譜儀的量測，合成後的奈米碳管在適當條件下的氫電漿前處理可使非晶質碳與非序結構降低，進而提升奈米碳管之品質。此外，藉由奈米壓痕壓縮測試，從壓力控制模式，可發現到奈米顆粒之楊氏模數與硬度值皆比鎳層為低，因而證實前處理奈米顆粒的特性。

　　在表面特性上，經由四氟化碳與氧氣電漿後處理，奈米碳管表面非晶質碳明顯降低。由拉曼光譜儀顯示，短時間之後處理可提升品質比值，而長時間卻降低品質比值。此外，傅立葉光譜儀可證實表面存在碳氧與碳氟的鍵結。由熱脫附量測顯示出，奈米碳管表面氟氧鍵確實有脫附的現象。X 光電子能譜亦印證出表面確實具有氟化之增益。

　　在電子傳輸研究中，以曝光顯影製作橫向之結構，讓奈米碳管連接於兩邊之電極。藉由四氟化碳與氧氣電漿後處理，證實電漿後處理確實具有修飾奈米碳管與增進電子傳輸之效益，而使得元件在室溫下可表現出蕭特基(Schottky)接觸特性。

　　至於機械特性部分，本論文選用奈米壓痕針頭對頂部奈米碳管薄膜作測試，可得到相對的韌性並展現出奈米碳管薄膜的特點。此外，利用拉曼光譜儀量，印

證當增加施力所產生的裂痕越大，量測品質變化量(I_D/I_G)上升，由此可印證奈米碳管之非序結構確實提升。

　　整體實驗中，無論是觸媒的形成，奈米碳管的吸附能力，電性、機械方面的測試上，均可藉由實驗證實其特性。

The Effect of Plasma Treatment on the Synthesis and Surface Characteristics of Carbon Nanotubes

Student：Hua-Chiang Wen   Advisors：Prof. Chang-Pin Chou

Dr. Wen-Fa Wu

Institute and Department of Mechanical Engineering, National Chiao Tung University

ABSTRACT

In the semiconductor industry, silicon devices are being scaled down to smaller dimensions. Carbon nanotubes (CNT) are of particular interest for future nanoelectronic applications, because of their high aspect ratio, small radius of curvature, high chemical stability, and large mechanical strength. Plasma surface treatments are promising techniques in the design and development of new materials because surfaces can be modified without altering the bulk properties of the material. Accordingly, more sensitive surface analysis approaches are being used to obtain more precise information regarding the plasma-treated surface chemistry. An experiment was conducted to elucidated pretreatment, the adsorption (desorption) in plasma surface treatment, the electronic conduction property associated with surface treatments, and the mechanical characteristics of CNTs.

In the pretreatment, CNTs were synthesized by microwave plasma chemical vapor deposition (MPCVD) on Ni/TiN/Si and Ni/TaN/Si systems. The effect of the pretreatment period and flow rate on the growing characteristics of the Ni catalyst layer and the properties of the CNTs was examined. The mechanical response of particle aggregates to the compression of substrates is emphasized. The improvement of the surface performance of the catalyst is using H_2 plasma is suggested. Therefore, small agglomerates of catalyst nanoparticles formed on TiN buffer substrates, helping to elucidate the mechanical properties of relatively large pretreated nanoparticles. The deformation behavior of the agglomerates under loaded control-mode nanoindentation was investigated. Nanoparticle testing demonstrated a lower modulus (from 238.9±8.4

to 176.2±6.1 GPa) and hardness (from 17.2±1.6 to 11±0.8 GPa) than those of the Ni film. The effects of the H_2 plasma flow rate during pretreatment on the synthesis of CNTs using an MPCVD system are also studied. Raman spectroscopy was employed with a change-coupled detector is used to elucidate the effect of the flow rate on the intensity ratio of G and D bands (I_D/I_G), which in turn yields the amounts of amorphous carbon and carbonaceous particles in the CNTs.

The effect of CF_4/O_2 plasma on the surface performance of CNTs in the post-treatment is elucidated. SEM and TEM studies reveal changes in the surface morphologies of CNTs that were exposed to the CF_4/O_2 plasma. Additionally, the I_D/I_G ratios reveal that chemical treatment with CF_4/O_2 plasma for 2 min reduces the degree of disorder. After 10 min, however, the degree of disorder in CNTs is increased. FTIR absorption spectra include peaks that correspond to C-O and C-F stretching vibrations. The TDS results yield adsorption information. XPS datum reveals fluorination in CF_4/O_2 plasma-treated CNTs and the absence of a significant of physisorbtion on CNTs. This result shows that adding oxygen to the plasma increases the decomposition efficiency.

A CNT bridge on SiO_2 that is patterned photolithographically in an electronic device is described. The CNTs grow laterally to the substrate over a Ta vertical growth barrier and connect to the side of the electrode pad. The CF_4/O_2 post-treated has a higher current-voltage curve than the surface-modified. The typical Schottky contact characteristics at room temperature are discussed. The surface of the CNT interacts with the surrounding plasma, breaking C-C bonds and creating active sites to bond the functional groups (fluorination). C-F binding in the amorphous carbon can be reduced by modifying the CNTs.

A CNT film was studied using nanoindentation equipment (Berkovitch indenter) by varying the loading force. CNT films exhibit features that are associated with toughening against cracks caused by indentation. The quantitative indentation force is utilized to determine the CNTs axial modulus, depending on the Raman shift. The I_D/I_G ratios of the CNTs films are associated with an increase in the force. Such features follow in part from the fact that CNTs films generally contain some disordered regions.

The experiment on plasma treatments yields information on the formation of the catalyst, the adsorption (desorption) capacity, the electronic conduction and the mechanical behavior in CNTs.

Contents

LIST OF TABLES

LIST OF FIGURES

1. Introduction

1.1   A Brief History of Nanomaterials

1.1.1   Buckminsterfullerene

The molecule was named for Richard Buckminster Fuller, a noted architect who popularized the geodesic dome. Since buckminsterfullerenes have a similar shape to that sort of dome, the name was thought to be appropriate. Fullerenes are similar in structure to graphite, which is composed of a sheet of linked hexagonal rings, but they contain pentagonal (or sometimes heptagonal) rings that prevent the sheet from being planar. The smallest fullerene in which no two pentagons share an edge is C_{60} (buckminsterfullerene), and as such it is also the most common. The structure of C_{60} is that of a truncated icosahedron, which resembles a round soccer ball of the type made of hexagons and pentagons, with a carbon atom at the corners of each hexagon and a bond along each edge. A polymerized single-walled nanotubule (P-SWNT) is a substance composed of polymerized fullerenes in which carbon atoms from one buckytube bond with carbons in other buckytubes [1].

1.1.2 The origin of carbon nanotubes

The physics of CNTs has rapidly evolved a research field since their discovery by Iijima in multiwall in 1991, and as single-walled two year later. Since then, the-oretical

and experimental studies in different areas, such as mechanics, optic, and electronics

have focused on both the fundamental physical properties and the potential application

of nanotubes.

Carbon is remarkable element showing a variety of stable from ranging from 3D

semiconducting diamond to 2D semi-metallic graphite to 1D conducting and

semiconducting CNTs to 0D fullerenes [2]. One distinction between these forms of

carbon relates to the many possible configurations of the electronic states of a carbon

atom, which is known as the hybridization of atomic orbitals and relates to bonding of a

carbon atom to its nearest neighbors.

Carbon is the sixth element of the periodic table and has the lowest atomic number

of any element in column IV of the periodic table. Each carbon atom has six electrons

which occupy $1s^2$, $2s^2$, and $2p^2$ atomic orbitals. The $1s^2$ orbital contain two strongly

bound core electrons. Four more weakly bound electrons occupy the $2s^2 2p^6$ valence

orbitals. In the crystalline phase, the valence electrons give rise to 2s, $2p_x$, $2p_y$, and $2p_z$

orbitals which are important in forming covalent bonds in carbon materials [3].

1.1.3 Single-walled nanotubes

The (n,m) nanotube naming scheme can be thought of as a vector (C_h) in an

infinite graphene sheet that describes how to 'roll up' to graphene sheet to make the

nanotube. T denotes the tube axis, and a^1 and a^2 are the unit vectors of graphene in real space. Most SWNTs have a diameter of close to 1nm, with a tube length that can be many thousands of times larger. The structure of a SWNT can be conceptualized by wrapping a one-atom-thick layer of graphite (called graphene) into a seamless cylinder. The way the graphene sheet is wrapped is represented by a pair of indices (n,m) called the chiral vector. The integers n and m denote the number of unit vectors along two directions in the honeycomb lattice of graphene. This is often thought of as representing the number of carbon atoms around the circumference of the tube, and the number of atoms down the tube axis. If m=0, the nanotubes are called "zigzag". If n=m, the nanotubes are called "armchair". Otherwise, they are called "chiral".
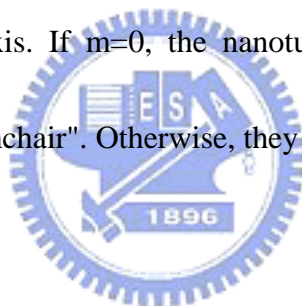
1.1.4 The Graphite structure of carbon nanotubes

Although the properties of graphite with bulk are now well understood, carbon science has focused on the synthesis and preparation of improved graphite materials, the development of more sensitive characterization method, and the introduction of more powerful tools as nanotechnology. Interest in graphite nanostructures and new synthesis capabilities of thin graphite films has stimulated study of the electronic structure of carbon materials.

Graphite edge sites are more reactive than bulk sites because of the availability of

dangling bonds. However, carbon clusters have been investigated in terms of their

potential for the uptake of active species which could be of interest for carbon-based

device.

1.1.5 The potential of carbon nanotubes

CNTs are cylindrical carbon molecules with novel properties that make them

potentially useful in a wide variety of applications (e.g., nano-electronics, optics,

materials applications, etc.). They exhibit extraordinary strength and unique electrical

properties, and are efficient conductors of heat. Inorganic nanotubes have also been

synthesized.
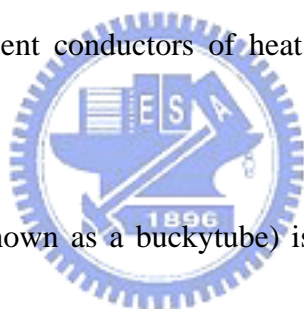
A nanotube (also known as a buckytube) is a member of the fullerene structural

family, which also includes buckyballs. Whereas buckyballs are spherical in shape, a

nanotube is cylindrical, with at least one end typically capped with a hemisphere of the

buckyball structure. Their name is derived from their size, since the diameter of a

nanotube is on the order of a few nanometers (approximately 50,000 times smaller than

the width of a human hair), while they can be up to several centimeters in length.

Nanotubes are composed entirely of sp² bonds, similar to graphite. Stronger than

the sp3 bonds found in diamond, this bonding structure provides them with their unique

strength. Nanotubes naturally align themselves into "ropes" held together by Van der

Waals forces. Under high pressure, nanotubes can merge together, trading some sp2 bonds for sp3 bonds, giving great possibility for producing strong, unlimited-length wires through high-pressure nanotube linking.

1.2 Motivation

1.2.1 The role of carbon nanotubes

The covalent bonding undergone in CNTs means they have very high tensile strengths. A SWNT was tested to have a tensile strength of 63GPa (in comparison, high-carbon steel has a tensile strength of approximately 1.2GPa). They also have very high elastic modulus, in the order of 1TPa [4]. Under excessive tensile strain, the tubes will undergo plastic deformation, which means the deformation is permanent. This deformation begins at strains of approximately 5% [5-6] and can increase the maximum strain the tube undergoes before fracture by releasing strain energy [7]. CNTs are not nearly as strong under compression. Due to their hollow structure, they tend to undergo buckling, when placed under compressive, torsional or bending stress. Due to the symmetry and unique electronic structure of graphene, the structure of a nanotube strongly affects its electrical properties. For a given (n,m) nanotube, if $2n+ m=3q$ (where q is an integer), then the nanotube is metallic, otherwise the nanotube is a semiconductor. Thus all armchair (n=m) nanotubes are metallic, and nanotubes (5, 0), (6,

4), (9, 1), etc. are semiconducting [8-9]. An alternative (equivalent) representation of this condition is if (n-m)/3=integer, then the SWNT is metallic. In theory, metallic nanotubes can have an electrical current density more than 1,000 times stronger than metals such as silver and copper.

All nanotubes are expected to be very good thermal conductors along the tube, exhibiting a property known as ballistic conduction but good insulators laterally to the tube axis [10]. As with any material, the existence of defects affects the material properties. Defects can occur in the form of atomic vacancies. High levels of such defects can lower the tensile strength by up to 85%. Due to the almost one-dimensional structure of CNTs, the tensile strength of the tube is dependent on the weakest segment of it. In terms of the tube's electrical properties, they too are affected by the presence of defects. A common result is the lowered conductivity through the defected region of the tube. Some defect formation in armchair type tubes (which are metallic) can cause the region surrounding that defect to become semiconducting.

1.2.2 Objective

This investigation elucidates the use of nanomaterials in CNT applications. In this thesis, chapter 2 is reviews the characteristics of CNTs, the synthesis of CNTs, and the mechanism of the growth of CNTs.

Chapter 3 introduces the experimental procedures. (i) CNTs are grown using Ni as a catalyst and hydrogen pretreatment by MPCVD with buffer layers (TiN, TaN) is conducted. (ii) The effects of CF_4/O_2 plasma post-treatment on the surface performance of multiwalled CNTs and lateral CNTs are elucidated. (iii) Indentation on CNT films is examined.

Chapter 4 investigates the pretreatment of Ni/TiN/Si and Ni/TaN/Si systems. The effect of the pretreatment of the Ni catalyst layer on the growth characteristics and properties of CNTs are studied with reference to the pretreatment conditions. The surface and electronic properties were examined using CF_4/O_2 plasma via the PECVD method. TDS and XPS results reveal information on adsorption on CNTs that have undergone CF_4/O_2 plasma post-treatment. The relationship between the process of the formation of the surface and the characteristics thereof is discussed. The surface performance can probably be modified by CF_4/O_2 plasma. Finally, in a mechanical study, CNTs were grown and subjected to nanoindentation using a Berkovitch nanoindenter. Quantitative indentation data are used to determine the axial modulus of the CNTs, depending on the Raman shift.

The last chapter summarizes the major results of this study and elucidates areas that required further attention.

Chapter 2 Literature review

2.1 Introduction

Carbon nanotubes (CNTs) are fullerene-related structures which consist of graphene cylinders closed at either end with caps containing pentagonal rings. They were discovered in 1991 by the Japanese electron microscopist Sumio Iijima who was studying the material deposited on the cathode during the arc-evaporation synthesis of fullerenes [11]. He found that the central core of the cathodic deposit contained a variety of closed graphitic structures including nanoparticles and nanotubes, of a type which had never previously been observed. A short time later, Thomas Ebbesen and Pulickel Ajayan, from Iijima's lab, showed how nanotubes could be produced in bulk quantities by varying the arc-evaporation conditions. Subsequently, in 1993, Iijima's group at NEC and Donald Bethune's group at IBM's Almaden Research Center in California independently discovered single-wall nanotubes. Whereas the multiwall CNTs were tens of nanometres across, the typical diameter of a single-wall CNTs was just one or two nanometers. The past decade has seen an explosion of research into both types of nanotube.

2.2 Structures of CNTs

CNTs are extremely small, thin, hollow cylinders structure formed by rolling up

seamlessly a single layer of graphite whereas buckyballs are graphite sheets rolled into a ball as shown as Fig. 2-1 [12]. Nanotubes can be either multiwall tubes, having several concentric shells, or single-wall tubes, having one single shell. Scanning tunneling microscopy (STM) offers the potential to probe this prediction, as shown as Fig. 2-2 [13]. Depending on the growth process single-wall or multiwall CNTs can be selectively produce by the carbon arc discharge method. CNTs come in a variety of diameters and lengths. Depending on the growth process, the length of the tubes can be from approximately 100 nanometers to several microns and the diameters vary from 1 to 20 nanometers, as shown as Fig. 2-3 [14]. CNTs are formed in the synthesis process. The CNTs physical properties range from 2-20 nm in diameter and 100 nm to several microns long with 5-20 graphitic layers, as shown as Fig. 2-4 [15].
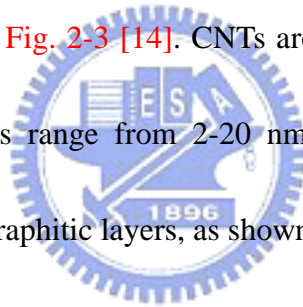
A nanotube can be considered as a single sheet of graphite that has been rolled up into a tube, as shown as Fig. 2-5 [16]. The electronic properties of the resulting nanotube depend on the direction in which the sheet was rolled up, as shown as Fig. 2-6 [16]. A CNT of the chiral vector is defined on the hexagonal lattice as $C_h = n\hat{a}_1 + m\hat{a}_2$, where $\hat{a}_1$ and $\hat{a}_2$ are unit vectors, and n and m are integers. The chiral angle, q, is measured relative to the direction defined by $\hat{a}_1$. This diagram has been constructed for $(n, m) = (4, 2)$, and the unit cell of this nanotube is bounded by OAB'B. To form the nanotube, imagine that this cell is rolled up so that O meets A and B meets B', and the

two ends are capped with half of a fullerene molecule. Different types of CNTs have

different values of *n* and *m*. (b) Zigzag nanotubes correspond to (*n*, 0) or (0, *m*) and have

a chiral angle of 0°, armchair nanotubes have (*n*, *n*) and a chiral angle of 30°, while

chiral nanotubes have general (*n*, *m*) values and a chiral angle of between 0° and 30°, as

shown as Fig. 2-7 [17]. According the theory, nanotubes can either be metallic or

semiconducting. Some nanotubes are metals with high electrical conductivity, while

others are semiconductors. Nanotubes also have remarkable mechanical properties [18]

that can be exploited to strengthen materials or to act as "tips" in scanning probe

microscopes, as shown as Fig. 2-8 [19]. And since they are composed entirely of CNTs

also have a low specific weight. MWNTs are close to hollow graphite fibers, except that

they have a much higher degree of structural perfection. The interlayer spacing in

MWNT ($d_{(002)}$ = 0.34 nm) is slightly larger than that in single crystal graphite ($d_{(002)}$ =

0.335 nm). This is attributed to a combination of tubule curvature and van der Waals

force interactions between successive graphene layers. The single-walled nanotubes

(SWNTs) and possess good uniformity in diameter about 1.2 nm. They are close to

fullerenes in size and have a single-layer cylinder extending from end to end. Qin et al.

also reported that high-resolution transmission electron micrograph of an 18-shell CNT

produced. The innermost shell has a diameter of 4 Å. The cylindrical structure of the
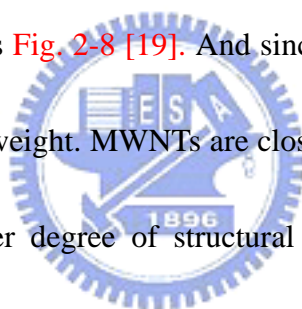
nanotube is shown by the reduced contrast towards the centre of the nanotube, where there are fewer atoms in the smaller tubes, as shown as Fig. 2-9 [20].

Carbon is the elemental equivalent of the perfect neighbor, friendly, and easygoing, as shown as Fig. 2-10 [21]. Under intense pressure, carbon atoms form co-valence bonds with four neighbor atoms, creating the pyramidal arrangement of diamond. However, the activation energy of diamond is very high and carbon usually links up with just three neighbors, creating the hexagonal rings of graphite network.

The arrangement of graphite has a host of unpaired electrons, which essentially float above or below the plane of carbon rings. In this arrangement, the electrons have more freedom to move around the graphite surface, which makes the material a good electrical conductor. S. Paulson et al. reported that junction resistance between a CNT and a graphite substrate and show that details of momentum conservation also can change the contact resistance, as shown as Fig. 2-11 and Fig. 2-12 [22].

CNTs consist of concentric hexagon-rich cylinders, made up of sp^2 hybridized carbon, as in graphite, and terminated by end-caps arising from the presence of 12 pentagons (six per end). It is possible to construct a cylinder by rolling up a hexagonal graphene sheet in different ways. Two of these are "non-helical" in the sense that the graphite lattices at the top and bottom of the tube are parallel. These arrangements are

named "armchair" and "zig-zag". In the armchair structure, two C-C bonds on opposite sites of each hexagon are perpendicular to the tube axis, whereas in the zig-zag arrangement, these bonds are parallel to the tube axis. In all other conformation, the C-C bonds lie at an angle to the tube axis and a helical structure is obtained [15].

Theoretical calculations have predicted that all the armchair tubes are metallic whereas the zig-zag and helical tubes are either metallic or semiconducting. The electronic conduction process in nanotubes is unique since in the radial direction, the electrons are confined in the singular plane of the graphene sheet. The conduction occurs in the armchair (metallic) tubes through gapless modes as the valence and conduction bands cross each other at the Fermi energy, as shown as Fig. 2-13[23]. In most helical tubes, which contain large numbers of atoms in their unit cell, the one-dimensional band structure shows an opening of the gap at the Fermi energy, and this leads to semiconducting properties. This unique electronic behavior only occurs for small nanotubes. As the diameter of the tubes increases, the band gap (which varies inversely with the tube diameter) tends to zero, yielding a zero-gap semiconductor that is electronically equivalent to the planar graphene sheet. In a SWNT, the outer planar graphene-like tubes superimpose the electronic structure of the inner tubes. The band structure obtained from individual SWNT resembles that of graphite. Experiments have indicated that the pentagonal defects present at the tips can induce metallic character by

introducing sharp resonance in the local density of states, as shown as Fig. 2-14[24].

2.3 Characteristics of carbon nanotube

2.3.1 Mechanical properties

In a sheet of graphite each carbon atom is strongly bonded to three other atoms, which makes graphite very strong in certain directions. However, adjacent sheets are only weakly bound by van der Waals forces, so layers of graphite can be easily peeled apart - as happens when writing with a pencil. As we shall see, it is not so easy to peel a carbon layer from a multiwall CNTs. Carbon fiber is already used to strengthen a wide range of materials. A simple method was used to assemble single-walled CNTs into indefinitely long ribbons and fibers, as shown as Fig. 2-15[25]. The processing consists of dispersing the nanotubes in surfactant solutions, recondensing the nanotubes in the flow of a polymer solution to form a nanotube mesh, and then collating this mesh to a nanotube fiber, as shown as Fig. 2-16[25].

The special properties of CNTs mean that they could be the ultimate high-strength measured the Young's modulus of CNTs. The Young's modulus of a material is a measure of its elastic strength. Yu et al. reported that the tensile strengths of individual CNTs were measured with a nanostressing stage located within a scanning electron

microscope, as shown as Fig. 2-17[26]. The tensile-loading experiment was prepared

and observed entirely within the microscope and was recorded on video. Analysis of the

stress-strain curves for individual MWCNTs indicated that the Young's modulus E of the

outermost layer varied from 270 to 950 gigapascals, as shown as Fig. 2-18[26].

It is now known that the Young's modulus should approach a value of 1.25

terapascals. This is true both for multiwall and single-wall CNTs because the modulus is

mainly determined by the carbon-carbon bonds within the individual layers.

The bending stiffness can also be measured by placing the nanotubes across probe

and using an atomic force microscope to bend them in the middle. Wong et al. reported

that atomic force microscopy was used to determine the mechanical properties of

individual, structurally isolated silicon carbide (SiC) nanorods (NRs) and CNTs that

were pinned at one end to molybdenum disulfide surfaces. The bending force was

measured versus displacement along the unpinned lengths, as shown as Fig. 2-19 [27].

The CNTs were about two times as stiff as the SiC NRs. Continued bending of the SiC

NRs ultimately led to fracture, whereas the MWNTs exhibited an interesting elastic

buckling process. The strengths of the SiC NRs were substantially greater than those

found previously for larger SiC structures, and they approach theoretical values.

Because of buckling, the ultimate strengths of the stiffer MWNTs were less than those

of the SiC NRs, although the MWNTs represent a uniquely tough, energy-absorbing material, as shown as Fig. 2-20 [27]. The Young's modulus, strength, and toughness of nanostructures are important to proposed applications ranging from nanocomposites to probe microscopy.

Occasionally a nanotube spanned one of the pores and the microscope was used to measure how the deflection, which is inversely proportional to the Young's modulus, varied with the applied force. Tombler et al. show that the effects of mechanical deformation on the electrical properties of CNTs are of interest given the practical potential of nanotubes in electromechanical devices. He reports an experimental and theoretical elucidation of the electromechanical characteristics of individual SWNTs under local-probe manipulation. Use AFM tips to detect suspended SWNTs reversibly, without changing the contact resistance; in situ electrical measurements reveal that the conductance of an SWNT sample can be reduced by two orders of magnitude when deformed by an AFM tip. The tight-binding simulations indicate that this effect is owing to the formation of local sp^3 bonds caused by the mechanical pushing action of the tip, as shown as Fig. 2-21 and Fig. 2-22 [28]. One recent experiment used the tip of an AFM to manipulate CNTs, revealing that changes in the sample resistance were small unless the nanotubes fractured or the metallic-tube contacts were perturbed. But it remains unclear how mechanical deformation affects the intrinsic electrical properties of

nanotubes.

CNTs are different: first they will bend over to surprisingly large angles, before they start to ripple and buckle, and then finally develop kinks as well. The amazing thing about CNTs is that these deformations are elastic - they all disappear completely when the load is removed.

2.3.2 Electronic properties

CNTs are giant molecular wires in which electrons can propagate freely, just as they do in an ordinary metal. This contrasts strongly with conventional "conducting" in which the electrons are localized. These molecules are actually insulators and only become conductors if they are heavily doped, as shown as Fig. 2-23 [29]. CNTs can be doped either by electron donors or electron acceptors. After reaction with host materials, the dopants are intercalated in the intershell spaces of the CNTs, and in the case of single-walled nanotubes either in between the individual tubes or inside the tubes, as shown as Fig. 2-24 [29]. The reaction of intercalation can be carried out in the vapour or liquid phase, and electrochemically.

Graphite, on the other hand, can conduct electricity because one of the four valence electrons associated with each carbon atom is delocalized and can therefore be shared by all the carbon atoms. However, it turns out that a single sheet of graphite (also known as graphene) is an electronic hybrid. Although not an insulator, it is not a semiconductor or a metal either. Graphene is a "semimetal" or a "zero-gap" semiconductor. This peculiarity means that the electronic states of graphene are very sensitive to additional boundary conditions, such as those imposed by rolling the graphene into a tube. A CNT can be thought of as being formed by folding a piece of graphene to give a seamless cylinder. The description of this process in terms of the chirality vector and the naming of nanotubes are given in Fig. 2-25(a) [30]. The interesting electrical properties of CNTs are due in a large part to the peculiar electronic structure of the graphene. Its band-structure (E vs. k relation) and the hexagonal shape of its first Brillouin zone are shown in Fig. 2-25(b) [30].

It can be shown that a stationary electron wave can only develop if the circumference of the nanotube is a multiple of the electron wavelength. This boundary condition means that a nanotube is either a true metal or a semiconductor - a fact that has been confirmed in experiments with single-wall nanotubes.

The high stability of metallic CNTs is maintained as long as the electron (hole)

energy is not high enough to excite optical phonons. When these vibrational modes become excited the resulting energy dissipation eventually leads to the breakdown of the CNT structure. Since in defect-free CNTs transport is ballistic, high-energy carriers can be formed by hot carrier injection at the contacts. Thus, the stability of a CNT depends on the nature of the contacts. Another factor that influences the stability of a CNT is the gaseous environment it is in. Experiments have shown that the threshold power that is needed to induce breakdown in a CNT is drastically lower in air than it is in vacuum. Particularly interesting is the breakdown behavior of MWCNTs. Fig. 2-26 [30] shows the variation with time of the current flowing through a MWCNT under a bias leading to breakdown. A very regular current staircase is clearly seen.
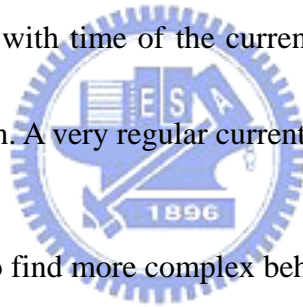
One would expect to find more complex behavior for CNTs because of interactions between adjacent layers, and this is the subject of ongoing research. Moreover, by combining different nanotubes, and supplementing them with gate electrodes, there is the potential to make a wide variety of electronic devices, ranging from quantum wires to field effect transistors.

On the fundamental side, a perfect metallic nanotube should be a ballistic conductor. In other words, every electron injected into the nanotube at one end should come out the other end. Although a ballistic conductor does have some resistance, this

resistance is independent of its length, which means that Ohm's law does not apply.

Indeed, only a superconductor (which has no electrical resistance whatsoever) is a better

conductor. Any wave that hits two semireflective barriers, one after the other, will

produce an interference pattern. This pattern consists of regular oscillations in the

intensity of the transmitted wave across the double barrier, as a function of wavelength.

Liang et al. report such oscillations in the transmission of electrons through a metallic

SWNT hundreds of nanometres long that is held between two electrodes, as shown as

Fig. 2-27 [31]. This experiment demonstrates the quantum-mechanical wave nature of

electrons. It also shows that the propagation of electrons in the nanotube is

ballistic-largely free from scattering-over distances of thousands of atoms. A few years

ago, we predicted theoretically the possibility of ballistic propagation of electrons over

such distances in metallic SWNTs. The creation by Liang et al. of a device that relies on

this effect for its operation confirms this and other results that indicate ballistic transport

through metallic CNTs, and is a stunning achievement.

2-3-3. Quantized conductance

This method for making electrical contact with nanotubes is very different to

techniques that rely on sub-micron fabrication technology. Quantized conductance will

only be observed if ideal contacts are made to the nanotube, and these can be very

difficult to achieve. (In an ideal contact none of the electrons entering or leaving the

nanotube will be backscattered by the contact.) Early experiments with microfabricated

contacts found strong evidence that electrons were scattered. The transport therefore

appeared to be diffusive rather than ballistic.   Limiting the length of a CNT leads to a

"particle-in-a-box" quantization of the energy levels. Such discrete energy levels have

been observed in transport experiments on individual nanotubes and ropes. The electron

wave functions corresponding to these discrete states can in principle be imaged by

scanning tunneling microscopy (STM). The well-known STM work on quantum corrals

demonstrated that wave patterns could be directly imaged in the local density of states

of a 2D metal surface, as shown as Fig. 2-28 [32]. The wave functions of several

adjacent energy levels can be displayed simultaneously by plotting the differential

conductance dI/dV as a function of the voltage and the position x along the tube (Fig.

3A). Wave patterns can be observed for four different energy levels appearing at bias

voltages of 0.11, 0.04, 0.00, and –0.05 V (15), as shown as Fig. 2-29 [32]. At each level,

a horizontal row of about seven maxima is resolved in dI/dV as a function of position x

along the tube (see Fig. 2-28 for the 1D spatial profile of the wave functions belonging

to these states).
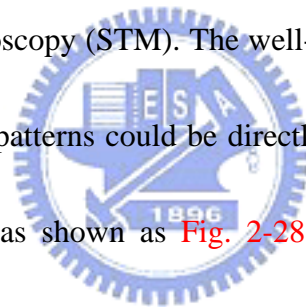
2.3.4 Thermal properties

Many phenomena in nature occur as the result of some kind of imbalance. For instance, heat is transported when there is a temperature gradient between two boundaries of a material. Despite their ubiquity in everyday life, many aspects of such phenomena are still the subject of debate among theoretical physicists. One central issue is the role of spatial constraints, caused by the dimensionality of a system: the response of a system to external forces is intimately related to statistical fluctuations within it, and these, in turn, depend strongly on whether the system is one-, two or three-dimensional. Because of the variety and complexity of specific interactions, simplified microscopic models are an invaluable tool for the study of transport mechanisms in reduced dimensions, as shown as Fig. 2-30 [33]. The old problem of heat conduction on the thermal conductivity should increase with the system size. In other words, the larger the system, the more efficiently heat is transported (assuming that the density of the material and the temperature gradient are fixed)-in physical terms, the mean free path of the 'heat carriers' increases with the length of the sample.

A system of fewer than three dimensions-confirming that space dimensionality is crucial in anomalous transport properties. More specifically, the thermal conductivity diverges as the length of a one-dimensional system increases, following a power law

with exponent 1/3; for a two-dimensional system, the divergence is much weaker and logarithmic. But such anomalous behaviour disappears in three dimensions. Transport anomalies such as this have been found in many microscopic models, including one-dimensional crystals. Although it may seem strange to consider a one-dimensional crystal as a fluid, it is nonetheless well known that mechanical vibrations in a crystal structure can be described by hydrodynamic equations similar to those used in a fluid, as interacting phonons in a crystal behave similarly to particles in a fluid.can the anomalous behaviour actually be described by universal scaling laws, and to what extent does it depend on the nature of the microscopic interactions? The conceptual challenge is not the only reason for studying energy transport in spatially constrained systems-there is also a variety of real systems in which these anomalies are important.
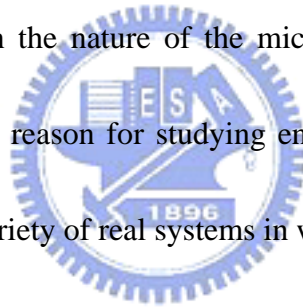
SWNTs (Fig. 2-30 [33]) are known through experiment to have an unusually high thermal conductivity, which is attributed mainly to quasi-one-dimensional lattice vibrations, and it is reasonable to expect that the scaling laws derived for simple models should apply to nanotubes as well. Although, so far, an experimental test is lacking, molecular-dynamics simulations that use realistic energy potentials for the carbon atoms support this idea. If the thermal conductivity did increase with nanotube length in a well-defined way, this would be a very promising feature to use in technological applications, such as the design of components that dissipate heat efficiently in

nanocircuits. In building models of energy-transport processes, the aim is to single out

generic physical features, although this might sometimes be at the price of drastic

simplifications. Hopefully, in the end the results will go beyond pure academic interest

and suggest new ideas for technological applications-perhaps the reader is astonished

that so many interesting and innovative ideas are still emerging from classical

mechanics [33].

2.3.5 Magnetic fields properties

Nanotubes have also been used to help demonstrate the Aharonov-Bohm effect,

one of the most fundamental phenomena in quantum physics. In the Aharonov-Bohm

effect a beam of quantum particles, such as electrons, is split into two partial beams that

pass on either side of a region containing a magnetic field, and these partial beams are

then recombined to form an interference pattern. The interference pattern can be altered

by changing the magnetic field-even though the electrons do not come into contact with

the magnetic field, as shown as Fig. 2-31 [34].

2.3.6 Field emission

The small diameter of CNTs is very favorable for field emission - the process by which a device emits electrons when an electric field or voltage is applied to it. Field emission is important in several areas of industry, including lighting and displays, and the relatively low voltages needed for field emission in nanotubes could be an advantage in many applications. However, as with all new technologies, there are formidable obstacles to be overcome. CNTs can act as electron sources with very rigid structures, making them particularly interesting for use as point electron sources in high-resolution electron-beam instruments, as shown as Fig. 2-32 [35].

Two parameters of an electron source affect the resolution of these instruments: the energy spread of the emitted electrons and a parameter called the reduced brightness, which depends on the angular current density and the virtual source size. To measure the reduced brightness, and find a value that is more than a factor of ten larger than provided by state-of-the-art electron sources in electron microscopes. In addition, an individual CNT emits most current into a single narrow beam, as shown as Fig. 2-33 [35].

On the basis of these results, we expect that CNT electron sources will lead to a significant improvement in the performance of high-resolution electron-beam instruments, as shown as Fig. 2-34 [35].

2.3.7 Biology and nanotube

Since the discovery of their one dimensional electronic band structure, the leading candidate that has emerged for nanodevice applications is SWNTs. Their unique properties with the specific molecular-recognition features of DNA by coupling SWNTs to peptide nucleic acid (PNA, an uncharged DNA analogue) and hybridizing these macromolecular wires with complementary DNA. The findings provide a new, versatile means of incorporating SWNTs into larger electronic devices by recognition-based assembly, and of using SWNTs as probes in biological systems by sequence-specific attachment, as shown as Fig. 2-35 [36]. The recognition properties imparted to SWNTs by oligonucleotide adducts could be used to programme the attachment of SWNTs to each other and to substrate features, such as electrodes, on which monolayers of complementary sequences are self-assembled. The antisense properties of PNA–SWNTs might also be exploited in a biological context, for example in biosensors.

2.4 The method of carbon nanotubes synthesis

2.4.1 Arc-discharge methods

The observed nanotubes synthesized from the electric-arc discharge technique. Shown schematically in Fig. 2-36 [37], the arc discharge technique generally involves the use of two high-purity graphite rods as the anode and cathode. The rods are brought together under a helium atmosphere and a voltage is applied until a stable arc is achieved. The exact process variables depend on the size of the graphite rods. As the anode is consumed, a constant gap between the anode and cathode is maintained by adjusting the position of the anode. The material then deposits on the cathode to form a build-up consisting of an outside shell of fused material and a softer fibrous core containing nanotubes and other carbon particles. To achieve single walled nanotubes, the electrodes are doped with a small amount of metallic catalyst particles.
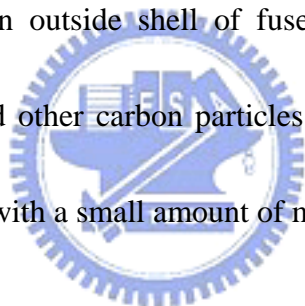
2.4.2 Laser vaporization

Laser ablation was first used for the initial synthesis of fullerenes. Over the years, the technique has been improved to allow the production of SWNTs. In this technique, a laser is used to vaporize a graphite target held in a controlled atmosphere oven at temperatures near 1200 °C. The general set-up for laser ablation is shown in Fig. 2-37 [37]. To produce SWNTs, the graphite target was doped with cobalt and nickel catalyst. The condensed material is then collected on a water-cooled target. Both the

arc-discharge and the laser-ablation techniques are limited in the volume of sample they can produce in relation to the size of the carbon source (the anode in arc-discharge and the target in laser ablation). In addition, subsequent purification steps are necessary to separate the tubes from undesirable by-products.

2.4.3 Chemical vapor deposition

Since separation of CNTs is difficult and the yield is low, they are very expensive. However, the catalytic CVD technique, which employs the catalytic decomposition of short-chain hydrocarbons, can produce relatively large amounts of CNTs under mild conditions. Moreover, this process makes it possible to control the size and growth density of CNTs by dispersing the catalyst particles on supports and adjusting the reaction parameters at relatively lower temperatures in comparison with the former processes. These limitations have motivated the development of gas-phase techniques, such as Thermal Chemical Vapor Deposition (Thermal CVD), as shown as Fig. 2-38 [38], where nanotubes are formed by the decomposition of a carbon-containing gas. The gas-phase techniques are amenable to continuous processes since the carbon source is continually replaced by flowing gas. In addition, the final purity of the as-produced nanotubes can be quite high, minimizing subsequent purification steps.

2.5 The mechanism of carbon nanotubes growth

2.5.1 The diffusion path of carbons atom

A typical growth condition may involve the following step in Fig. 2-39 [39].

(1) Hydrocarbon dissociate and deposit carbon on surface.

(2) Carbon diffuses through solid metal.

(3) Carbon precipitates as curved graphitic layers.

2.5.2 Tip growth mode and base growth (root growth) mode

Based on the position of metal particle on the tube, there were two kinds of growth mode: one is called "base-growth" and the other is called "tip-growth". The "base-growth" mode meant that the tube grew upward from metal particles, which attached to the substrate. If the metal particle detached and moved to the head of the growing tubes, it was the "tip-growth" mode in Fig. 2-40 [40].
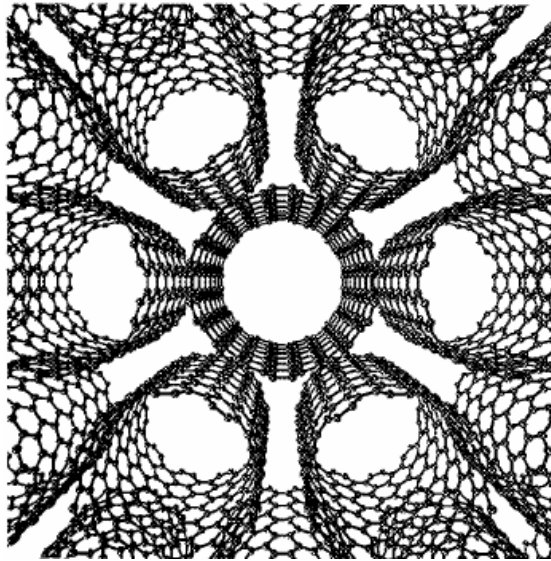
Fig. 2-1 Perspective view of a rope of (10,10) carbon nanotubes. [12]
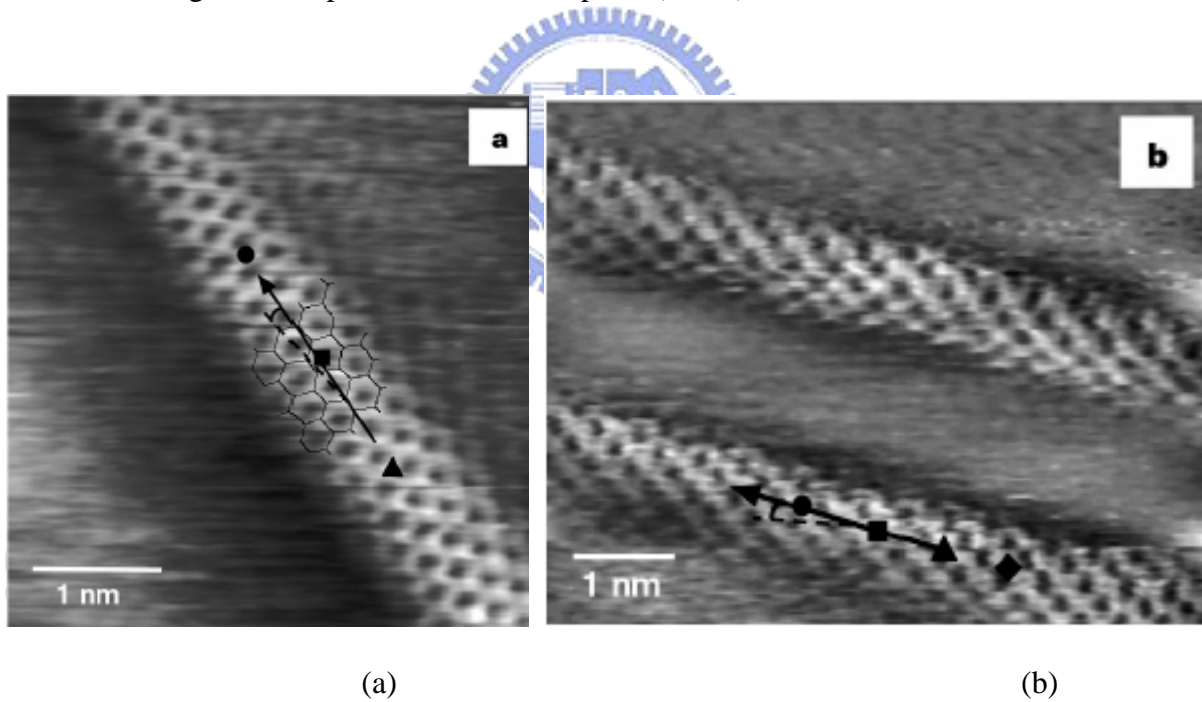
(a)   (b)

Fig. 2-2 Atomic structure and spectroscopy of metallic SWNTs. STM images of a SWNT [13]
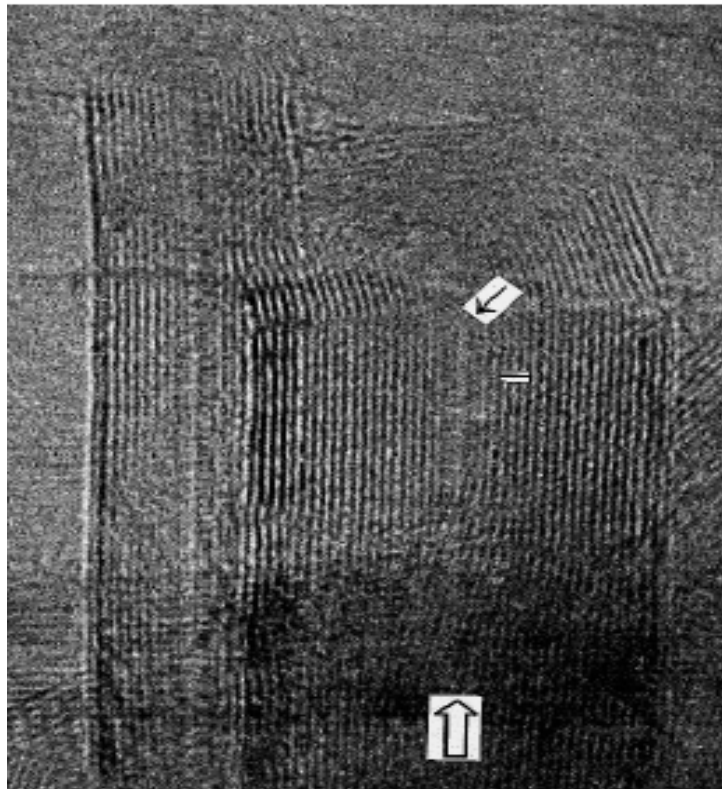
Fig. 2-3 HRTEM image of two nanotubes with outer diameters of 6 nm and 16 nm. [14]

(a)   (b)   (b)
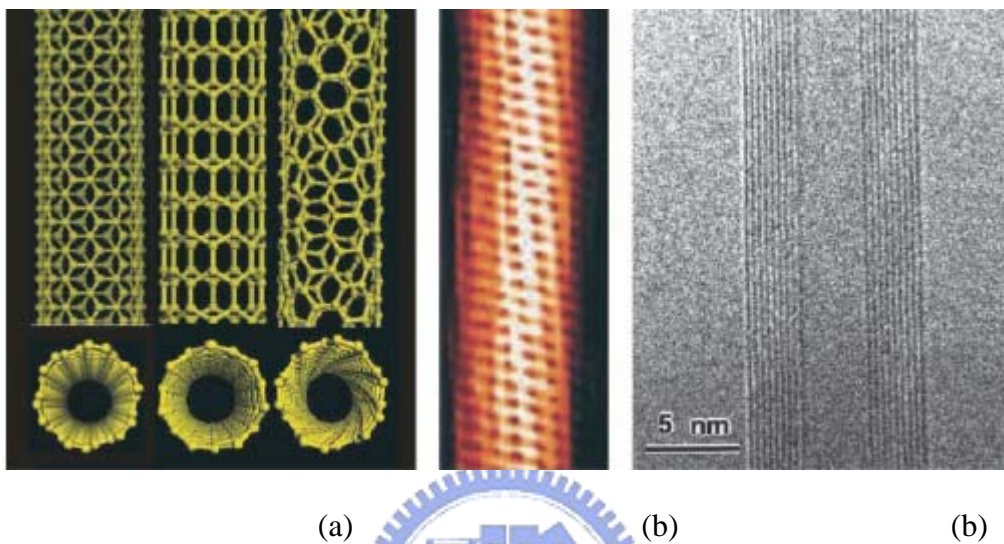
Fig. 2-4 (a) armchair, zigzag, and chiral SWNTs. (b) Tunneling electron microscope image of a 1.3-nm-diameter chiral SWNT. (c) Transmission electron microscope (TEM) image of a MWNT [15]
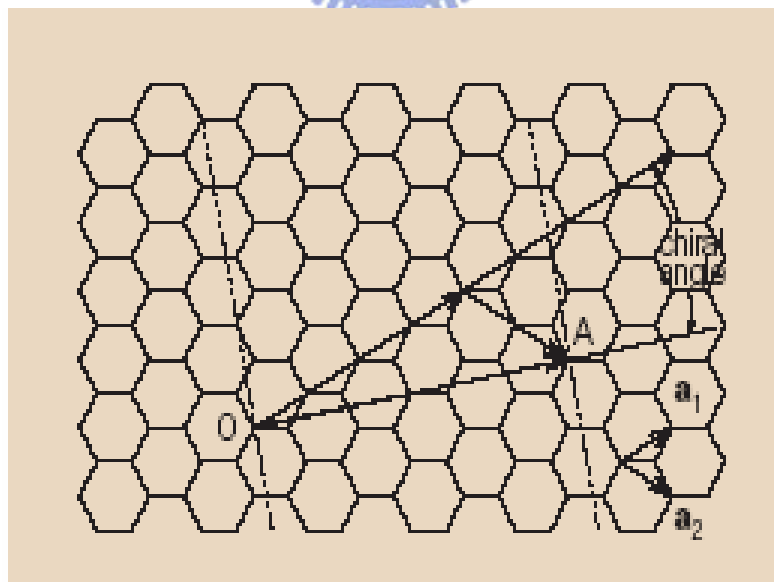
Fig. 2-5 Nanotube coordinates. [16]
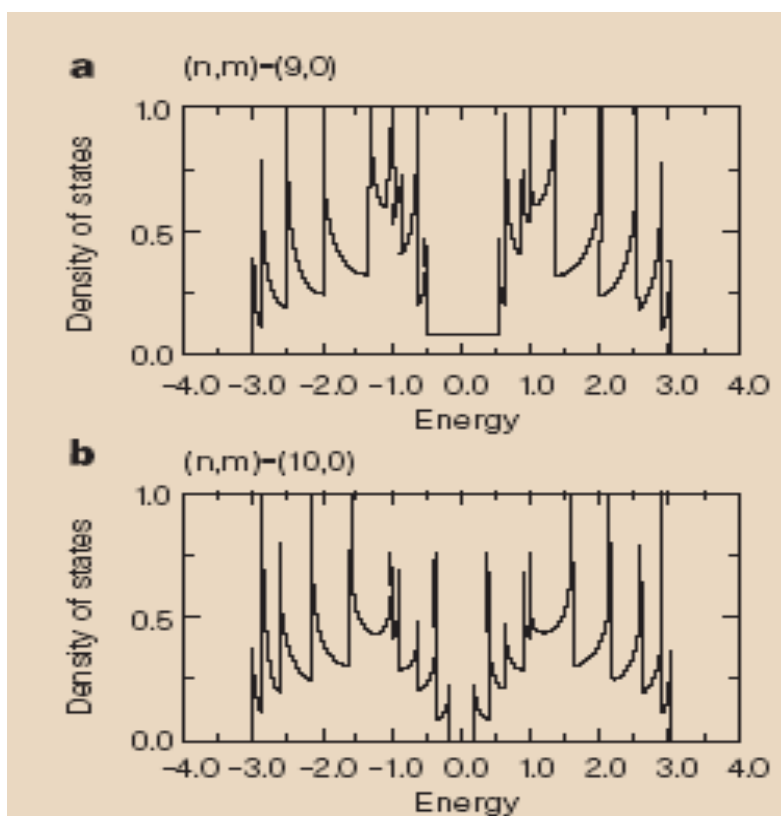
Fig. 2-6 Calculated one-dimensional electronic density of states on single-wall nanotubes.

[16]
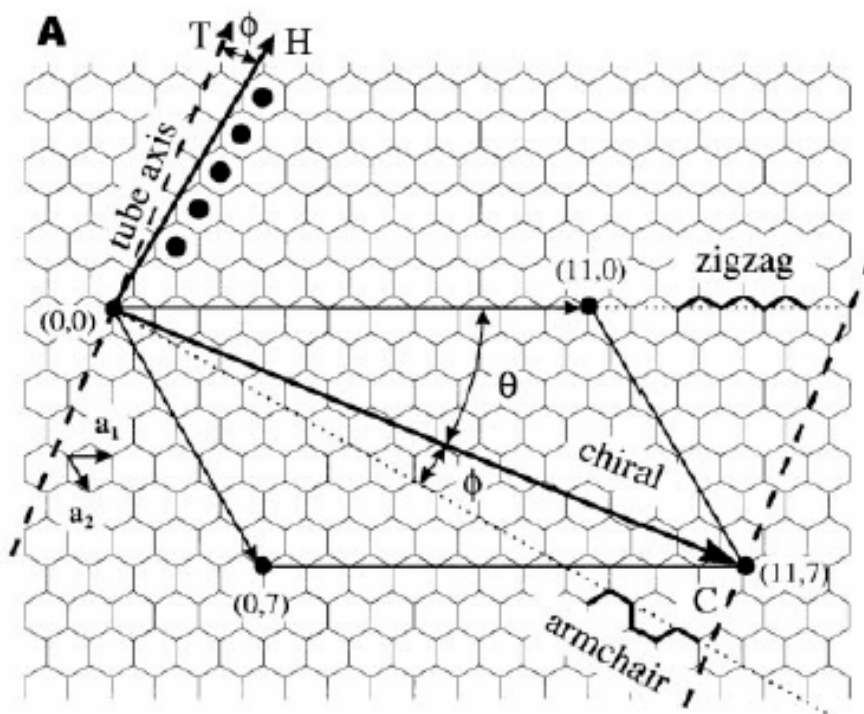
Fig. 2-7 Relation between the hexagonal carbon lattice and the chirality of carbon nanotubes.
[17]

(a)   (b)

(c)   (d)
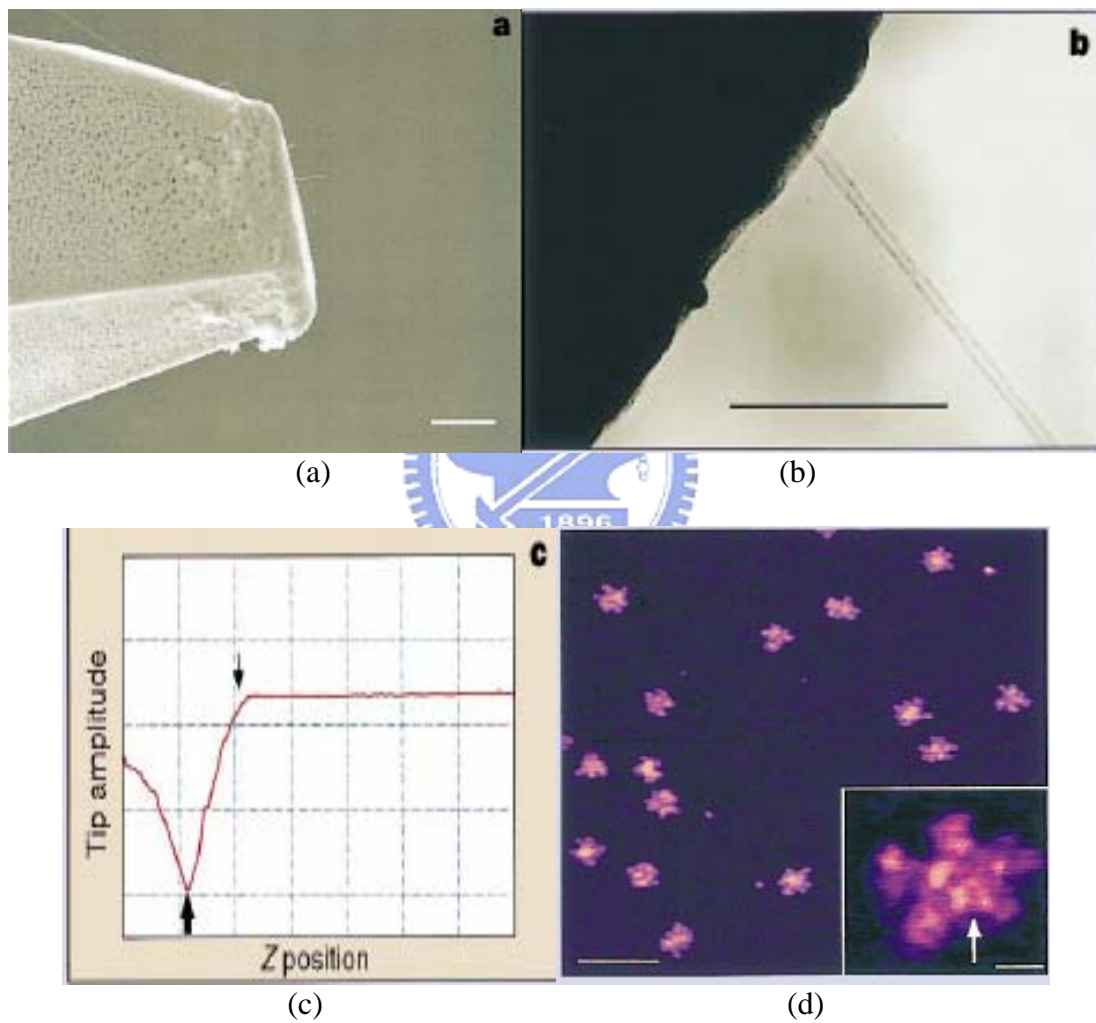
Fig. 2-8 (a) Characterization of CVD nanotube tips. (b) Transmission electron microscope (TEM) image of a CVD nanotube tip. (c) Tip oscillation amplitude (d) Imaging IgM macromolecules with a CVD nanotube tip at high resolution. [19]
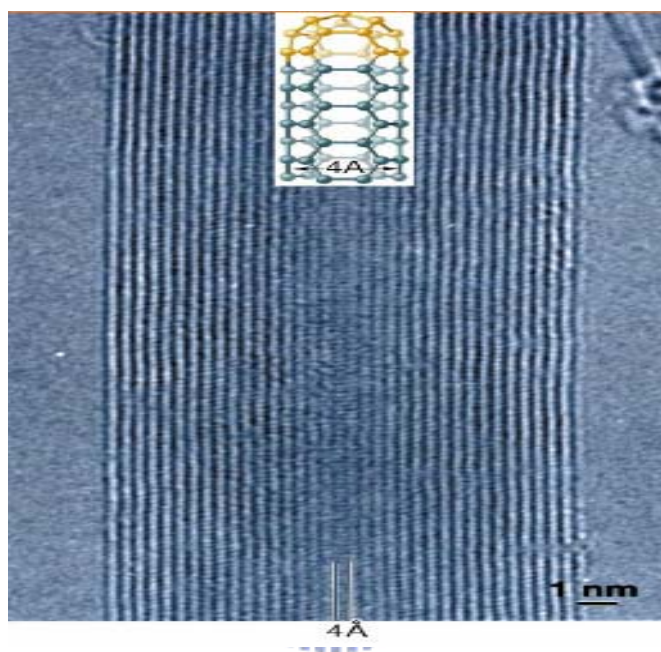
 Fig. 2-9 High-resolution electron microscope image of a 4 Å tubule (side walls are marked by lines) confined inside an 18-shell carbon nanotube. [20]
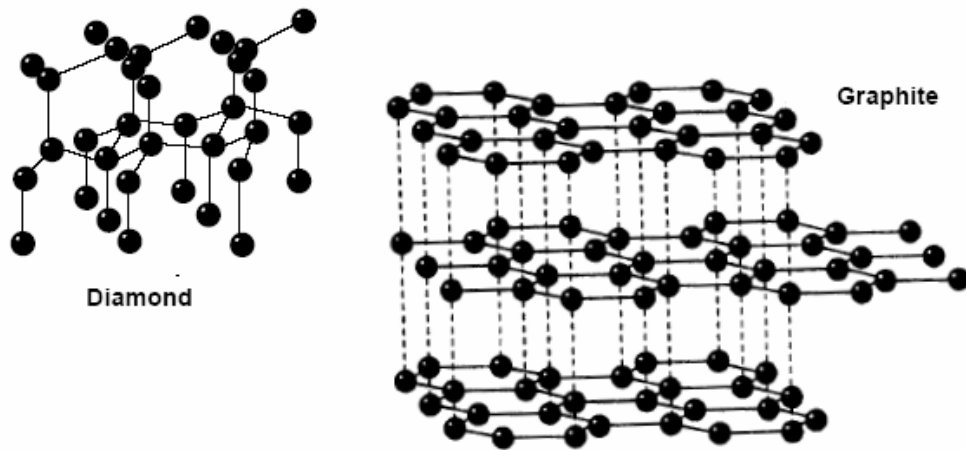
Fig. 2-10 Diamond and Graphite structures [21]
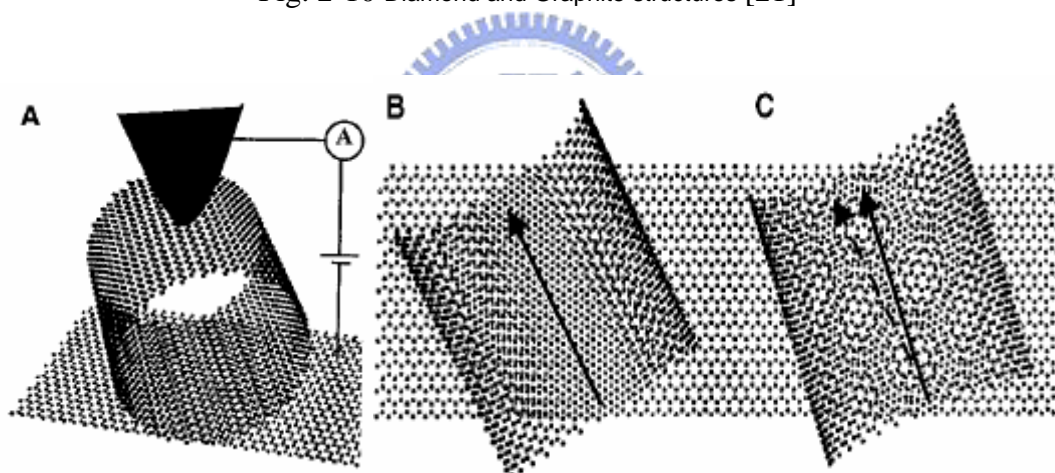
Fig. 2-11 (A) A conducting AFM tip is used to measure the resistance of the NT-HOPG interface. (B) The NT is in registry. (C) The NT Fermi-level states (dotted arrow) [22]
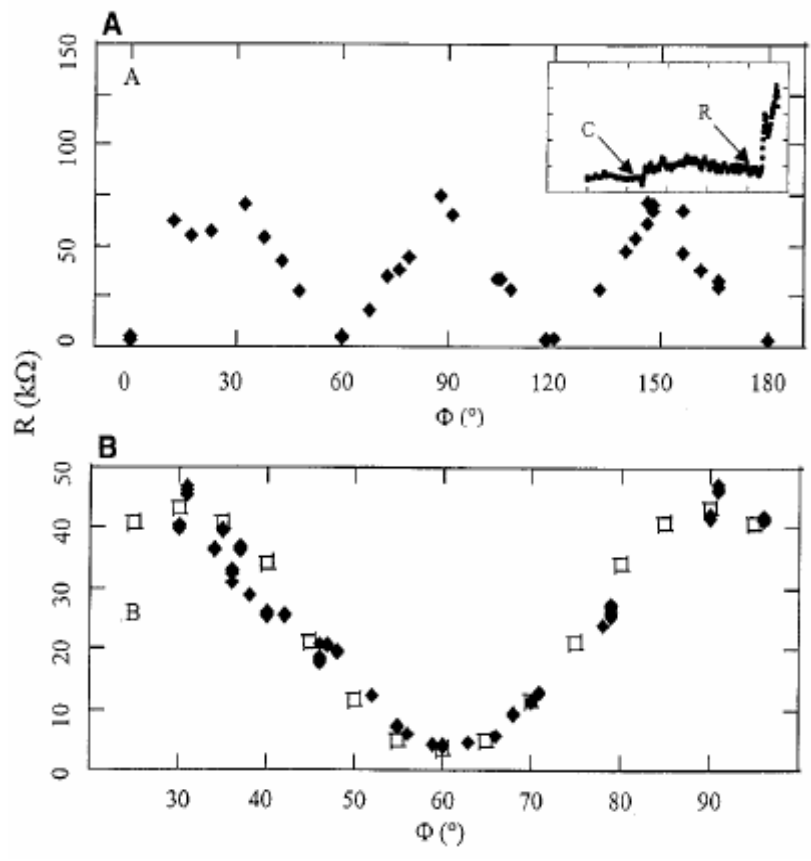
Fig. 2-12 (A) A tube that has been rotated through 180¡. (B) More dense data over one period on a different tube gives us a better indication of the shape of the curve. [22]
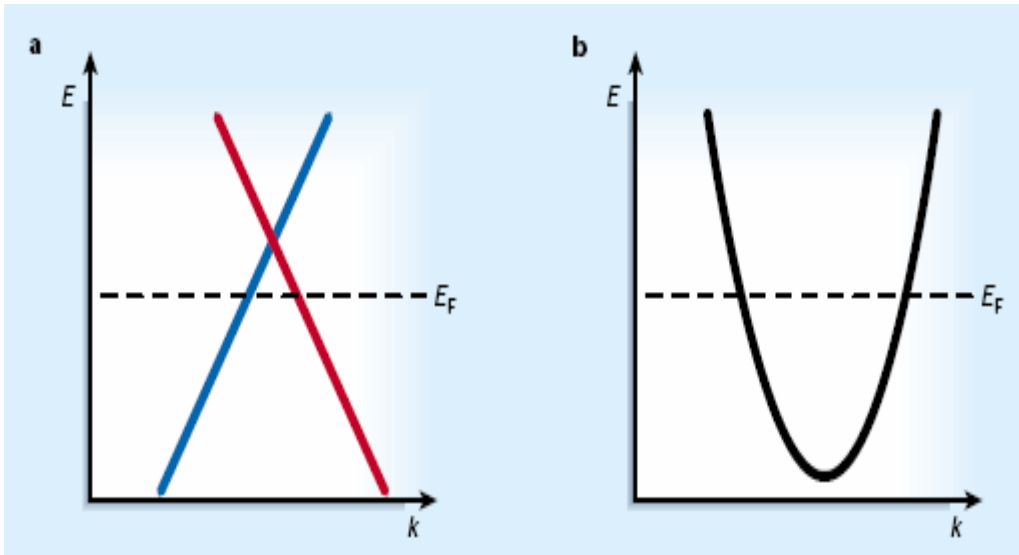
Fig. 2-13 In a metallic carbon nanotube, left-moving electrons (red) and right-moving electrons (blue) belong to two different bands with distinct microscopic structures. [23]
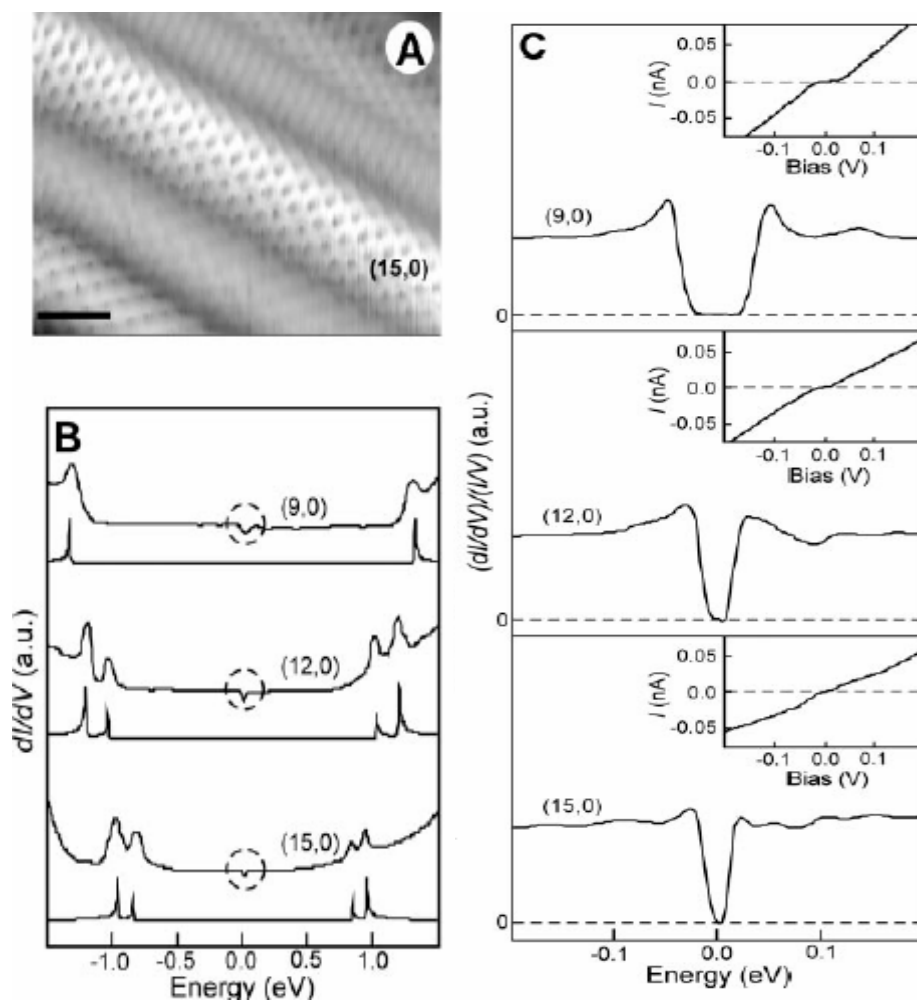
Fig. 2-14 (A) Typical atomically resolved STM image of a (15,0) SWNT. Scale bar, 1 nm. (B) Tunneling conductance data (C) Typical high-resolution normalized conductance (dI/dV)/(I/V) curves and measured I-V curves [24]
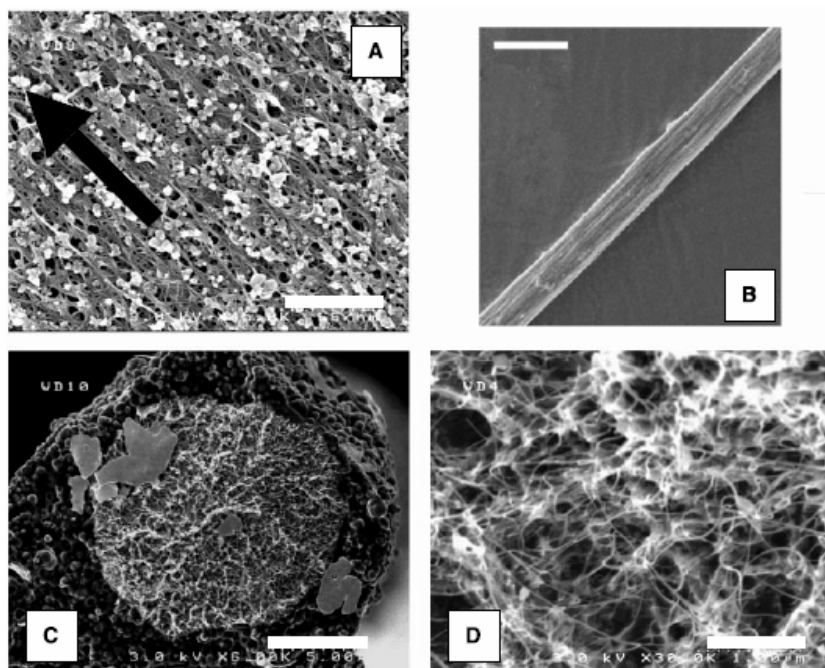
Fig. 2-15 (A) A dry ribbon deposited on a glass substrate. (B) A nanotube fiber (scale bar 5 25 mm). (C) Cross section of a nanotube fiber. (scale bar 5 16.7 mm). (D) Magnification of the bright region in (C) (scale bar 5 1 mm). [25]
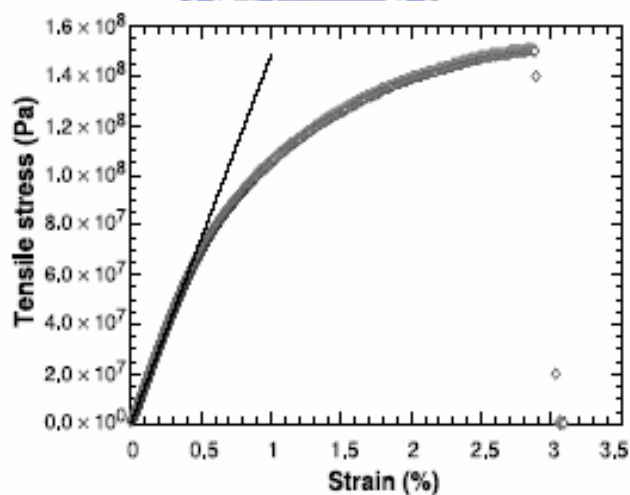
Fig. 2-16 Mechanical measurements under tensile loading performed at a strain rate of 1% per minute.. [25]
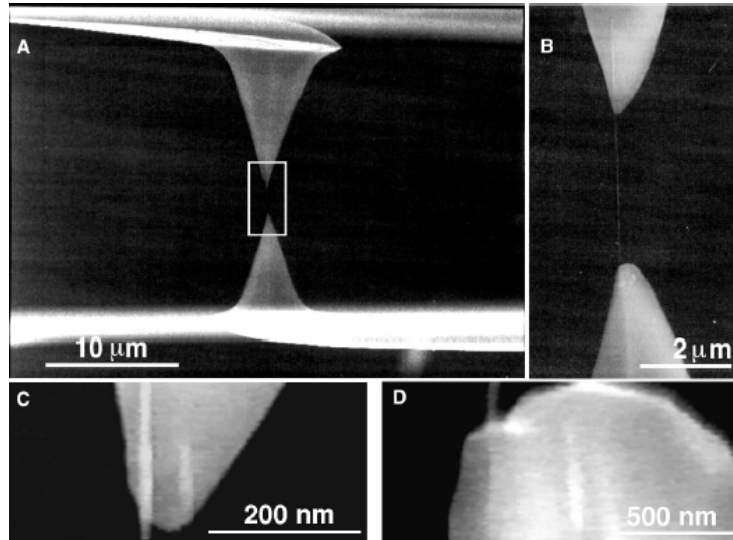
Fig. 2-17 (A) An SEM image of two AFM tips holding a MWCNT.(B) High-magnification
SEM image of the indicated region in (A), showing the MWCNT between the AFM tips. (C)
Higher magnification SEM image [26]
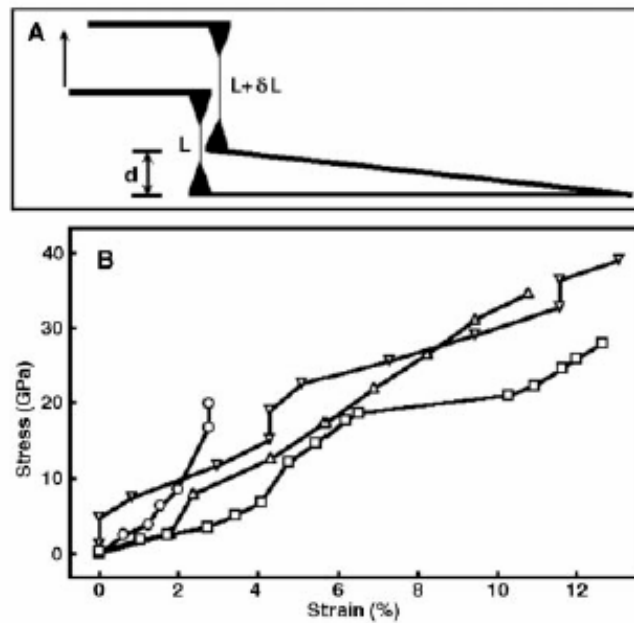
Fig. 2-18 (A) Schematic showing the principle of the tensile-loading experiment. (B) Plot of
stress versus strain curves for individual MWCNTs. [26]
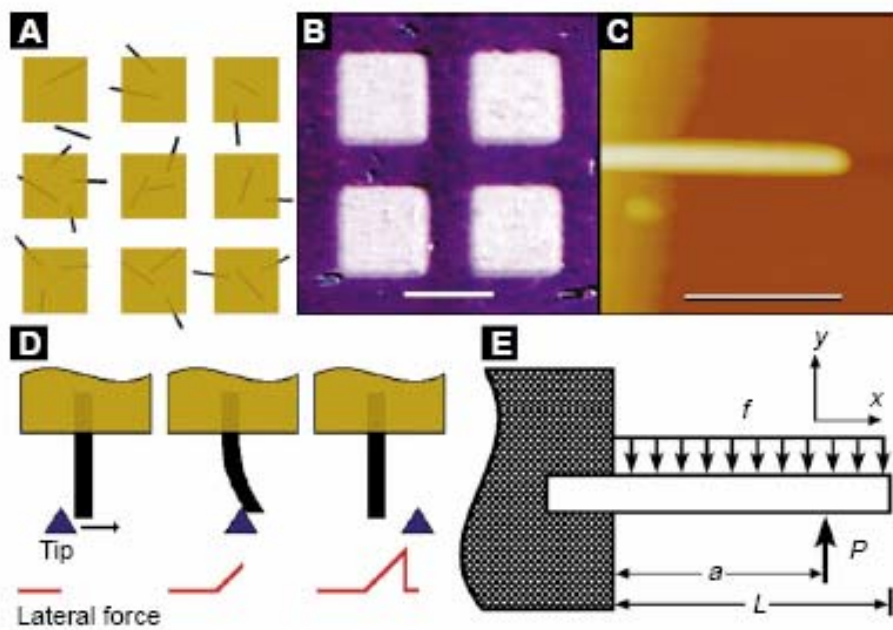
Fig. 2-19 (A) SiC NRs or carbon nanotubes (B) Optical micrograph of a sample showing the SiO pads (white) and the MoS2 substrate (blue).. (C) An AFM image of a 35.3-nm-diameter SiC NR (D) Schematic of beam bending with an AFM tip. The tip (blue triangle) [27]
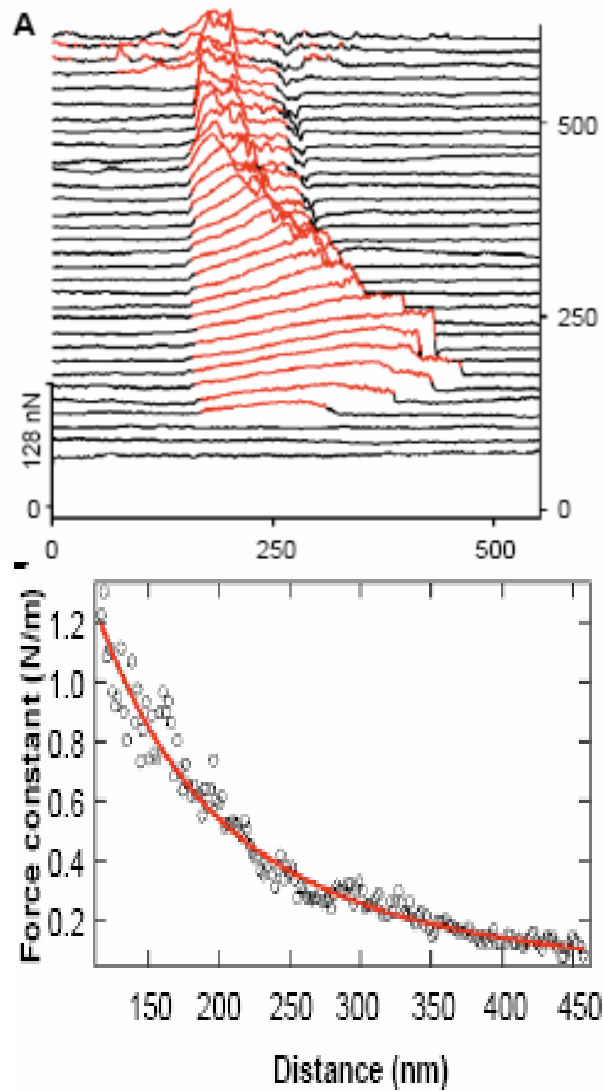
Fig. 2-20 (A)Surface plot showing the F-d responseof a 23.0-nm-diameter SiC NR (B) Dependence of the force constant k(x) on position x along the axis of the same NR [27].
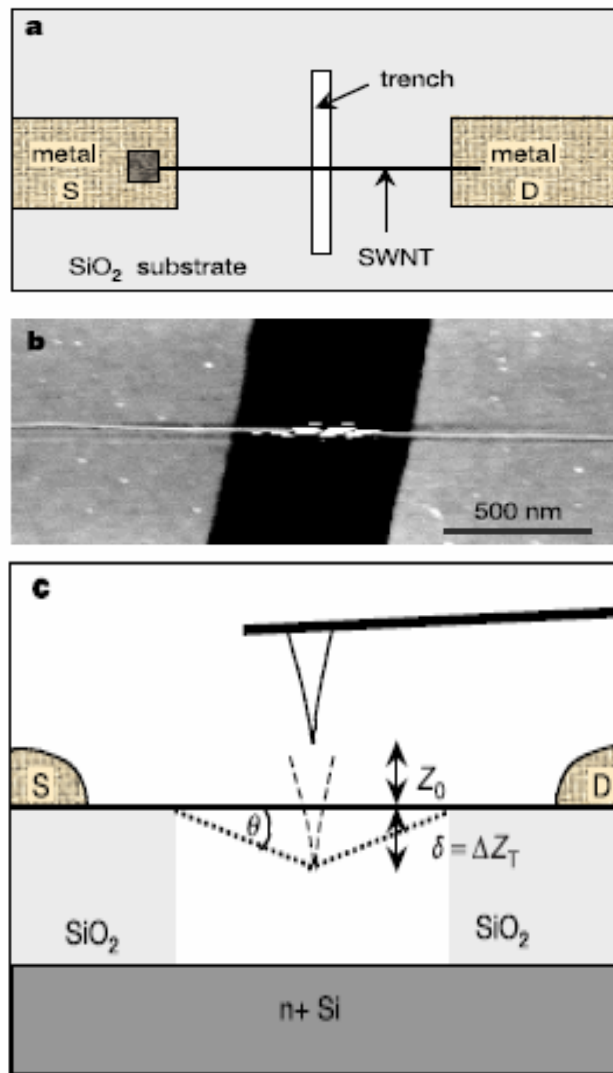
Fig. 2-21. a. Device viewed from above. Preparation of samples involves chemical vapour deposition of SWNTs b, AFM image of an SWNT c. Side-view of the AFM pushing experiment. [28]
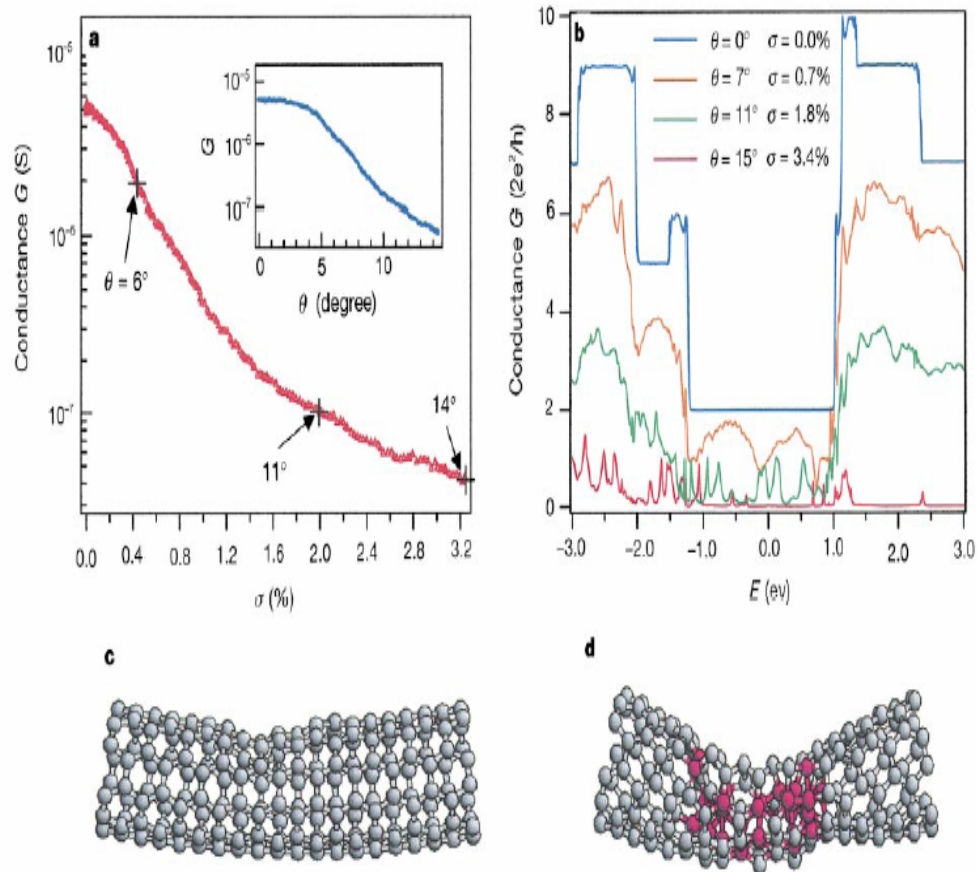
Fig. 2-22 a. Experimental result of conductance. b. Conductance versus band energy calculated for an ideally contacted (5,5) SWNT. c,d. Simulated atomic configurations of the nanotube pushed to 78 and 158 respectively. [28]
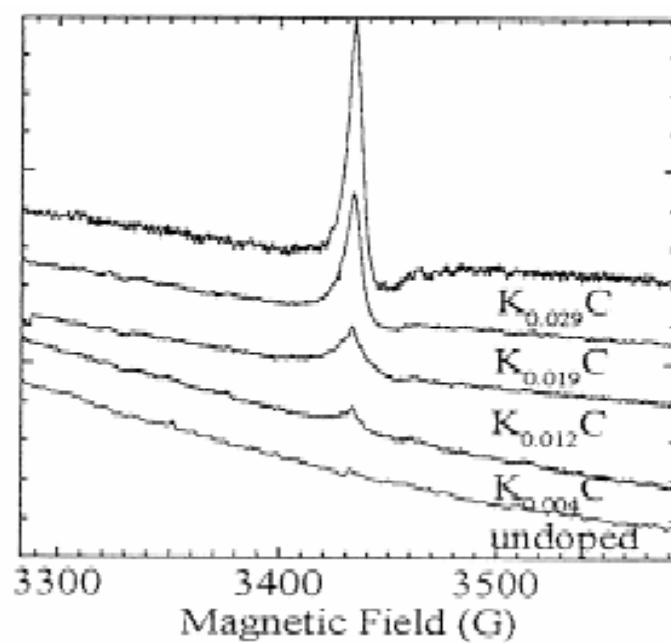
Fig. 2-23 CESR (conduction electron spin resonance) of SWNT bucky paper films electrochemically doped by K for K C various x compositions. [29]
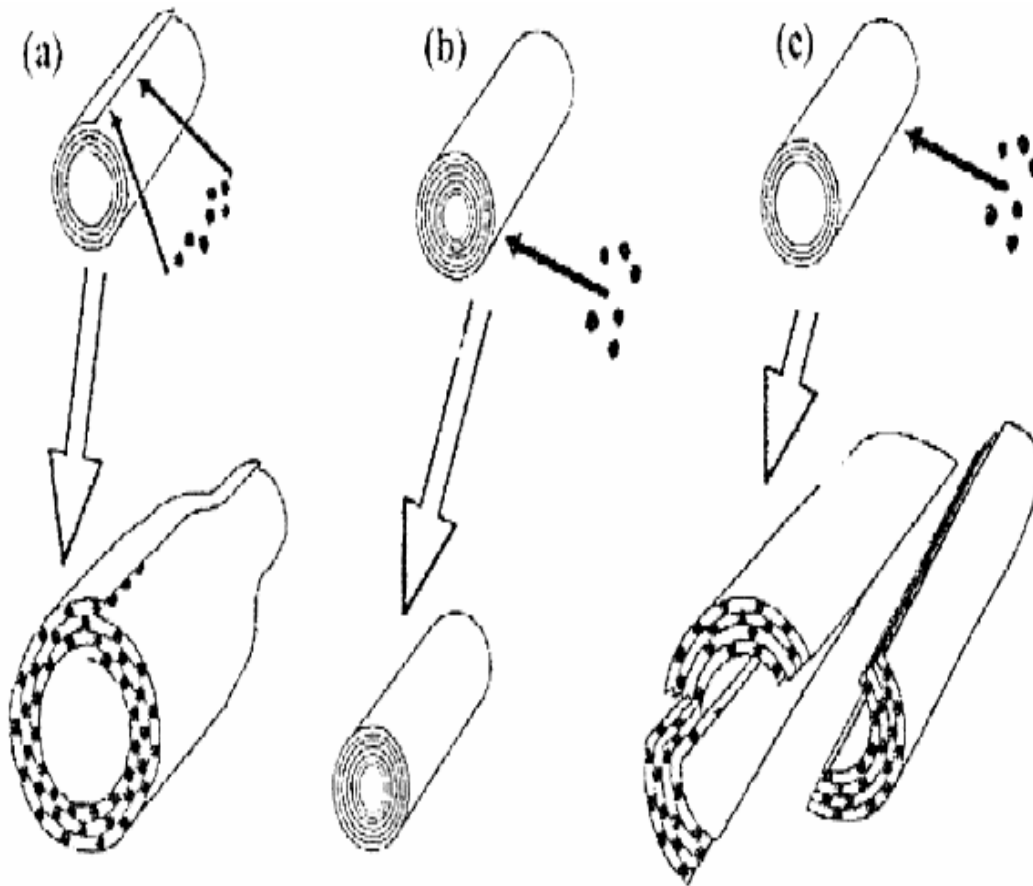
Fig. 2-24 Schematic of three types of MWNT (a) intershell intercalation; (b) no reaction; (c) intercalation-assisted break-up. [29]
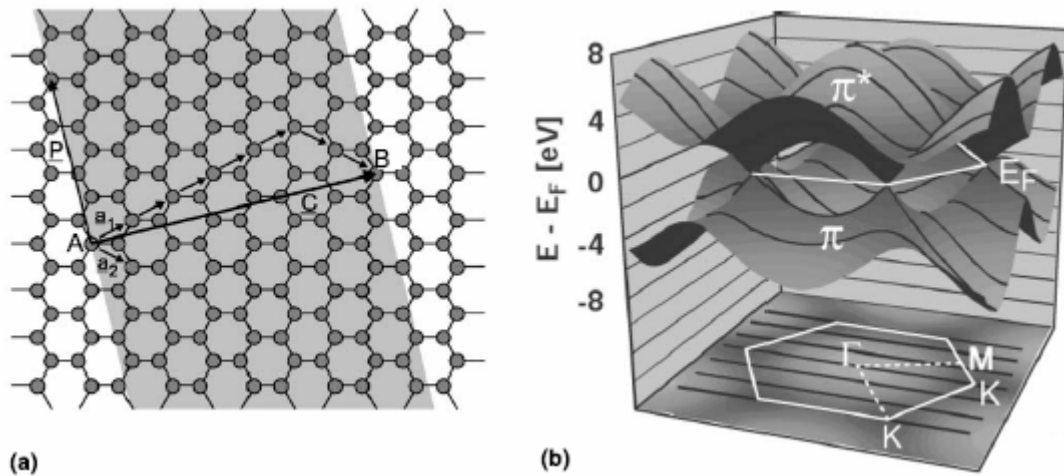
Fig. 2-25 (a) Schematic illustration of the generation of a nanotube (b)Top: Band-structure of the 2D graphene sheet (in gray). [30]
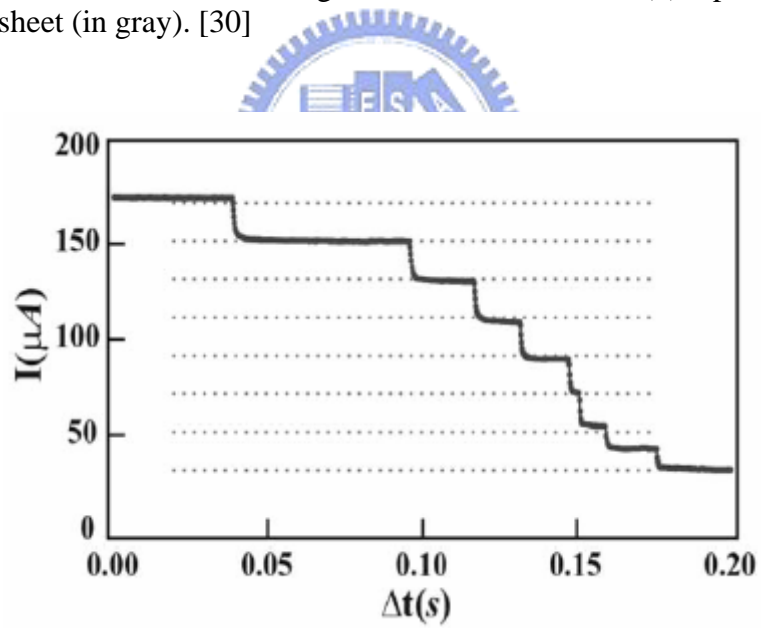
Fig. 2-26 Time-dependence of the current flowing through a multi-walled nanotube during current-induced breakdown. [30]
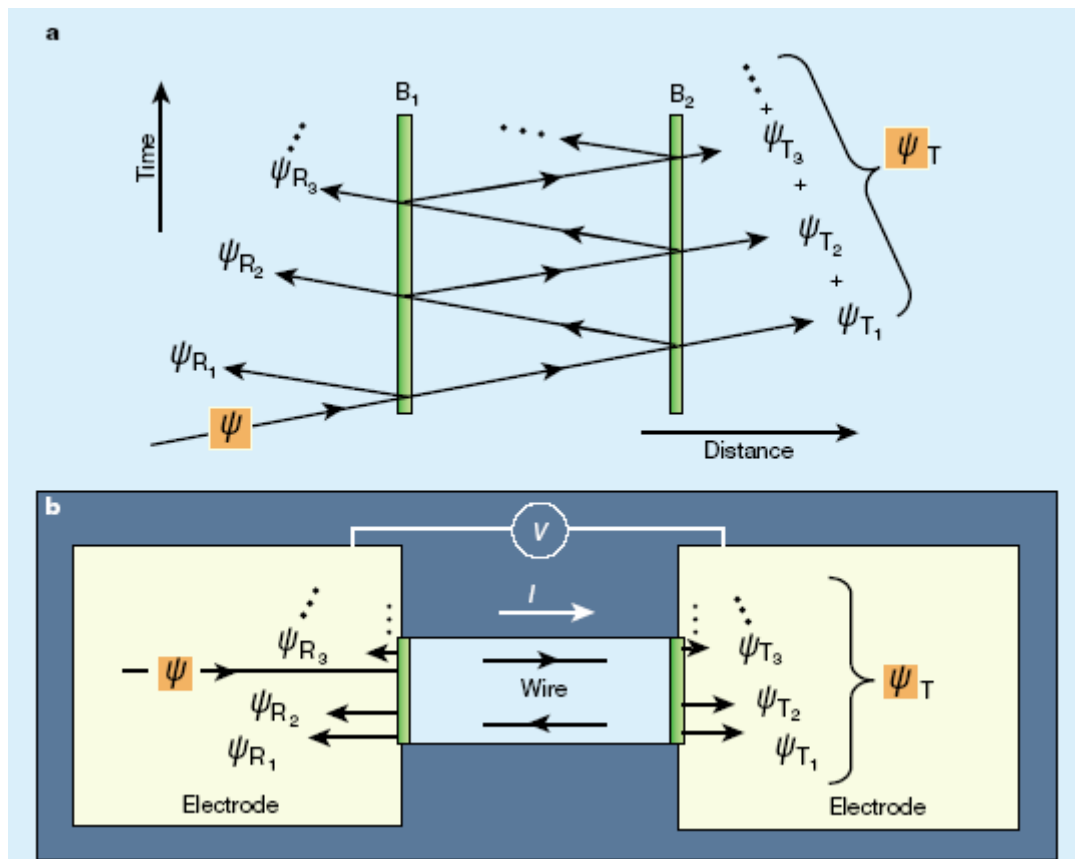
Fig. 2-27 A wave hitting two partially reflective barriers. [31]
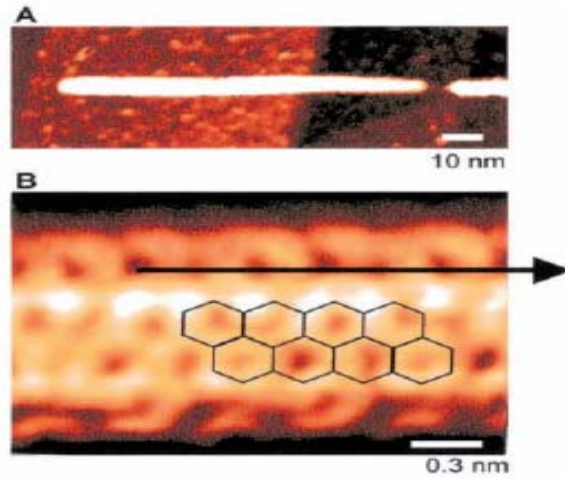
Fig. 2-28 (A) Example of a nanotube (B) Atomically resolved image of an armchair nanotube. [32]
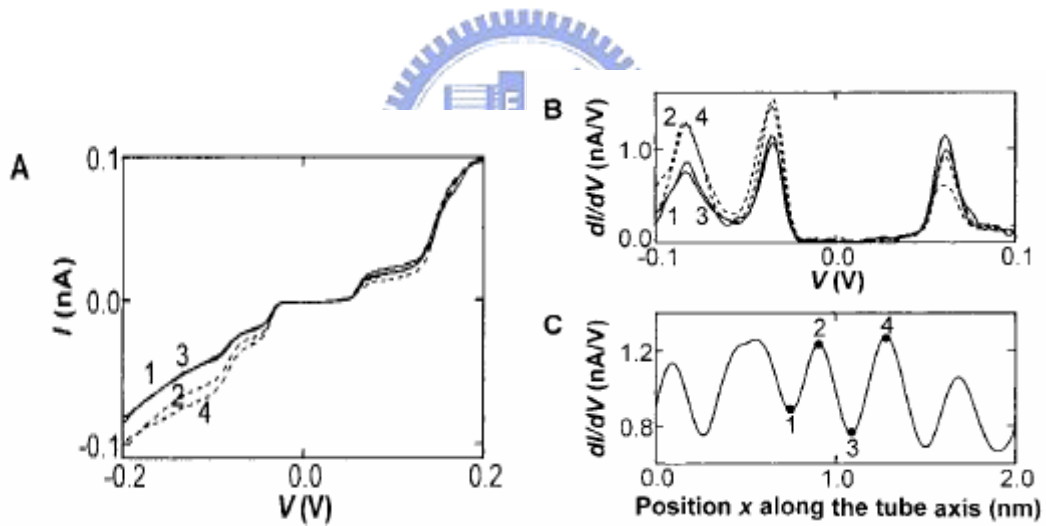
Fig. 2-29 (A) I-V characteristics of the tube. (B) Differential conductance dI/dV versus V, as calculated from the I-V curves. (C) Differential conductance dI/dV as a function of position along the tube. [32]
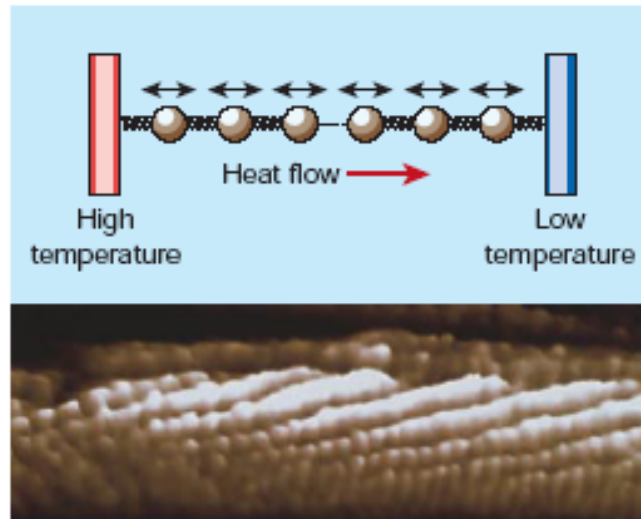
Fig. 2-30 Simple models and real materials. [33]
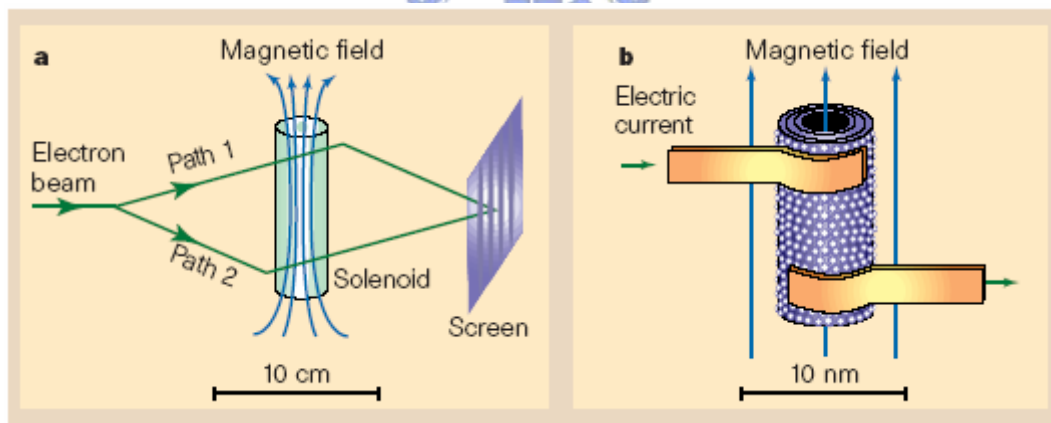
Fig. 2-31 Observing the Aharonov–Bohm effect.[34]

(a) (b)
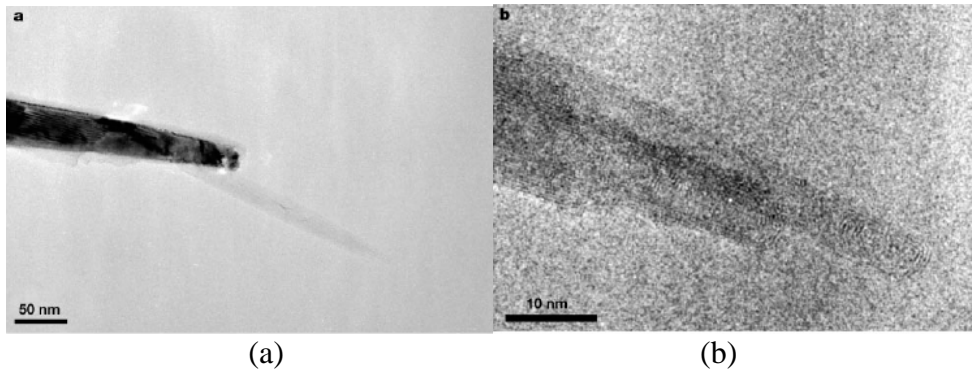
Fig. 2-32 TEM images of an individual multi-walled carbon nanotube b, High-resolution TEM image of the apex of the tube.[35]
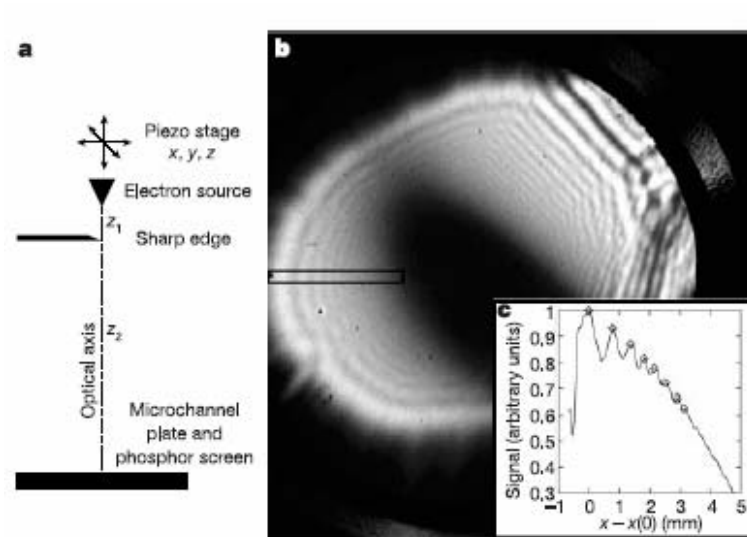
Fig. 2-33 a. Schematic overview of the point projection microscope. b. The Fresnel interference pattern of a hole in a thin carbon film [35]
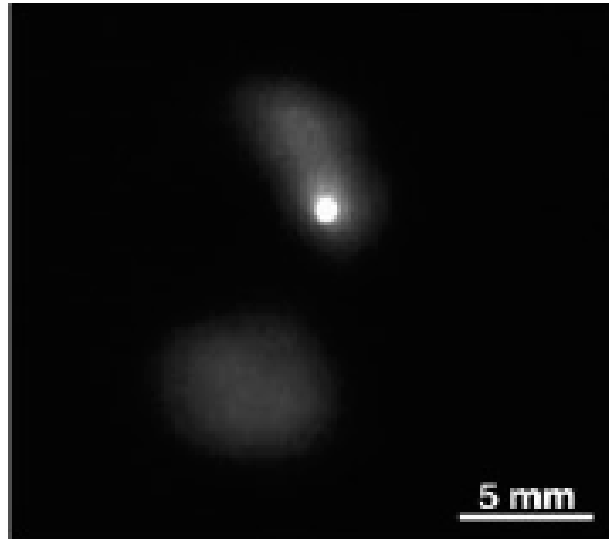
Fig. 2-34 The emission pattern on a phosphor screen of an electron source consisting of an individual multi-walled carbon nanotube. [35]
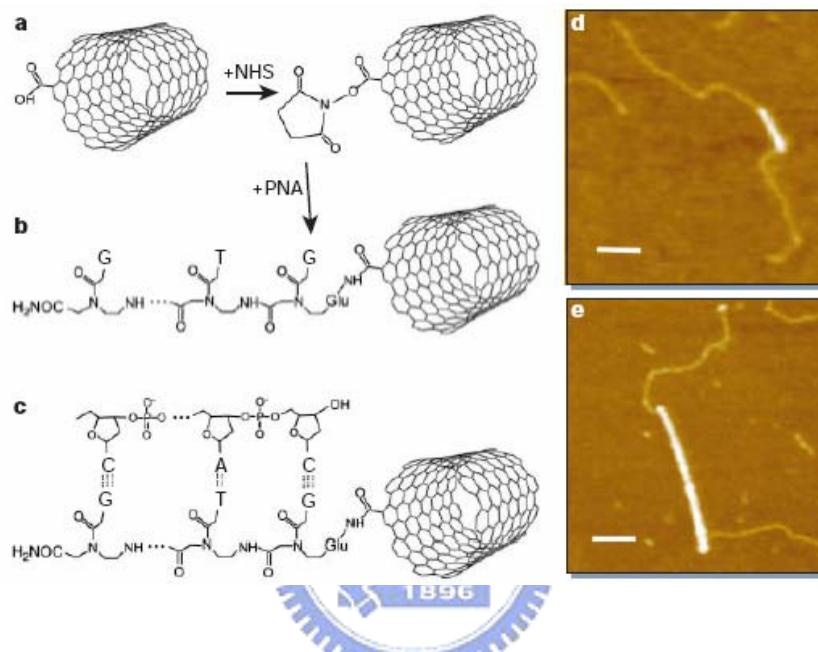
Fig. 2-35 a, b, N-hydroxysuccinimide (NHS) esters formed on carboxylated. d, e, Atomic-force microscope (Tapping Mode) images of PNA–SWNTs. [36]
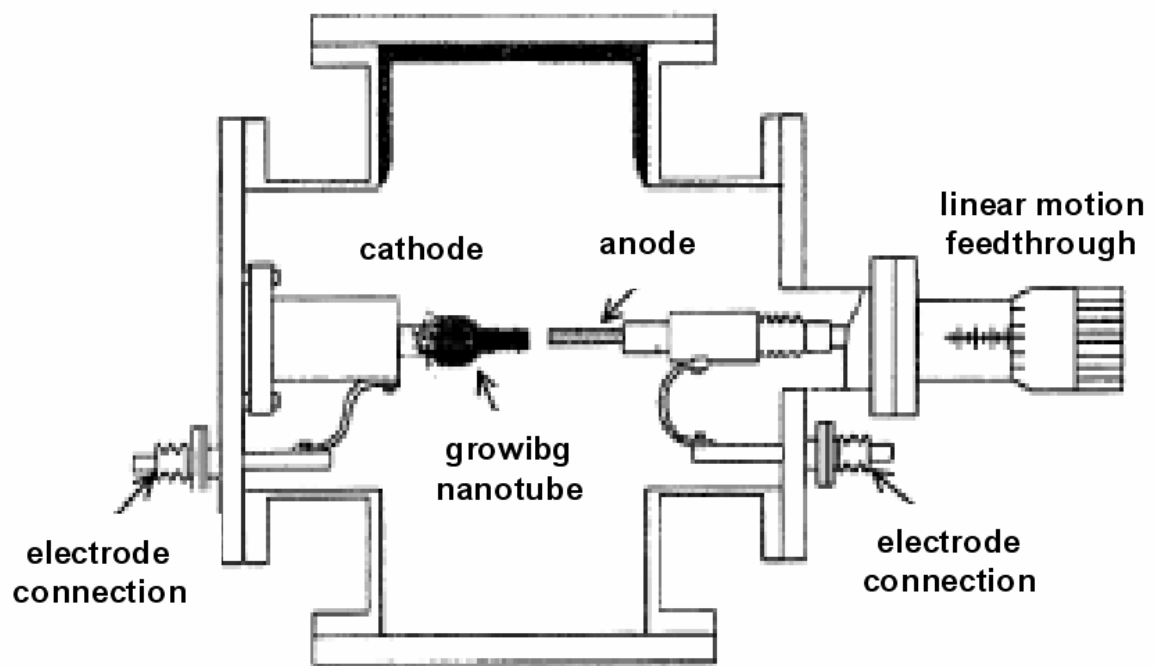
Fig. 2-36 Schematic illustration of the arc-discharge technique. [37]
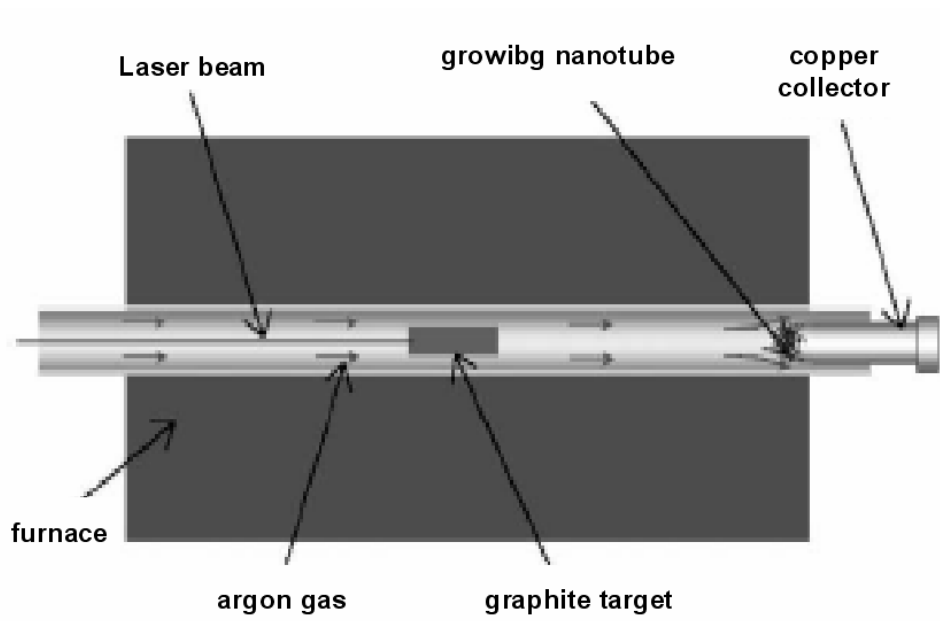
Fig. 2-37 Schematic of the laser ablation process. [37]
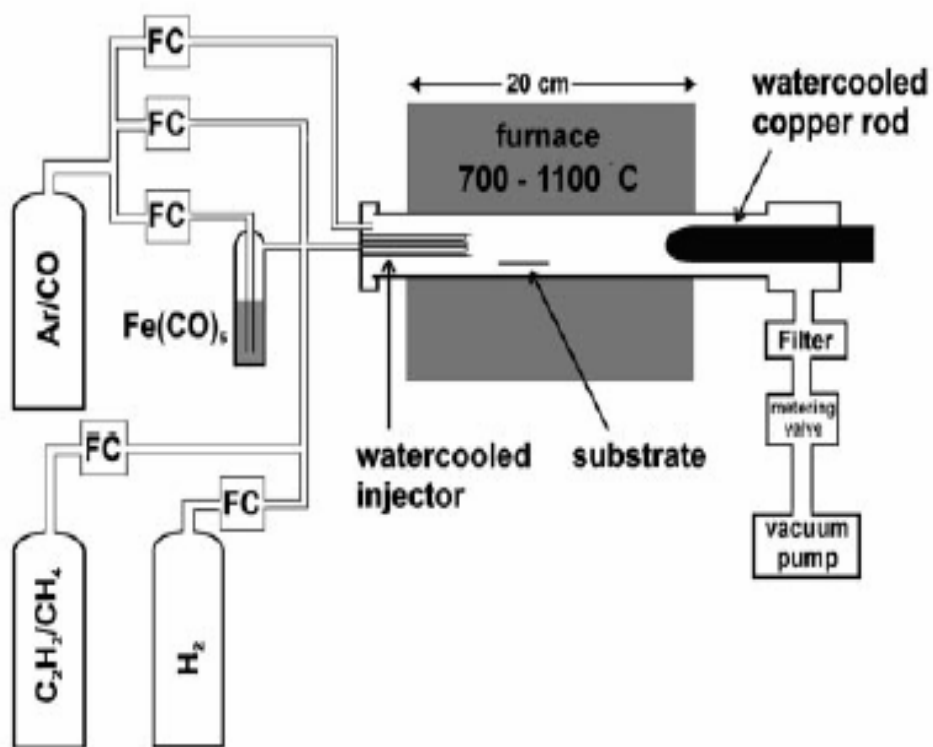
Fig. 2-38. The CVD production apparatus. [38]
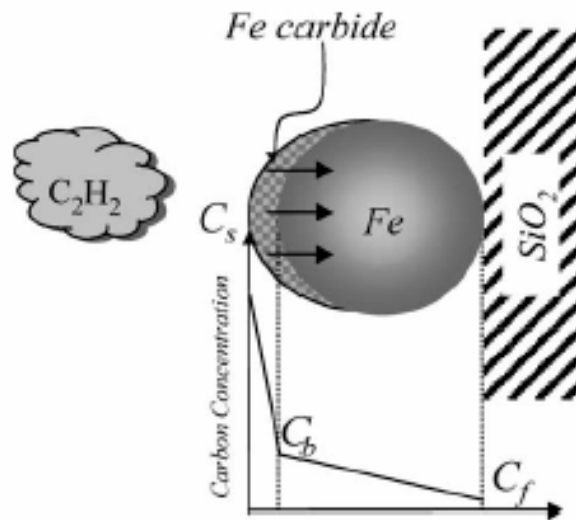
Fig. 2-39 Scheme with some parameters involved in the reaction kinetics of the growth mechanism of CNTs. [39]
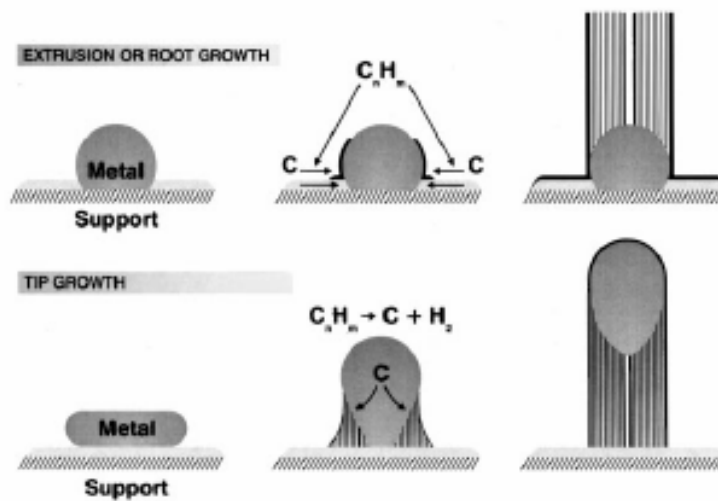
Fig. 2-40 Schematics of tip-growth and extrusion mechanisms for carbon filament growth after Baker and Harris. [40]

Chapter 3 Experimental apparatus and procedures

3.1 Experimental procedures

In the experiment, the primary design is reveal in Fig.3-1.
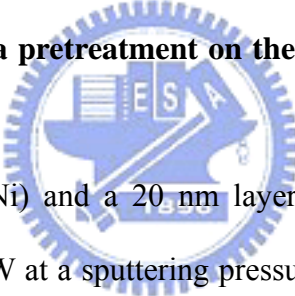
(a) Characterization of carbon nanotubes density through Ni nanoparticle formation using hydrogen plasma treatment on the TiN buffer layer and nanoindentation:

The substrates used in the experiments were 6-inch p-type (100) orientated silicon wafers and cleaned using RCA cleaning procedures in order to remove chemical impurities and particles. A 7 nm layer of nickel and a 20 nm layer of tantalum nitride were deposited with a power of 800 watt at a sputtering pressure of 6.4 mTorr (0.85 Pa). A 915 MHz microwave chemical vapor deposition (MPCVD) system was used to grow CNTs. The base pressure of the system was less than 2×10^{-3} torr. During the deposition of CNTs, the substrates were heated using a graphite heater. The nickel-coated substrates were first pretreated with hydrogen plasma at 550°C for 3, 5, 10 and 15 minutes, respectively. The pretreatment process is also illustrated in Fig.3-2.

The catalyst particles were examined by field-emission scanning electron microscopy (FE-SEM), atomic force microscopy (AFM) and high-resolution transmission electron microscopy (HR-TEM). Also, the catalyst particles on the substrate surface were indented using a nanoindentation tester (MTS NanoIndenter XP System), a device for measuring the displacements and loads during indentation and the Young's modulus and hardness. The indent was prepared by moving the indentation positions in arrays using the stage-scan function of the nano-indentation tester with the Berkovich indenter (tip radius ~50 nm), the loadings and unloadings were performed with an

approximately constant rate of 0.0166 mNs^{-1}. In MPCVD system, the substrate heated directly by a resistively heated graphite stage. The substrate temperature was measured using a thermocouple attached directly to the upper surface of the stage. Gas flow rates were controlled independently using mass flow controllers. After nickel-coated catalysts were pretreated for 3, 5, 10 and 15 minutes, respectively, hydrogen (90 sccm) and methane (10 sccm) flowed into the chamber at 550°C for 10 minutes (The flow unit sccm means standard cubic centimeter per minute). The total pressure in the chamber was kept at 20 Torr. The resulting CNTs were characterized by FE-SEM, TEM, and Raman spectroscopy.

(b) Effects of hydrogen plasma pretreatment on the TaN buffer layer for growth of carbon nanotubes:

A 7 nm layer of nickel (Ni) and a 20 nm layer of tantalum nitride (TaN) were deposited with a power of 800 W at a sputtering pressure of 6.4 mTorr. MPCVD system was used to grow CNTs. The base pressure of the system was less than $2x10^{-3}$ Torr. During the growth of CNTs, the substrates were heated using a graphite heater. The Ni-coated substrates were first pretreated with hydrogen plasma at 550 °C for 10 min with various H_2 flow ratio (100, 200 and 300 sccm). Ni nanoparticles were examined by SEM and HR-TEM. In MPCVD system, the substrate heated directly by a resistively heated graphite stage. The substrate temperature was measured using a thermocouple attached directly to the upper surface of the stage. Gas flow rates were controlled independently using mass flow controllers. H_2 (90 sccm) and CH_4 (10 sccm) gases flowed into the chamber at 550 °C for 10 min. Prior to CNTs growth the catalyst films

were pretreated in H_2 plasma for 10 min to promote the formation of catalyst particles and elemental Ni. The synthesis process is illustrated in Fig.3-3. The total pressure in the chamber was kept at 20 Torr while the gas flow rates were increased from 100 to 300 sccm. Synthesizing of aligned CNTs was investigated by using SEM, TEM techniques. In addition, Raman spectroscopy (Raman spectroscopy equipped, Condensed matter sciences (CCMS) in National Taiwan University (NTU)) with a change coupled device detector (Nd-YAG laser), operating at a wavelength of 532 nm and a power of 100 mW was employed in our experiment.

(c) Effects of fluorocarbon/oxygen plasma post-treatment on the surface performance of multiwalled carbon nanotubes:

A 7 nm layer of nickel and a 20 nm layer of titanium nitride were deposited with a microwave power of 800 W at a sputtering pressure of 6.4 mTorr. MPECVD system was used to grow the CNTs. The nickel catalysts were formed on titanium nitride/Si substrates. The base pressure of the system was less than 2 mTorr. During the deposition of CNTs, the substrates were heated using a graphite heater. The nickel-coated substrates were first pretreated with hydrogen plasma at 550°C for 10 min with hydrogen gas flow (200 sccm). After pretreated was finished, hydrogen (80 sccm) and methane (20 sccm) were flowed into the chamber at 550°C for 10 minutes. And, the surface characteristics on both of fluorination and oxidation are promoted by mixture of fluorocarbon and oxygen (CF_4/O_2) as the reaction gases (at 20 Torr for 2 and 10 min).

FE-SEM and HR-TEM were used to characterize the morphology and microstructures of CNTs. Fourier transform infrared spectroscopy (FTIR, ASTeX

PDS-17 System), thermal desorption atmospheric pressure ionization mass spectrometry (TDS-APIMS) and, X-ray photoelectron spectroscopy (XPS, VG Scientific Microlab 310F) was used to explore the changes in the chemical components of CNTs under various stages of CF_4/O_2 post-plasma treatment, as illustrated in Fig.3-4.

In addition, the as-grown and the plasma treated CNTs were studied with Raman spectroscopy by means of a Jobin Yvon micro-Raman LabRam system in a backscattering geometry. A 632.8 nm He-Ne laser was used as the light source and the power of the laser was adjusted by optical filters (Raman spectroscopy equipped, Department of materials science and engineering at NCTU)

. By using a 100× objective les, the illuminated spot on the CNTs samples was focused to approximately 2 μm in diameter. The resolution of the Raman spectra was 1 cm^{-1} with the typical acquisition time of 30 sec.
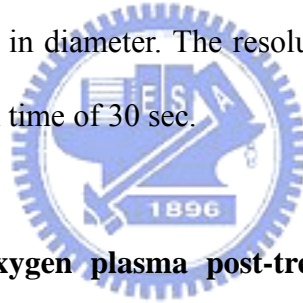
(d) Effect of fluorocarbon/oxygen plasma post-treatment on the lateral carbon nanotubes:

The wafers were cleaned by the standard procedures for removing the chemical impurities and particles on surface. The layer structure was prepared by stacking Ti-Ni-TiN-SiO$_2$ layers on Si substrate. Though process steps varied according to the electrode structures, the basic sequences of experiment process are as follows:

(i) The SiO$_2$ layer was grown on the p-Si (100) wafer by a wet oxidation process at 1100°C.

(ii) The stacking layer on the Ta electrodes, catalyst, and TiN buffer layer were deposited by sputtering using argon plasma.

(iii) The selected region follow patterned by photolithography and plasma etching. The spacing of the two electrode pattern was 1 μm. The top Ta electrodes layer is introduced as a barrier layer for vertical growth, covering the top of the Ni catalytic layer.

(iv) The CVD chamber temperature was steadily raised to the process temperature of 750 °C within 10 min in atmosphere. During the synthesis of CNT, the total flow rate of process gases was maintained at 200 sccm. For instance, the flow rate of the hydrocarbon source, C_2H_4 (ethylene), was 10 sccm and the remaining 190 sccm was hydrogen gases. After the CNT synthesis, the chamber was purged continuously with a mixture of N_2 until the chamber temperature reached room temperature, as illustrated in Fig.3-5 (a).

(v) We subsequently exposed the CNT to 20 sec of CF_4/O_2 gas (200 sccm) treatment at 20 Torr pressure. FE-SEM, AFM was used to characterize the morphology and microstructures of CNT. The surface performance of CNT was investigated by XPS. The devices were measured using standard dc techniques with a semiconductor parameter analyzer (HP-4156B).The process is simple illustrated in Fig.3-5 (b).

(e) Characteristics of indentation on carbon nanotubes films:

The Ni layer (70Å) was deposited as catalyst, and then grown CNTs using Thermal CVD at 600°C and 15 minutes. The reaction gases were CH_4, C_2H_4, N_2, and H_2, and flow rates were 200, 10, 500, and 500 sccm, respectively. The resulting morphologies were investigated by SEM. CNTs were subjected to nanoindentation, using a Nanoindenter with a Berkovitch indenter, on the top and side of the CNTs films, loads are increasing by 50, 100, 300, 500 mN, respectively. The crystallization was measured by Raman spectrum (Raman spectroscopy equipped, Department of materials science and

engineering at NCTU). The valuation of quality of CNTs was characterized using Gaussian curves fitting in order to obtain the I_D/I_G ratio. The Nanoindenter with a Berkovitch indenter process is also simple illustrated in Fig.3-6.

3.2 Deposition system

(a) Physical vapor deposition (sputtering) system

The system can provide the buffer layer of thin film deposition, such as TiN or TaN and Ni metal layer.

(b) Micro wave plasma chemical vapor deposition (MPCVD) system

A 915 MHz micro wave plasma chemical vapor deposition (MPCVD) system was used to pretreatment and grow CNTs. The nickel catalysts were formed metal substrates.

(b)Thermal chemical vapor deposition (Thermal CVD) system

Thermal CVD system was used to grow lateral CNTs.
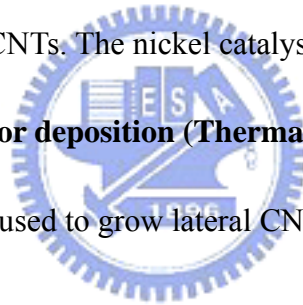
3.3 Measurement System

(a) Scanning electron microscopy (SEM)

Scanning electron microscopy (SEM, Hitachi S-4000) was utilized to observe the, lengths, diameters, density and the morphologies of the CNTs arrays.

(b) Atomic force microscope (AFM)

Digital Instruments DI 5000 were utilized to observe the particles size, diameters, density and the morphologies of the catalysts after pretreatment.

(c) Raman spectroscopy

Raman's spectrum in the highest vibration of balanced location promptly, and offer the information between the crystallization and atom band.

(d) High-Resolution transmission electron microscopy (HR-TEM)

High resolution transmission electron microscope (JEM-2010F) at 300 kV was utilized to discover the microstructural analysis of the CNTs.

(e) An energy dispersive X-Ray (EDX)

An EDX analyzer was used to investigate the composition if Fe-Ni surface before and after plasma post treatment

(f) Fourier transform infrared spectroscopy (FTIR, ASTeX PDS-17 System)

FTIR analyzer was used to explore the changes in the chemical components of CNTs under various stages of post-plasma treatment.

(g)Thermal desorption atmospheric pressure ionization mass spectrometry (TDS-APIMS)

TDS analyzer was used to measurement the changes in the chemical components.

(h) X-ray photoelectron spectroscopy (XPS, VG Scientific Microlab 310F)

XPS analyzer was used to measurement the chemical bonding.

(i) I-V system: Semiconductor parameter analyzer (HP-4156B).

I-V system was used to measurement thelateral CNT device.
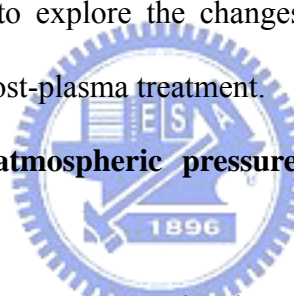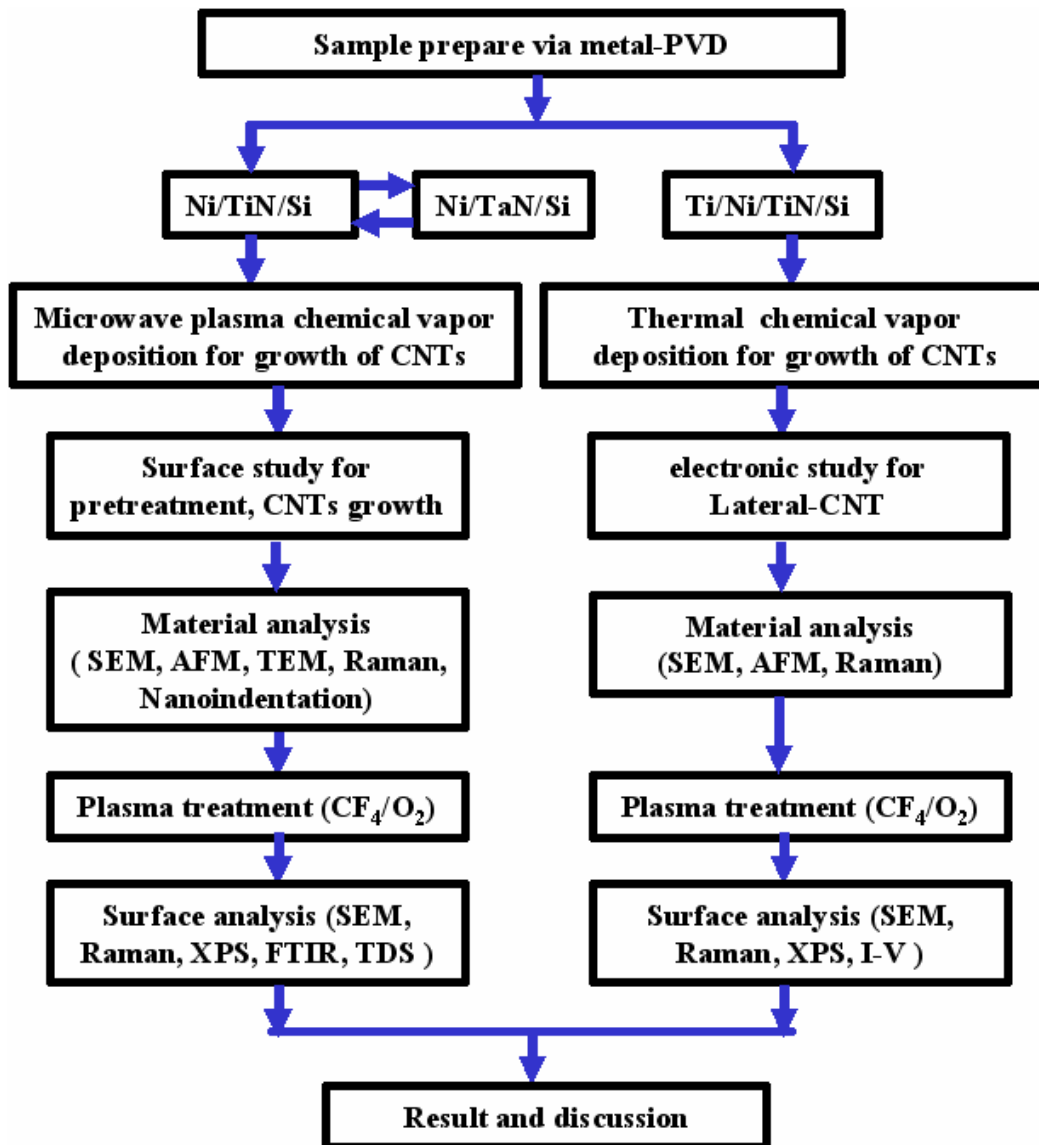
Fig.3-1. The primary experimental design
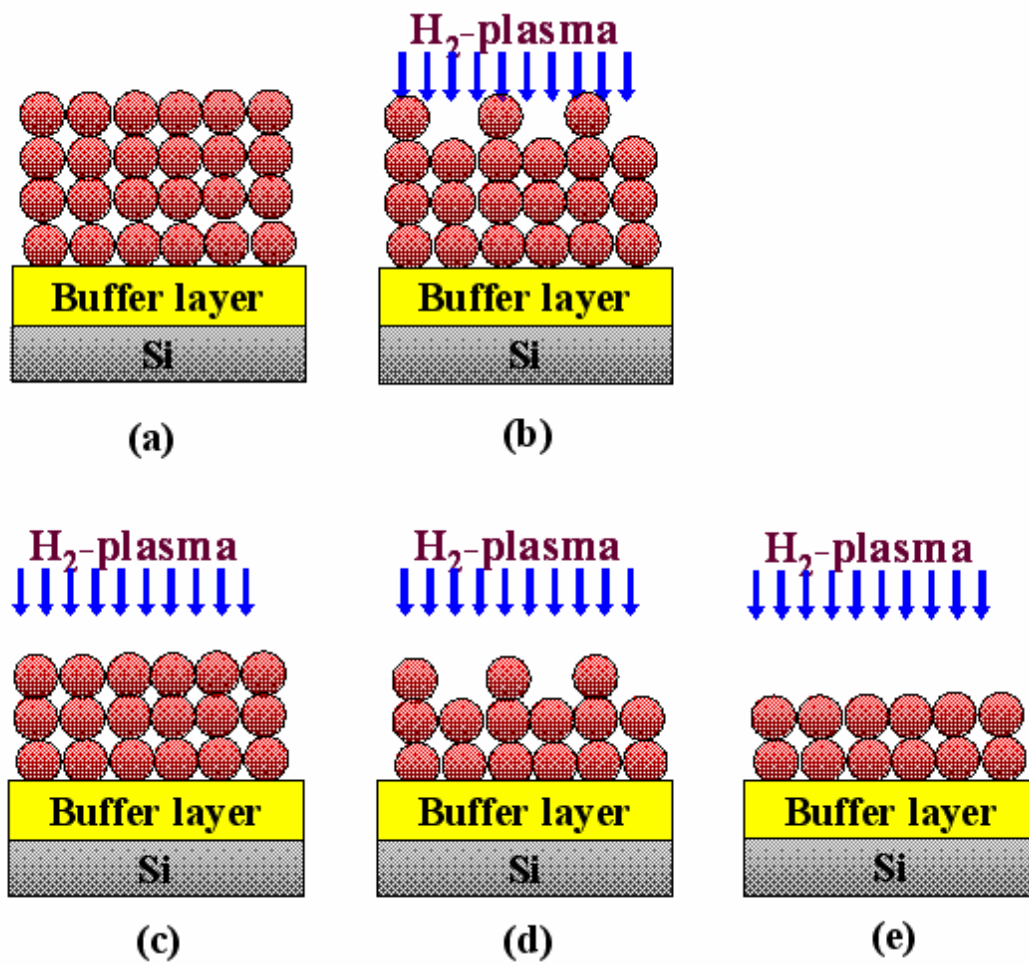
Fig.3-2 The nickel-coated substrates via pretreatment process with hydrogen plasma.
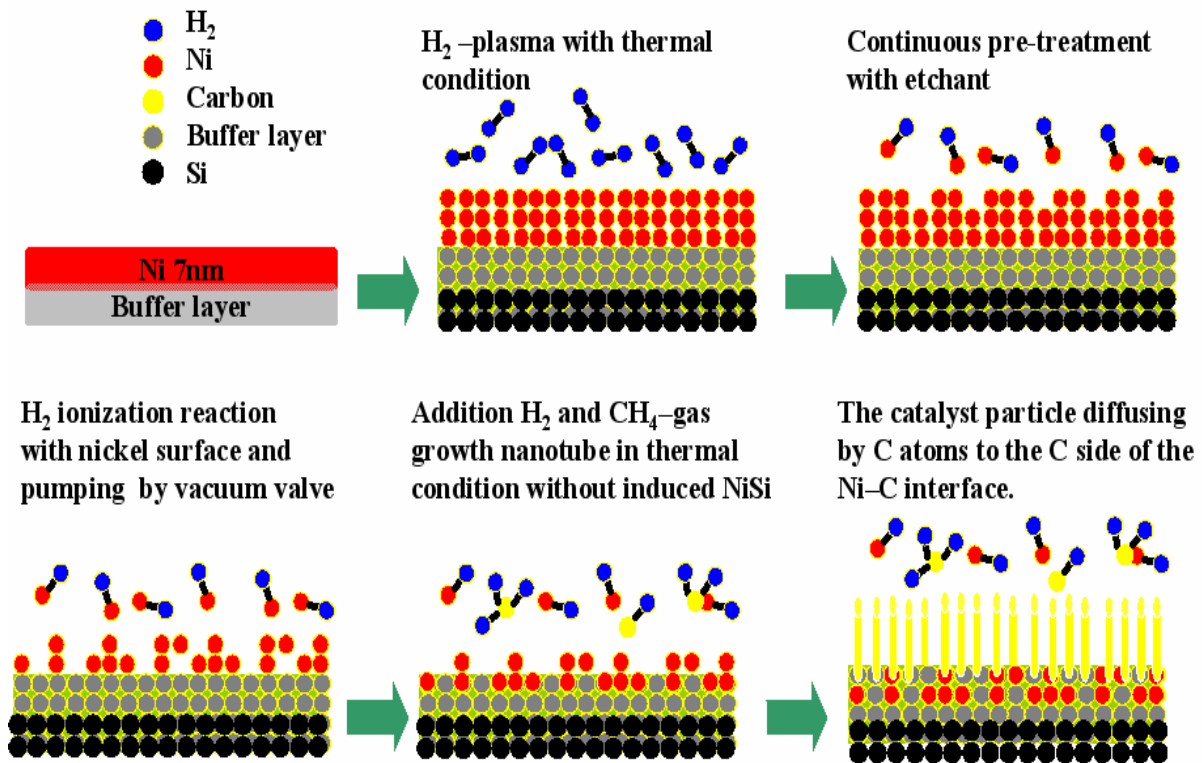
Fig.3-3 The CNTs growth from catalyst films were pretreated in H_2 plasma to promote the formation of catalyst particles and elemental Ni.
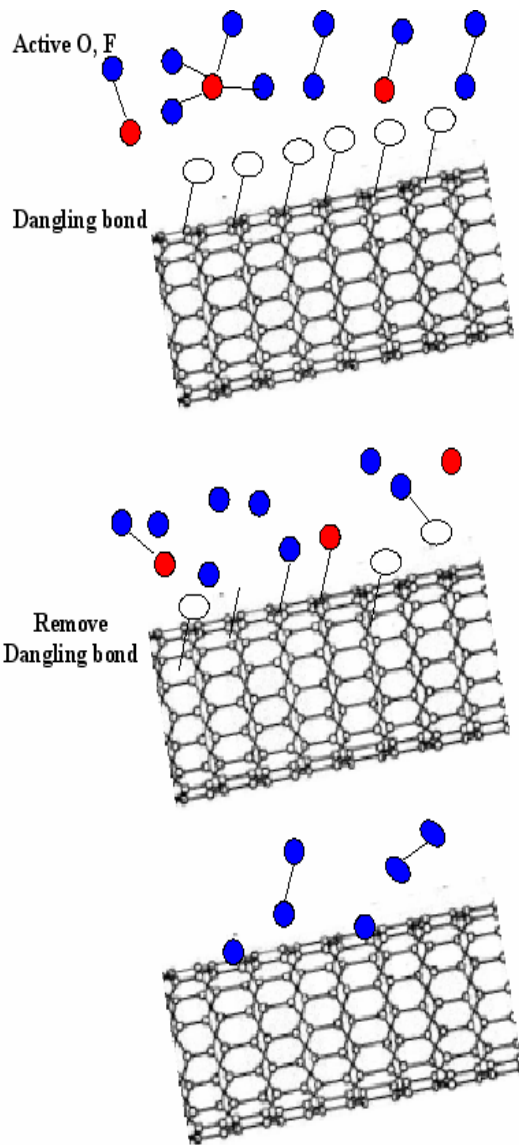
Fig.3-4 The changes in the chemical components of CNTs under various stages of CF_4/O_2 post-plasma treatment.

(a)
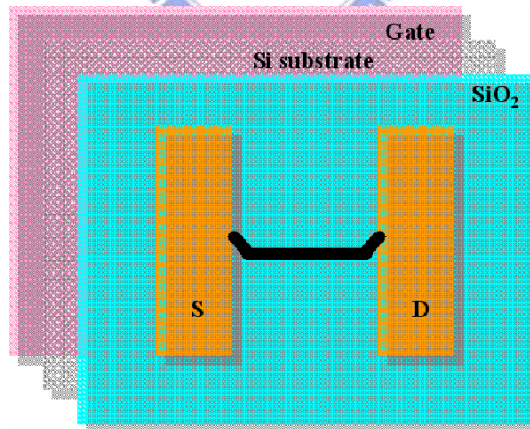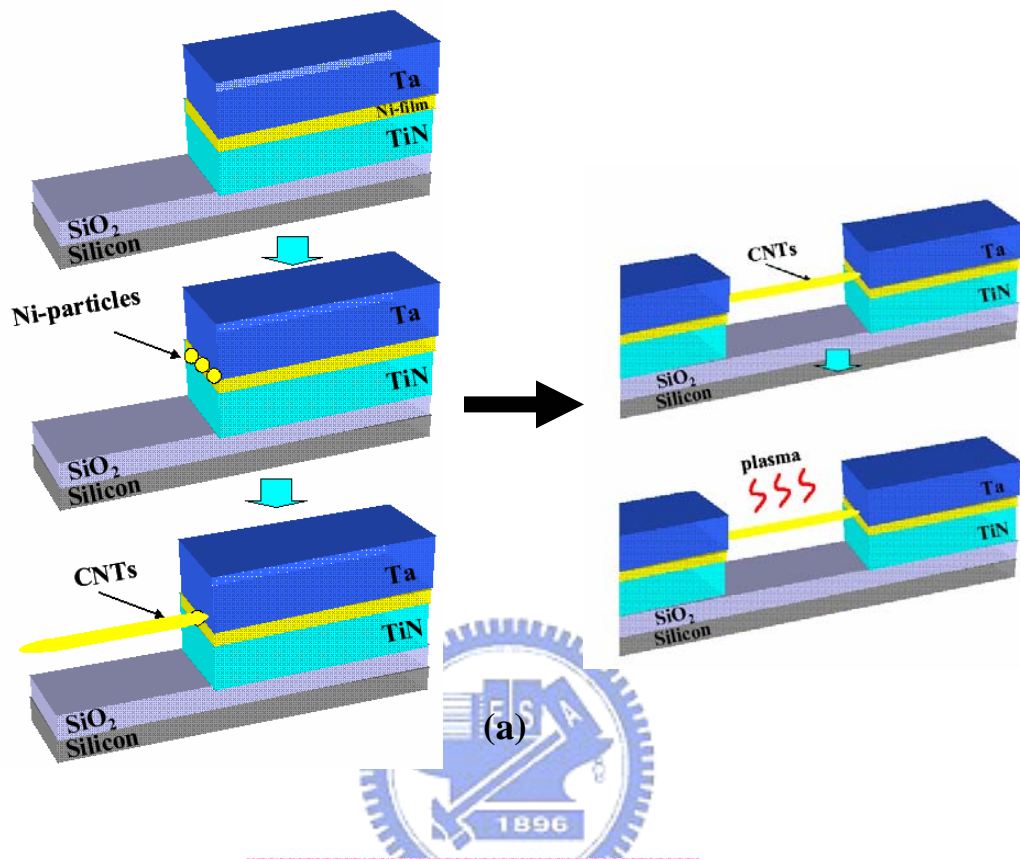
(b)

Fig.3-5 (a) The layer structure was prepared by stacking Ta-Ni-TiN-SiO$_2$ layers on Si substrate. (b) The design is simple illustrated.
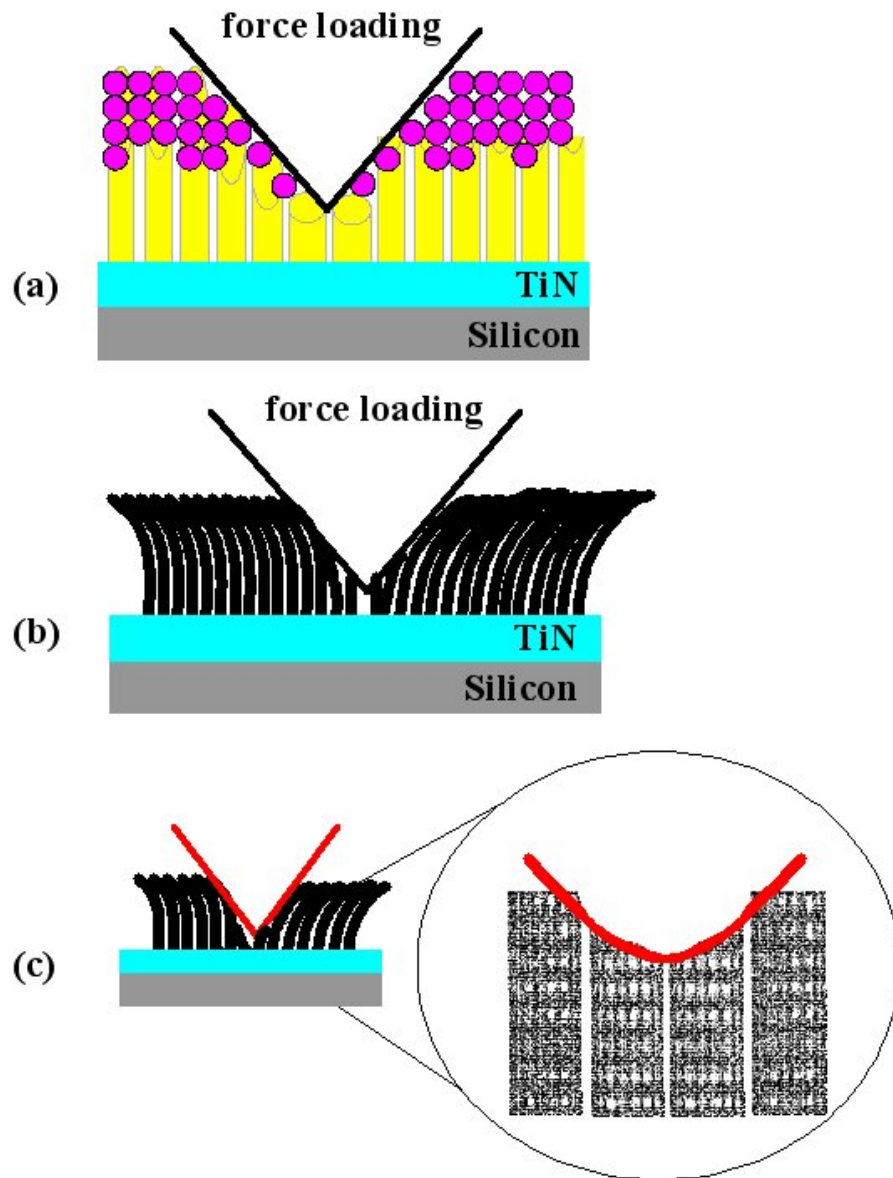
Fig.3-6 The Nanoindenter with a Berkovitch indenter process.

Chapter 4 Primary Result

4.1 Characterization of carbon nanotubes density through Ni nanoparticle formation using hydrogen plasma treatment on the TiN buffer layer and nanoindentation

4.1.1 Introduction

Carbon nanotube (CNT) is the most important material [41], exhibit unique electronic and extraordinary mechanical properties. The control of such structure has technical significance in the sense that the structural diversity leads to different electronic, mechanical and other physical properties. These useful properties of CNTs make themselves good candidates for various application fields, such as a transistor [42, 43], sensor [44], field emission display [45-46], nanoscale interconnects [47]. The growth is in these cases usually achieved by means of catalytical chemical vapor deposition (CVD) with high purity, high yield CNTs for practical application. Thus, it was found that the CNTs would only be deposited under specific pretreatment conditions before CNTs growth [48~53]. Therefore, in order to avoid an undesired metal silicide formation at high temperature, the buffer layer was proposed in annealing process [54~56].

In the recent, some materials such as thin film [57~61], nanocomposite [62], CNTs [63], and nanoparticle [64] were measured using indenter technology with loaded in axial compression. It should be emphasized that special care is required when measuring the mechanical response of particle aggregates or thin films deposited on substrates, the tension, bending, vibration, and compression experiments can strongly contribute to the overall mechanical response of the film/substrate system. When dealing with metal nanoparticles from the pretreatment behaviors of the agglomerates mechanism to the substrate becomes an aim of issue for nanoindentation. In this cause, the resolution to measure directly the interparticle forces in the nanometer regime is lacked. Nevertheless, the relationship between both of the interparticle forces on metal particles and the effect of the grown CNTs is not yet being exposed in detail. In this chapter, we synthesized CNTs with a microwave plasma chemical vapor deposition (MPCVD) system on Ni/TiN/Si substrate. The effect of pretreatment of Ni catalyst layer on growing characteristic and properties of CNTs according to the pretreatment of period process was investigated. It is suggested that the surface performances of catalyst can be modified by hydrogen plasma [57]. Therefore, small agglomerates of catalyst nanoparticles were formed on TiN buffer substrates. The aid of focused is find out the relatively large particles mechanical property of pretreated nanoparticles, in the nanometer range. The

deformation behavior of the agglomerates under loads control-mode of nanoindentation

technique was studied.

4.1.2 Results and discussion

4.1.2.1 Catalysts pretreatment

Layers of Ni were not only etched, but also conglomerated, by hydrogen plasma

treatment at 3 minutes from SEM observation (Fig. 4-1 (a)). Above 5 minutes, the

conglomeration effect dominates so the heating and plasma power transform the film of

Ni catalysts film into large Ni particles (Fig. 4-1 (b)). The size and distribution of Ni

nanoparticles varied with the pretreatment time. The average diameter of the Ni

nanoparticles declined at 10 minutes, because small Ni nanoparticles were removed and

large particles were shrunk by long etching (Fig. 4-1 (c)). Ni nanoparticles tend to melt

away and conglomerate with each other over 15 minutes (Fig. 4-1 (d)).

Fig. 4-2 presents the AFM analysis on surface etching associated with pretreatment.

The results were shown that the flat nickel layer is arrived at island-like of catalysts by

pretreatment (3, 5, 10, and 15 minutes). The intermediate TiN layer was to be used as a

diffusion barrier to prevent reaction between Ni and Si. In fact, nucleation also induces

the formation of islands on the buffer layer in the presence of hydrogen plasma. Tab. 4-1

summarized that the RMS surface roughness of the catalytic-layer changed from 6.1 to

11.9 nm, as the pretreatment time increased from 3 to 15 minutes. Therefore, the

nucleation and etching by heating and hydrogen plasma treatment are obvious. This

treatment contributes to the formation of particles, which act as seeds for nucleation in

the growth of CNTs.

Fig. 4-3 presents HRTEM images of the metal particles from 3 to 15 minutes. In

the pretreatment, the metal film was being melting due to heated by thermal and plasma.

It is show that the flat Ni layers arrive at island-like of catalysts and become a droplet

upon buffer layer (Fig. 4-3 (a)). Because of continue treatment with 5 minutes, a droplet

is defined by decreasing size between island-like of catalyst in thermal equilibrium on a

horizontal surface (Fig. 4-3 (b)). At 10 minutes pretreatment, the droplet became

smallest due to the suitable interfacial tension force on horizontal surface. The Ni

nanoparticles are seemed corresponds to perfect forming from a film (Fig. 4-3 (c)). Over

15 minutes, large nanoparticles were occurred by unequal interfacial tension force (Fig.

4-3 (d)). It is indicates that increasing the period of pretreatment increased the change in

volume of the metal clusters, and conic particles were formed by pretreatment.

4.1.2.2 Indentation of catalyst from pretreatment

Fig. 4-4 illustrated the pretreatment Ni/TiN/Si substrate to endure the Berkovich

indenter tip (tip radius ~50 nm) (a) before and (b) after. The loadings and unloadings

were performed with an approximately constant rate of 0.0166 mNs^{-1}. Fig. 4-5(a) shows

that before the indentations, the SEM images were performed us with images of the

agglomerates. Thus, compare with after indentation (see in Fig. 4-5(b)), it is obvious

that the Ni nanoparticles on the surface were identified by the Berkovich indenter tip

within the indents part in low load force (0.25 mN). Especially, from the inset figure,

the area of tip is almost 1 micrometer. These images were actually convolutions of the

true surface and the shape of the tip, and therefore, were of limited resolution. However,

the imprints of the tip are clearly visible. In contrast, the particles on the indented

surface became enlarged, such that Ni particles are formation also occurred on the TiN

surface.
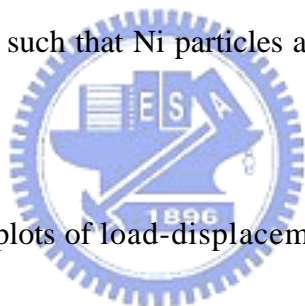
Fig. 4-6 reveals the plots of load-displacement curves for the (a) Ni/TiN/Si thin

film and (b) Ni particles/TiN/Si. From the Fig. 4-6(a), Ni/TiN was indented with

deformed material around the indents at low force. Based on the Fig. 4-6(b), the

particles were observed only inside the indented parts, thus lead the decreased in

modulus (from 238.9±8.4 to 176.2±6.1GPa) and hardness (from 17.2±1.6 to 11±0.8

GPa GPa) as compared in Tab. 4-2.

Fig. 4-7 shows the SEM image within the after Ni-coated catalyst were pretreated

for 3, 5, 10 and 15 minutes, hydrogen and methane (9:1) flowed into the chamber at

550°C for 10 minutes. The relationship among these conditions is presented in this

figure. CNTs were found variation of length, diameter, and morphology. Based on the pretreatment, the size of nanoparticle was depending on the increased pretreatment time (correspond in Fig. 4-1). Therefore, based on the constant grow time (10 minutes), it is induced that the CNTs have well aligned via 10 minutes pretreatment condition. It is believed that diffusion, nucleation and etching would occur during hydrogen plasma pretreatment and heating. The combined effects contribute to formation of nanoparticles with small spacing. These can act as the nucleation sites for growth of CNTs.

The crystal quality and structure of CNTs have been measured by Raman spectra according to the pretreatment condition. Fig. 4-8 shows Raman spectra of CNTs that were grown on the Ni/TiN systems. The Raman spectra of all samples show D-band peak and G-band peak around 1300 cm^{-1}, 1550 cm^{-1} respectively. The intensity increases according to increasing pretreatment time. The D and G-band correspond to sp^2 and sp^3 carbon stretching modes, relatively and their intensity ratio is a measure of the amount of disorder in the CNTs. The D-band has known to be attributed to the carbonaceous particles, defects in the curved graphitic sheet and tube ends. The intensity of D-band peak is higher than that of the G-band at all samples, and it indicates that there were many carbonaceous particles or clusters in the CNTs. The ratio of the intensities of the D-band and G-bands (I_D and I_G) was summarized in Fig. 4-9. The I_D to I_G ratio decrease indicating the effect of the sp^3 to sp^2 bonded carbon configuration. In case of

pretreatment, the ratio decrease according to pretreatment time, the I_D/I_G ratio is 0.90, 0.89, 0.86, and 0.96 respectively. This result shows that the increase of pretreatment time decrease the I_D/I_G ratio and the disorder of CNTs (correspond in Tab. 4-1), so it reduces amorphous carbon and carbonaceous particles in CNTs and this result is consistent with the SEM result.

Fig. 4-10 displays typical TEM image of the CNTs synthesized after hydrogen plasma pretreatment. TEM investigations reveal that the CNTs are not very straight at their root, their walls being corrugated. Particles at the CNTs root exhibit a faceted morphology. The CNTs associated to these particles exhibit outer diameter in the 50–80 nm range and inner diameter less than 30 nm. Particle size is considerably larger than the CNTs inner diameter and is often slightly larger than the CNTs outer diameter. Also, the critical value is related to the hydrogen plasma pretreatment, the CNTs quality also changes with the pretreatment and gas increases.
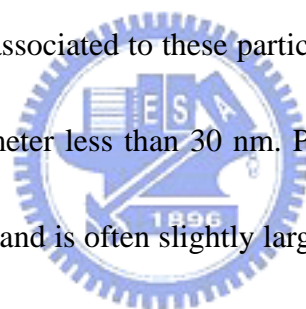
4.1.3 Conclusion

We have described the effect of pretreatment on the increasing time. From the SEM image of pretreated Ni catalyst layer, the increase time decrease the diameter of Ni catalyst grain size. The microstructure and properties of the pretreated Ni nanoparticles was characterized by in situ HR-TEM. The nanoindentation technique was used to study

the behavior of Ni nanoparticles. By the low load force testing, it is observed that the decreased in modulus (from 238.9 ± 8.4 to 176.2 ± 6.1GPa) and hardness (from 17.2 ± 1.6 to 11 ± 0.8 GPa) compared with the Ni film. Also, the density and vertical alignment of CNTs could be controlled by adjusting the density of nickel nanoparticles. From the Raman characterization indicates that the increase of pretreatment time decrease the I_D/I_G ratio and the disorder of CNTs, therefore, it indicates reducing amorphous carbon and carbonaceous particles in CNTs.

4.2 Effects of hydrogen plasma pretreatment on the TaN buffer layer for growth of carbon nanotubes

4.2.1 Introduction

The CNT undoubtedly occupies a unique position among advanced materials because of its novel electrical, mechanical and chemical characterizations [65,68]. These useful properties of CNTs make themselves good candidates for various application fields, such as the field-effect transistor [68], sensor [69], field emission display [45,70] and nanoscale interconnects [71]. CNTs can be synthesized by a variety of techniques, such as arc discharge, laser ablation, plasma-enhanced and thermal chemical vapor depositions (CVDs) [72~75]. While the former two techniques are suitable for large-scale production of CNTs, they cannot be used for self-assembly on material surfaces. CNTs synthesized by CVD are known to be longer than those obtained by other processes. It is possible to grow dense arrays of aligned CNTs by CVD [76] as well. Therefore, CVD is one of the prominent methods to synthesize high purity, high yield CNTs for practical applications.

Meanwhile, the control of CNT structure has technical advantage in the

sense that the structural diversity leads to different electronic and mechanical characterizations. There have been several attempts to control the structure of CNTs by various methods, including the pretreatment of the metal films on which CNTs are grown [77] and the direct control of structure by varying synthesis parameters [78]. In particular, the plasma etching can be used to transform a catalytic layer into catalytic nanoparticles, which may be applied to the density control of CNTs. In addition, however, in order to avoid the formation of metal silicide at a high temperature, a buffer layer was adopted in the annealing process [54].
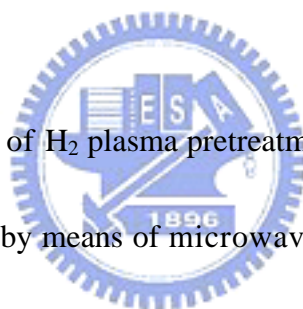
Herein, the effects of H_2 plasma pretreatment flow rate on the synthesis of CNTs on a Ni/TaN/Si substrate by means of microwave plasma chemical vapor deposition (MPCVD) system are investigated. The structure and composition of Ni catalyst nanoparticles are investigated using scanning electron microscopy (SEM) and transmission electron microscopy (TEM). Raman spectroscopy equipped with a change coupled device detector is used to study the effect of the flow rate on the intensity ratio of G and D bands (I_D/I_G), which in turn measures the amounts of the amorphous carbon and carbonaceous particles in the CNT.

4.2.2 Results and discussion

The synthesis of CNTs by CVD often involves three mainly steps: first, decomposition of hydrocarbon gas at the surface of the catalyst nanoparticles; then, diffusion of resultant carbon atom in the nanoparticles to form the nucleation seed; and finally, precipitation of carbon atoms at the nanoparticles interface to form CNTs. It is well known and often proposed that the size and chemical composition of metal nanoparticles determine the diameter and structural perfection of the CNT [79].

Ni catalyst metal layers transformed into nanoparticles after various H_2 plasma pretreatment flow rates are illustrated in Fig.4-11. From this figure, it is clearly observed that higher H_2 plasma pretreatment flow rates leads to denser Ni catalyst nanoparticles. With the treatment of etching by H_2 plasma, it can be found that the Ni catalyst metal layers breaks into small islands. From SEM observations, it is confirmed that the H_2 plasma pretreatment plays an important role in promoting the uniform formation of Ni nanoparticles. The particle sizes of Ni catalyst metal layers treated by H_2 plasma etching are approximately 20-30 nm, which are displayed in the cross-sectional TEM images in Fig.4-12. It is interesting to note that the geometries of the Ni catalyst particles were obviously affected by the H_2 plasma pretreatment flow rate. As shown in Fig.4-11, at the flow rates of 100 sccm and 200 sccm the Ni catalyst particles have broad-based shapes, while at the flow rate of 300 sccm the Ni catalyst

particle has a semicircle-like one. Such a morphology difference is not surprising to be

noticed because at a higher flow rate, the atoms in the catalyst particle can move around

more easily via H_2 plasma etching than at a lower flow rate. In the plasma environment,

the H_2 plasma plays a role in reducing Ni nanoparticles like the results proposed in Ref.

80. These observations also indicate that the geometry of a large catalyst particle can be

reshaped more easily at a higher flow rate for the CNT nucleation and growth.

Fig.4-13 shows the cross-sectional SEM images of the CNTs grown at the

synthesis flow rates 100, 200 and 300 sccm, respectively. It can be seen that amorphous

carbon and carbonaceous particles were decreased and denser vertically-aligned CNTs

were displayed at a higher flow rate, as shown in Fig.4-13. In addition, the CNTs shown

in Fig.4-13(c) were 30-40 nm in diameter and several micrometers in length. From this

observation, the ability of Ni catalyst particles to change their shape can also explain

why in the present experiment the highest density of CNTs was synthesized at the flow

rate of 300 sccm.

The structure of CNTs, which is obtained from the Ni catalyst particles treated by

H_2 plasma at the flow rate of 300 sccm, is displayed in Fig.4-14. An embryonic Ni

catalyst particle is formed in the course of H_2 plasma pretreatment because of the

difference of the interfacial energies between Ni catalyst particle/substrate and Ni

catalyst particle/gas, with its catalytic decomposition of CH_4 to liberate carbon atoms.

The change of elastic energy and surface energy of carbon layer caused the radius of curvature of Ni catalyst particle to become small. Then the rising gradient of the surface energy enhanced the surface diffusion of carbon atoms from bottom to top of the Ni catalyst particles. Therefore, significantly, a spindle-shaped Ni catalyst particle exists within the CNTs. The details of CNTs growth mechanisms can be found elsewhere [81]. In addition, the TEM image reveals that there are well-graphitized layer and the direction of graphite basal planes is parallel to the tube axis, as illustrated in Fig.4-14.

Raman spectroscopy (Raman spectroscopy equipped, CCMS in NTU) has been used to investigate the vibrational characterizations of the carbon samples. Raman spectra of CNTs obtained at H_2 plasma pretreatment flow rates of 100, 200 and 300 sccm, respectively, are illustrated in Fig.4-15. All of Raman spectra display two broad bands at 1330 cm^{-1} (D-band) and 1580 cm^{-1} (G-band), respectively. The D-band is associated with the vibrations of carbon atoms with dangling bonds in plane terminations of "disordered graphite" or glassy carbons. The G-band corresponds to the E_{2g} mode of graphite and, is related to the vibration of sp^2-bonded carbon atoms in the two dimensional hexagonal lattice of the graphite layer. In addition, G-band indicates the degree of crystallinity in the graphite structure, while the intensity of D-band represents the impurities, defects or lattice distortions in CNTs.

In 2000, Ferrari *et al*. [82] proposed that the intensity ratio of G and D bands (I_D/I_G)

is related to the sp^2 carbon cluster sizes in the graphene sheet and is nearly proportional to the defect density. The I_D/I_G ratio is 0.96, 0.92 and 0.84 of H_2 plasma pretreatment flow rates of 100, 200 and 300 sccm, respectively, which is shown in Fig.4-16. This shows that a lower degree of structural disorder exists after the CNTs were H_2 plasma pretreated. Results indicated that I_D/I_G ratio is decreased with increasing the flow rate. Further from the analysis of Raman spectra, we observed that the higher flow rate induces the amorphization of lattice and formation of defects in CNTs, indicating that the decrease of the degree of disorder in CNTs and this result is consistent with the SEM observations.

4.2.3 Conclusions

To summarize, we have combined SEM, Raman and TEM techniques to investigate the effects of H_2 plasma pretreatment flow rate on the synthesis of CNTs. We synthesized CNTs by using MPCVD system on Ni/TaN/Si substrates. From SEM observations, higher flow rates leads to denser Ni catalyst nanoparticles. Furthermore, the results of Raman spectra and TEM indicate that the morphologies of CNTs transform from amorphous carbon to crystalline graphite structure or finite sized graphite structure, depending on the H_2 plasma pretreatment flow rate. A decrease in the number of defects and optimized morphologies therefore is believed to play a

significant role in the improvement in the field emission characterizations observed in

the future.

4.3 Effects of fluorocarbon/oxygen plasma post-treatment on the surface performance of multiwalled carbon nanotubes

4.3.1 Introduction

CNTs have attracted tremendous interest from fundamental and technological aspects this last decade since their discovery in 1991 because of their special physical and chemical characteristics [83]. It is well-known that the multiwalled carbon nanotubes (MWCNTs) have mechanical characterizations quite different from those of single-waled carbon nanotubes (SWCNTs) [84~86]. These differences are reflected in either their macroscopic material characterizations or their processing and handling behaviors or both. Also, MWCNTs have been investigated widely on their electrical transport characterizations as the most promising material for nanoelectronics [87~88]. The electrical transport characterizations of MWCNTs are exported to depend on their structures such as multiplicity, chirality, and so on.

Among various methods (such as arc discharge, laser ablation and chemical vapor deposition) developed to grow CNTs, plasma-enhanced chemical vapor deposition (PECVD) methods are attracting great interest because of their specificities, such as vertical alignment of CNTs production, well-patterned nanotubes and relativity low

synthesis temperature [89]. To go further on the control of CNTs structure, an understanding of the growth mechanisms of CNTs is needed but it has not been clearly provided yet. The roles of various gases as precursors for applying the synthesis of CNTs have been presented [79, 90], but we have not fully understood the effects of each gas on the post-treatment of CNTs. In our previously study [91], the effects of ammonia plasma treatment on the surface characteristics of carbon fibers was analyzed during the plasma treatment procedure, but never, at the best of our knowledge, the role of fluorocarbon/oxygen plasma treatment in the characteristics of CNTs by PECVD.

The aim of this chapter is to present the results obtained with the CNTs grown by PECVD method via CF_4/O_2 plasma post-treatment. The structures of formed CNTs were characterized by using scanning electron microscopy (SEM) and transmission electron microscopy (TEM). CNTs were analyzed by Raman spectroscopy, Fourier transform infrared spectroscopy (FTIR), thermal desorption atmospheric pressure ionization mass spectrometry (TDS-APIMS) and X-ray photoelectron spectroscopy (XPS), as well.

4.3.2 Results and discussion

Fig.4-17 shows the SEM images of CNTs before and after CF_4/O_2 plasma treatment. Fig.4-17 (a) reveals that CNTs grown by PECVD have natural form and the length of CNTs was larger than 7 µm. Fig.4-17 (b) and 1(c) show that after 2 and 10

mins of CF$_4$/O$_2$ plasma treatment on surface of CNTs, respectively. From the image, it is

very obvious that there are many amorphous carbon particles on the surface of CNTs at

an appropriate plasma post-treatment, as illustrated in Fig.4-17(b). On the contrary, the

structural damage significantly of CNTs occurs at the longer plasma treatment time, as

displayed in Fig.4-17(c). Therefore, we suggest that the surface density of aligned CNTs

becomes reduced because of the formation of CNT bundles with an appropriate CF$_4$/O$_2$

plasma post-treatment time, in part, which helps to decrease screening effects between

adjacent emission sites resulting in larger emission currents[96]. The details of CF$_4$/O$_2$

post-plasma treatment on CNTs are discussed the following TEM and micro-Raman

studies.
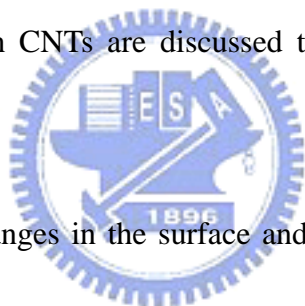
To examine any changes in the surface and/or structural characterizations via the

plasma treatment, we perform TEM results in Fig.2 which show TEM images of the

structural variation in CNTs occurring before and after CF$_4$/O$_2$ plasma treatment,

respectively. Fig.4-18(a) shows a TEM image of as-grown CNT used in this experiment.

Fig.4-18(b) and 4-18 (c) are TEM images of the CNTs structure at the CF$_4$/O$_2$ plasma

post-treatment time of 2 and 10 mins, respectively. After plasma treatment, the surface

topography of CNTs changed significantly and, amorphous structure and the

amorphous-crystalline interfaces are also observable. This change may be owing to the

defect generated on CNTs walls having partly weak structure. Nevertheless, the longer

the CF_4/O_2 plasma post-treatment time the more CNTs structure serious destroyed is.

Raman spectra (Raman spectroscopy equipped, MSE at NCTU) in the 1250-1650 cm^{-1} region for the as-grown CNTs, CF_4/O_2 plasma post-treatment time of 2 and 10 mins with a 632.8 nm laser wavelength excitation are illustrated in Fig.4-19, respectively. The two main features in the Raman spectra are the D and G peaks at approximately 1330 cm^{-1} and 1600 cm^{-1}, respectively. The G band corresponds to the symmetric E_{2g} vibrational mode in graphite-like materials, while the appearance of the strong D band can be interpreted as being owing to [94]: (i) the turbostratic structure of carbon sheet in tubes, namely the finite size nanometer-scale order of the crystalline domains and, (ii) the high density of the twisty tubes. Therefore, the enhancement of D bands at approximately 1330 cm^{-1} accounts for the large amount of crystalline domains on the nanometer-scale.

In addition, Ferrari and Robertson [84] proposed that the intensity ratio of I_D/I_G is related to the sp^2 carbon cluster sizes in the graphite sheet and is nearly proportional to defect density. We calculated the intensity of the D band to that of G band, as illustrated in Fig.4-20. Results indicated that the I_D/I_G ratios of the samples, which are 0.88, 0.86 and 0.94 for as-grown CNTs and, CF_4/O_2 plasma post-treatment time of 2 and 10 mins, respectively; reveals that the chemical treatment decreases the degree of disorder at longer plasma treated time. Because of its disorder origin, the D band is useful in

characterizing the defect density in CNT samples. The increase of I_D/I_G with the slightly appearance of non-crystalline subpeaks implies that the degree of disorder in CNTs increased with longer plasma treatment. Based on the results of TEM and Raman spectra, we propose that the longer plasma treatment caused the number of defects and the amorphous carbon, resulting in the collapse of crystalline graphite shells of MWCNT walls. Further, from the relatively intensity of both non-treated and CF_4/O_2 plasma post-treatment time of 2 min, it could be interpreted that the overall crystalline quality of the non-treated CNTs is lower than that of CF_4/O_2 plasma post-treatment time of 2 min on CNTs [95]. According to the above-mentioned results, it may be possible to get improved the field emission properties of CNT via an appropriate CF_4/O_2 plasma post-treatment in the future.
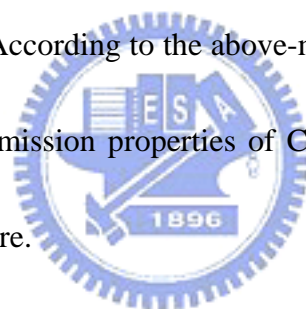
The FTIR absorption spectra of as-grown CNTs and the various CF_4/O_2 plasma post-treatment times on CNTs are illustrated in Fig.4-21. Therefore, at the CF_4/O_2 plasma post-treatment that can induce the number of binding on the surface, such as the peak at 1068-1088 cm^{-1} is attributed to C-O stretching vibration and other peak at 1233 is attributed to C-F stretching vibration. In addition, the TDS results indicate that the adsorption information on CNTs. The desorbed O and F gas phase (molecular weight value are 16 and 19) are observed at 277.5 °C for CNTs at the CF_4/O_2 plasma post-treatment time of 2 min, as shown in Fig.4-22(a). Comparing, there is higher F

desorbed are observed at 427 °C for CNTs at the CF_4/O_2 plasma post-treatment time of 10 min, as shown in Fig.4-22(b). This is probably the cause of increased chemical bond in CNTs by longer plasma treatment time, resulting in the adsorption capability.

The XPS measurements of as-grown CNTs and, 2 and 10 mins CF_4/O_2 plasma post-treated CNTs are shown in Fig.4-23(a), (b) and (c), respectively. From Fig.4-23(a), it can be seen that the intensity of C 1s peak reduces manifestly and two peaks near 286.7 eV and 291-292 eV are observed in C 1s spectra after CF_4/O_2 plasma treatment, which are attributed to C-F and C-F_2 binding [96]. Also, in Fig.4-23(b), two F 1s peaks appear near 689 eV from the original noise spectra of as-grown CNTs. Therefore, all these demonstrate that fluorine has chemically bonded into CNTs. In Fig.4-23(c), the analysis of O 1s spectra indicates that the concentration of oxygen-containing species on the CNTs increased significantly because of the CF_4/O_2 plasma post-treatment. From the XPS spectra, we observe that oxygen has been adsorbed on CNTs during the CF_4/O_2 plasma treatment process. Thereby, we can reasonably deduce that the fluorine atoms are decomposed by the reaction of oxygen and CF_4 and, further the plasma treated efficiency of CNTs surface is promoted; meanwhile, the amount of fluorine and oxygen atoms are also increased. That is, a no appreciable variation of oxygen physisorbed on CNTs (always present on the CNTs surface owing to samples exposure to atmosphere via CF_4/O_2 plasma post-treatment), which, as already pointed out, does not give

significantly contribution on C 1s spectra.

4.3.3 Conclusion

In summary, we have successfully demonstrated that the effects of CF_4/O_2 plasma post-treatment on surface performance of MWCNTs by SEM, TEM, Raman, FTIR, TDS and XPS analyses. SEM and TEM studies reveal changes in surface morphologies of CNTs exposed to the CF_4/O_2 plasma post-treatment. Moreover, I_D/I_G ratios indicate that the chemical treatment decreases the degree of disorder via CF_4/O_2 plasma post-treatment time of 2 min. On the contrary, the degree of disorder is increased in CNTs at 10 min CF_4/O_2 plasma post-treated. FTIR absorption spectra show the peak with C-O, C-F stretching vibration; in addition, TDS results indicate that the adsorption information on the CNTs at the various CF_4/O_2 plasma post-treatment times. XPS data reveals the fluorination in the CF_4/O_2 plasma treated CNTs and a no appreciable variation of oxygen physisorbed on CNTs, suggesting that the decomposed efficiency is promoted by adding the oxygen in the plasma.

4.4 Effect of fluorocarbon/oxygen plasma post-treatment on the lateral carbon nanotubes

4.4.1 Introduction

CNTs have attracted great attention due to their scientific interest and potential applications of technological importance [97~98]. To realize the commercialization of CNT-based nanoelectronic and optoelectronic devices, the development of a fabrication process of catalytic chemical vapor deposition (CCVD) growth of CNTs across electrodes is required [99~101]. However, to achieve the CNTs bridges device, there is particular interest in the electronic properties of CNTs for the nanoelectronic applications [102]. Furthermore, the controlled of the CNT bridges in length, linearity, and density by adjusting various synthetic process parameters was demonstrated [103]. Thus, some other device such as field-effect transistors [43,104], lateral emitters [45,46], sensor [44], and nanointerconnection [47] were proposed. Therefore, CNTs have been expected to be a promising candidate for next-generation electronics, and applied to nano-scale novel electronic devices and logic circuits.

The growth CNT owing to the presence of nitrogen was demonstrated [105]. The

CNT also play a crucial role in the domain of field emission [106], biosensor device [107]. In contrast, research on the surface properties of post-treatment on the lateral CNT has not drawn equal attention. So far, the measurements of the characterizations of CNT on a surface adsorption and the correlation with the microstructures are very important in recognizing their electrical behaviors.

In this chapter, we report the CNT on given substrates with precise control over the location and orientation in a lateral from thermal CVD. The CNT was further ex situ treated by CF_4/O_2 plasma, the relation of the surface formation and the characteristic is discussed. It is suggested that the surface performances can be modified by CF_4/O_2 plasma.

4.4.2. Results and Discussion

4.4.2.1 SEM and AFM

The Ta, as the upper layer on Ni pads, not only plays a role as a barrier to prevent vertical growth but also serves as a buffer site that helps in forming smaller nano-sized Ni particles. Fig. 4-24(a) reveals that CNT grown by thermal CVD have lateral form between both of the two metal-pads. Fig. 4-24(b) reveals that lateral CNT treated by CF_4/O_2 plasma have broken form between both of the two metal-pads. Fig. 4-25(a) is showed that the AFM image of CNT in the lateral growth was confirmed. Fig. 4-25(b) is

showed that the AFM section image of the grown CNT have multiwalled graphite in the structure. The CNT with outer diameter range is over 71.5 nm and consists of hollow compartments can be applied to selective lateral component in our experiment. Furthermore, the CNT is clearly perpendicular to the edges of the electrodes. From the image, it is very obvious that there is the lateral CNT on the surface of electrodes.

4.4.2.2 XPS spectra

The adsorption of CF_4/O_2 post-treatment has been checked by ex situ XPS. Fig. 4-26(a) and (b) correspond to the XPS spectrum curve of the as-CNT and the post-treated CNT sample, respectively. The XPS spectrum was presented non-peak of As-CNT example. Post-treated CNT shows the survey spectrum provides the fluorine concentration on the surface whereas the narrow scan spectrum of the F1s line gives the distribution by the corresponding components on the spectral graph. The fluorine are considered to react with the surface carbon layer of nanotubes if chemical bond formation, as illustrated in Fig. 4-27(a). As the treatments time increased, the surface chemical bonding were detected as CF^*-CF_2 (692 eV) functional group of the CNTs surface from 20s plasma treated, as illustrated in Fig. 4-27(b). This is because the fluorinated in the CNTs induce chemical shifts due to their inductive effects, resulting in prominent features in the F1s-XPS spectra. This peak identified as C-F component

correlated with the increase in the fluorine on the CNTs surface

4.4.2.3 I-V analysis

In order to examine the transport properties of the CNTs bridges across the trench, Fig. 4-28(a) shows their I-V characteristics for both non-treated and the post-treated CNT sample taken at room temperature. They show typical properties of Schottky contact characteristics at room temperature.

Fig. 4-28(b) is shows the middle CF_4/O_2 plasma post-treated at 20s have the improvement in current come through both of the electrode. Compared the both of the current-voltage from -10 to 10 V with a step of 200 mV, it shows in overall a nonlinear I-V relations, signifying nonohmic contact between CNT on SiO_2. This is in agreement with the proposed statement that the bridges may behave a metal-semiconductor junction because of defects parts and cause nonlinear electron transport characteristics. At appropriate plasma post-treatment, the structural damage significant of CNTs occurs at the shorter plasma treatment time. Therefore, we suggest that the lateral CNT becomes reduced because of the formation of CNT bundles with an appropriate CF_4/O_2 plasma post-treatment time, in part, which helps to decrease amorphous carbon between the each site of electrodes.

4.4.3. Conclusion

We have described a method for synthesizing a CNT bridge on a SiO_2 patterned by

a photolithography process. The CNT grow laterally to the substrate by a TiN vertical

growth barrier and connect to the side electrode pad. The CNT show the electrical

property appears at relatively higher current-voltage by the CF_4/O_2 post-treated due to

the surface modified.   The excited species within the plasma interacted with the

surface of the CNT breaking the C-C bonds and creating active sites for bonding of

functional groups. Furthermore, the CNT is clearly perpendicular to the edges of the

electrodes. From the image, it is very obvious that there is the lateral CNT on the

surface of electrodes. Thus, depending on the parameters used, it is possible to reduce

the amorphous carbon that the C-F binding used in the modification of CNT.
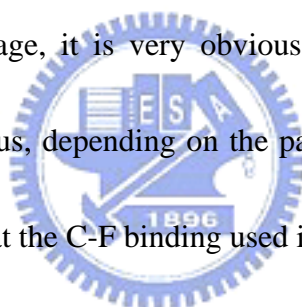
4.5 Characteristics of indentation on carbon nanotubes films

4.5.1 Introduction

The discovery of CNTs has sparked considerable interest in their use as reinforcements in various matrix materials to impart stiffness, strength, and toughness. Novel mechanical tests on individual CNTs [108-109] in polymer matrices and atomistic calculations [110~112] attestation that CNTs have high elastic moduli, approaching 1 TPa, and exceptional tensile strengths, in the range of 20-100 GPa. The transference of these properties into correspondingly good mechanical properties in actual composites depends on many other in situ features. Also, CNTs have attracted other applications such as electronic devices [113] sensors [117] due to their good electrical, and chemical properties owing to the high current density (109 Amps/cm^2) [114-115] and ballistic conductance [117]. CNTs play a crucial role in performance, reliability, stability, and reactive sites [116] in electron sources [118], for example, the flat panel displays device which prototypes have already been built [119]. The mastering of CNTs for composite applications passes by strength characterization studies that relate the dependence of indentation to the CNT surface.

In this chapter, CNTs were grown by thermal chemical vapor deposition (Thermal

CVD), subjected to nanoindentation, using a Nanoindenter with a Berkovitch indenter, on the top and side of the CNTs films, Loads between 50 and 500 mN were used. The quantitative indentation data is used to determine the multiwall CNT axial modulus, depending on the quality of Raman shift. The values of I_D/I_G ratio are increasing due to induced cracks on the CNTs films. The relation between the loading force and the intensity I_D/I_G ratio was studied

4.5.2 Results and discussion

Fig. 29 (a) ~ (d) shows the CNTs/Si surface structure was induced cracks using a Nanoindenter with a Berkovich indenter, on the top and side of the CNTs films, loads are increasing by 50, 300, 500 mN, respectively. By the high load force from 50 to 500, the more crack were performed at more indenter area on the surface the CNTs films, respectively.

In contrast, CNTs inside the indent holes were analyzed by Raman spectrum (Raman spectroscopy equipped, MSE at NCTU), this compare with various load forces on the CNTs films, as shown as Fig. 4-30. To verify the indentation-plane of CNTs films, the indent sections were used Raman spectra to identify the crack. In the other word, Raman shift have both sharp peaks in 1350 cm^{-1} (D-band) and 1596 cm^{-1} (G-band). This provided us the section area of both peaks for curves fitting. Thus, the loading force of

indenter on CNTs films are increasing from 50 to 500 mN, the Gaussian curves fitting were suggested (Fig. 4-31).

In contrast, the G-band and subpeaks (1550 to 1582 cm^{-1}) were observed at the indent positions (I_D/I_G ratio as illustrated in Fig. 4-32). This indicates that the CNTs films selectively broke with a Berkovich indenter, on the top and side of the CNTs films, variation of loads were used in the indented areas with good uniformity. In the unindented section, the flat CNTs films observed in other zone. The reason for the selectivity of the indented areas upon indentation to be demonstrated that CNTs films exhibit all of the features associated with toughening behavior in crack. Such features, in part because CNTs films have typically contained low volume fractions of highly disordered. Here, the damaged process was clearly observed by the Raman shift.
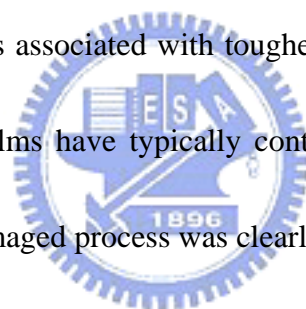
4.5.3 Conclusion

In summary, CNTs/SiO$_2$ was subjected to nanoindentation, using a Nanoindenter with a Berkovich indenter. This indicates that the CNTs films selectively broke with a Berkovich indenter, on the top and side of the CNTs films, loads from 50 to 500 mN were used in the uniform indented areas.

The quantitative indentation data is used to determine the CNTs films, depending

on the quality of Raman shift. The curves are fitting using Gaussian method for the

valuation of quality on CNTs. The values of I_D/I_G ratio are increasing due to induced

crack on the CNTs films. The relation between the loading force and the intensity I_D/I_G

ratio was pointed out the quality of CNTs can influence by the nanoindentation tester.

The reason for the selectivity of the indented areas upon indentation to be demonstrated

that CNTs films exhibit all of the features associated with toughening behavior.

Tab. 4.1 The summarized that the RMS surface roughness of the catalytic-layer changed from 6.1 to 11.9 nm, as the pretreatment time increased from 3 to 15 minutes.

Samples	A	B	C	D
Pre-treatment time (min)	3	5	10	15
RMS (nm)	6.1	8.8	8.4	11.9
I_D/I_G	0.90	0.89	0.86	0.96
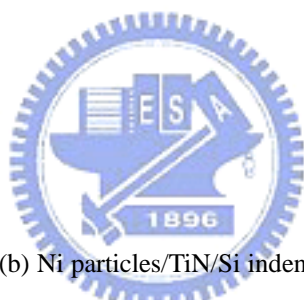
Tab. 4.2 (a) Ni/TiN/Si thin film and (b) Ni particles/TiN/Si indented with low force. The particles were observed only inside the indented parts, thus lead the decreased in modulus and hardness.

Samples	Load force(mN)	Modulus (Gpa)	Hardness (Gpa)
Ni film/TiN	0.25	238.9±8.4	17.2±1.6
Ni particles/TiN	0.25	176.2±6.1	11±0.8

(a)

1 um

100 nm

(b)

1 um

100 nm

(c)

1 um

100 nm

(*continue*)

104

(d)

1 um

100 nm
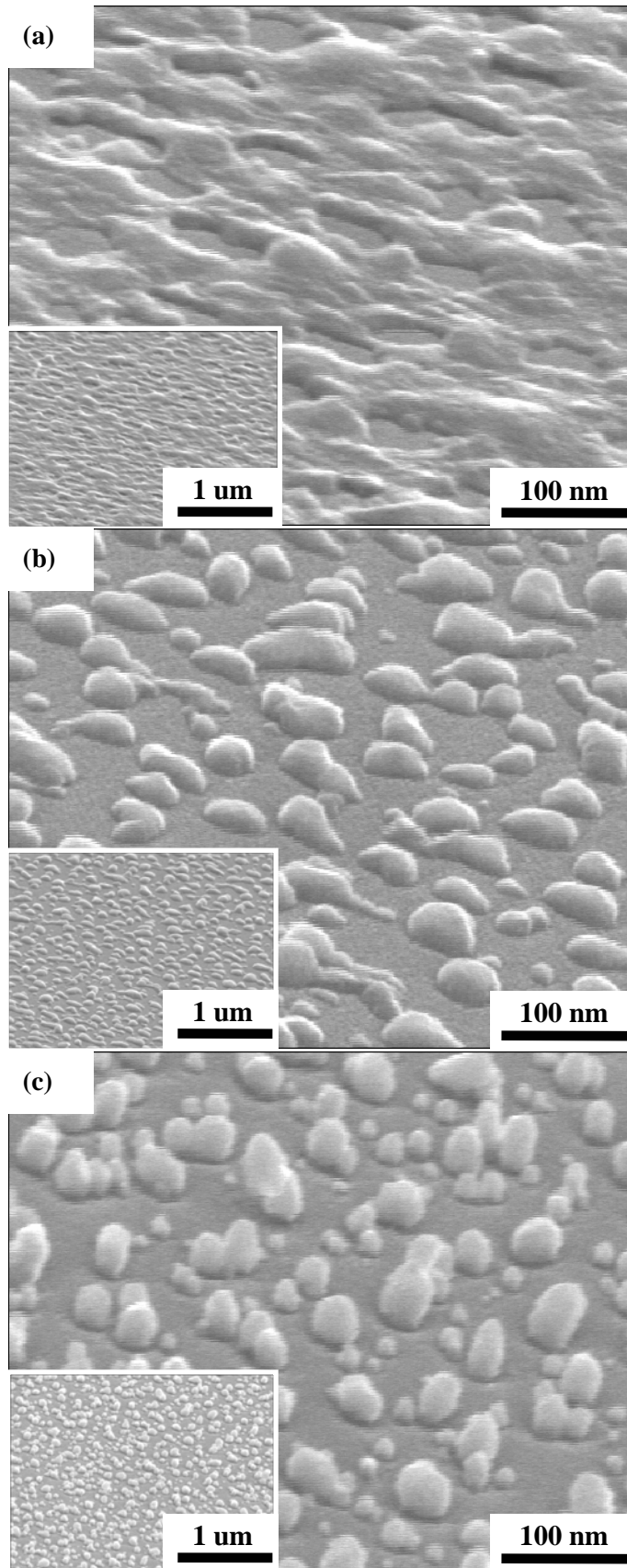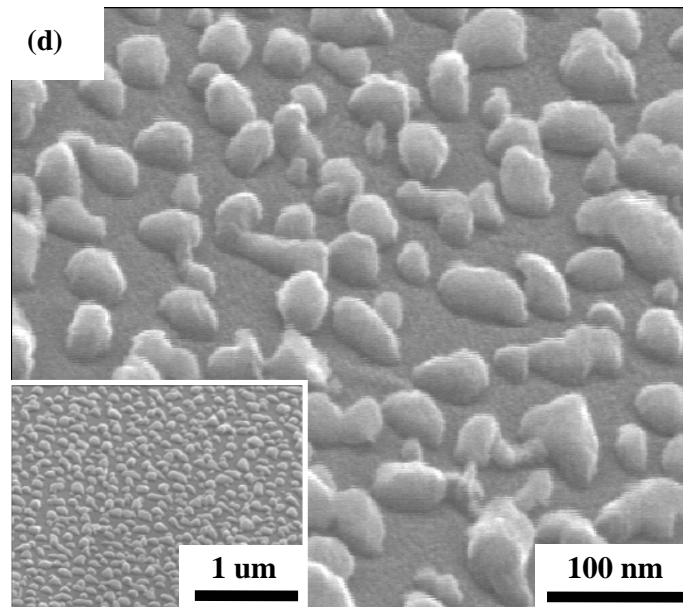
Fig. 4.1 Nickel catalysts layer pretreatment at various time (a) 3, (b) 5, (c) 10, and (d) 15 minutes. Nickel catalysts layer not only etched but also conglomerated by hydrogen plasma treatment.
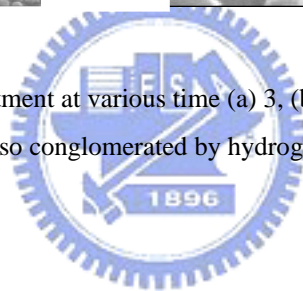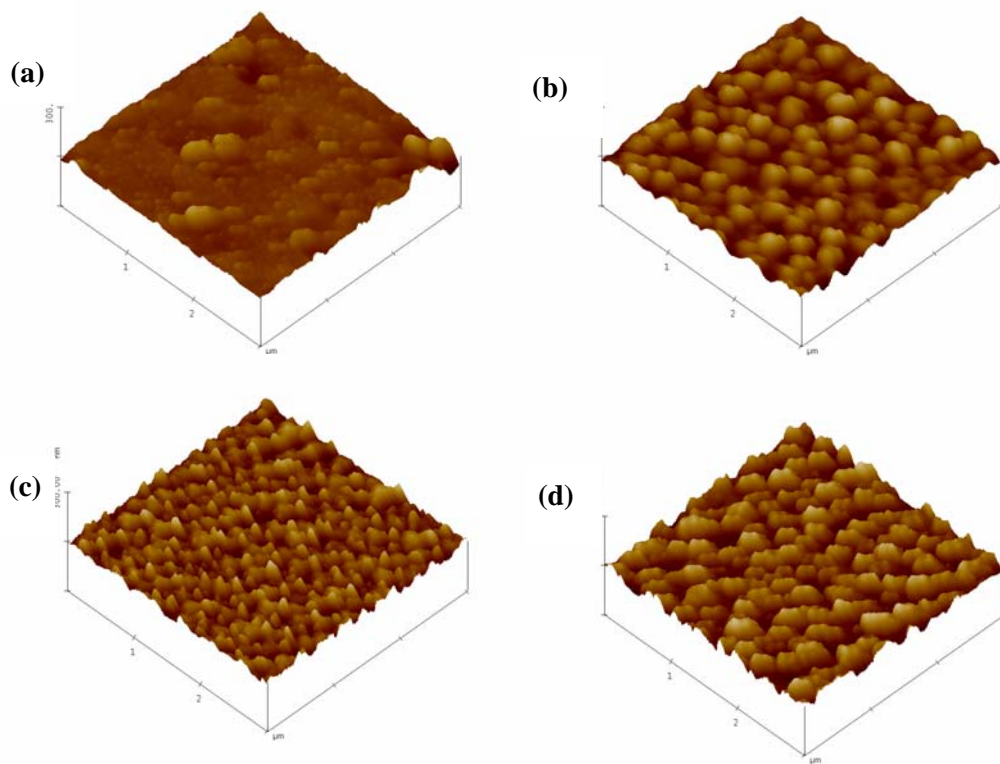
Fig. 4.2 Nickel catalysts surface etching was performed at various time (a) 3, (b) 5, (c) 10, and (d) 15 minutes. The flat nickel layers arriving at island with pretreatment process.

(a)

20 nm

(b)

20 nm

(c)

20 nm

(*continue*)

(d)

20 nm
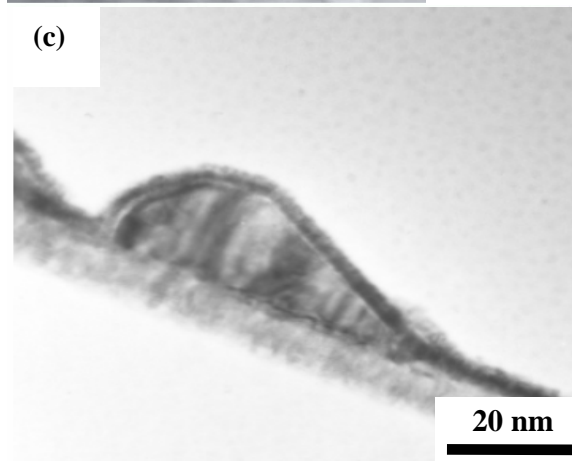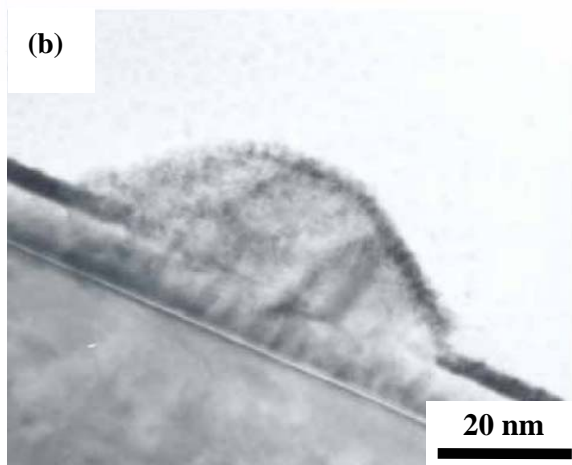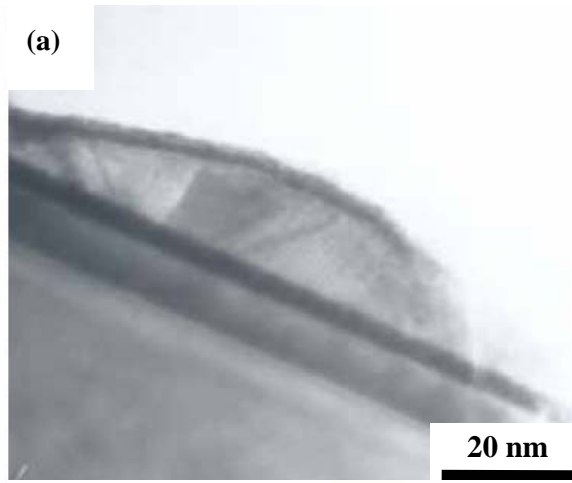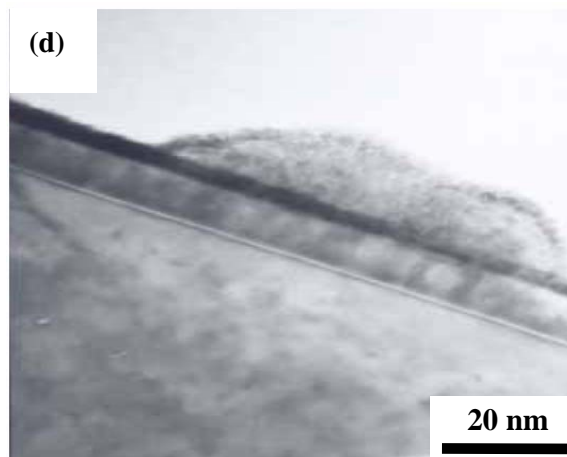
Fig. 4.3 Nickel catalysts surface etching was performed at various time (a) 3, (b) 5, (c) 10, and (d) 15 minutes.
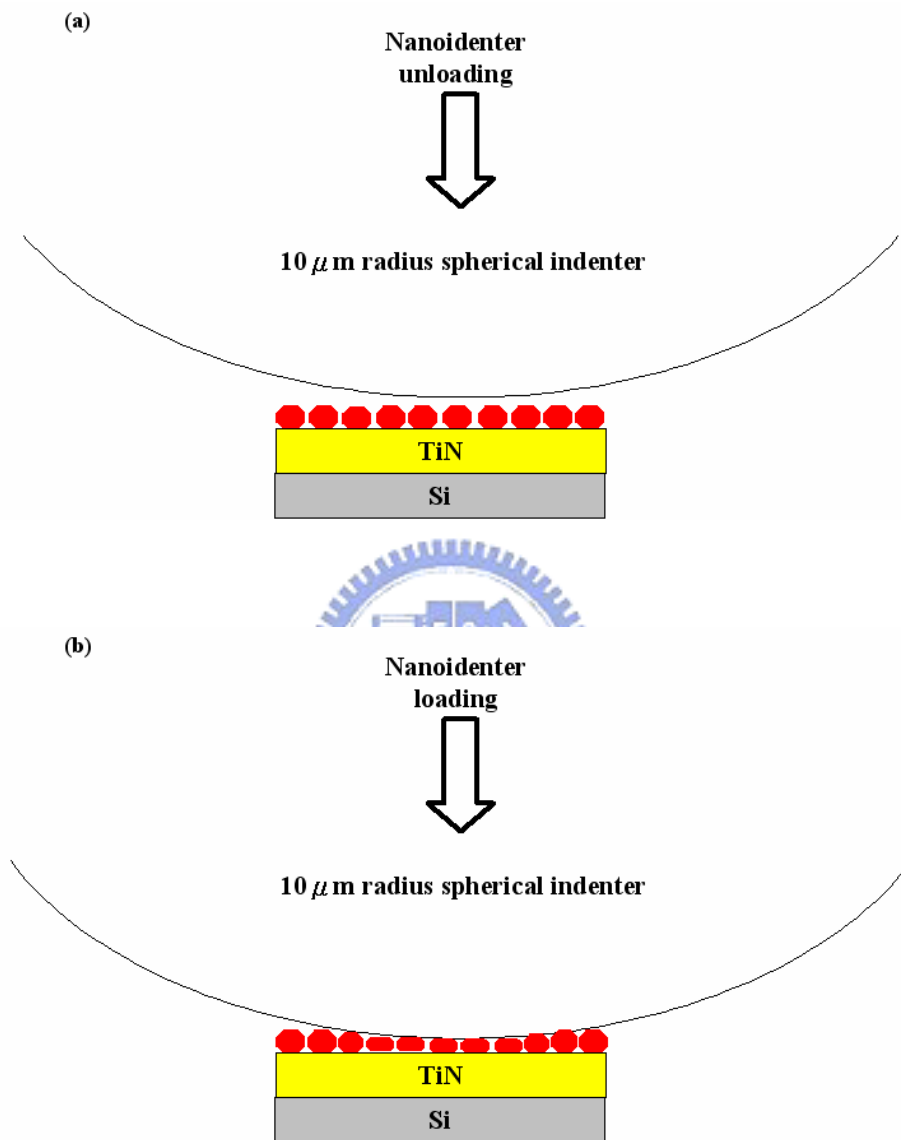
Fig. 4.4 The pretreatment Ni/TiN/Si substrate to endure the Berkovich indenter tip (a) before and (b) after.
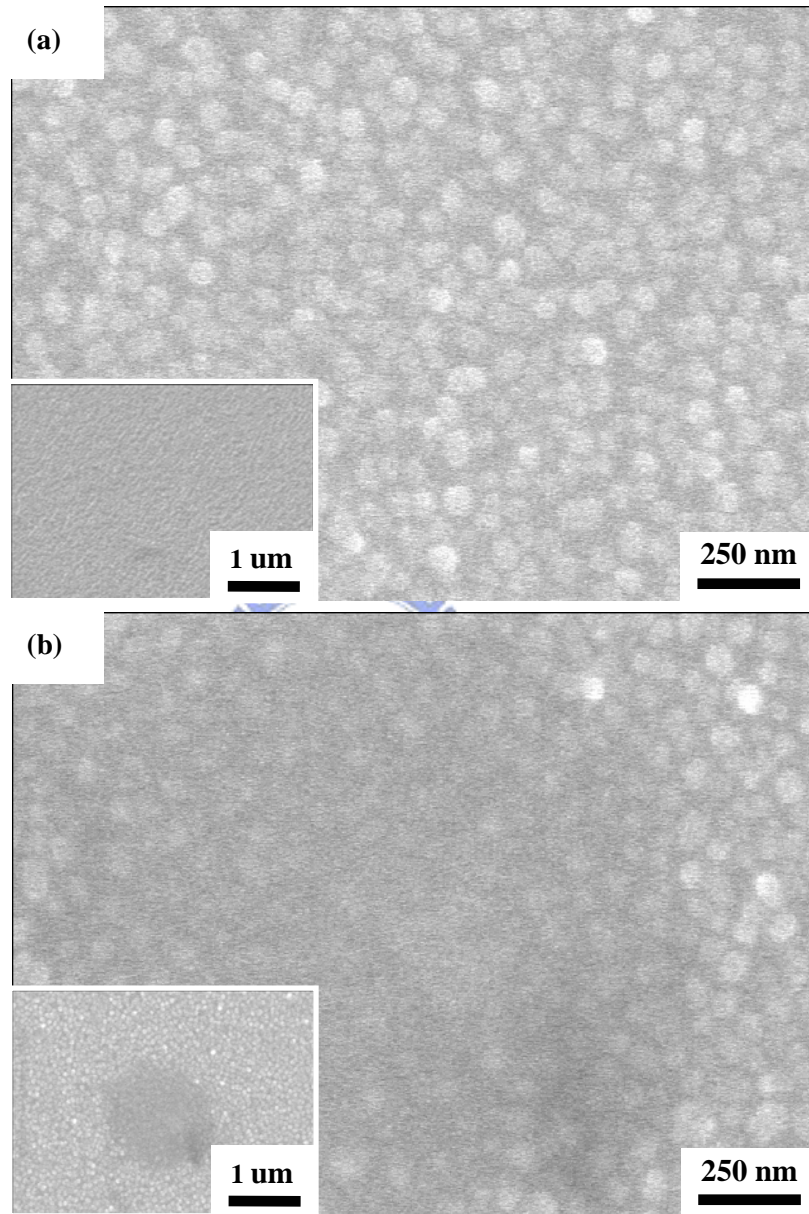
Fig. 4.5 The indentations of the SEM images were performed with images of the agglomerates (a) before and (b) after.
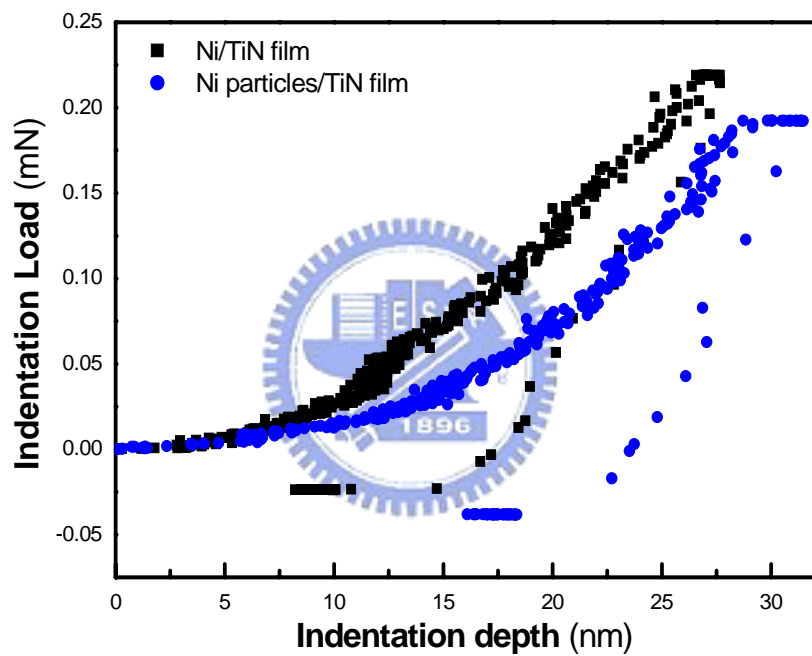
Fig. 4.6 The plots of load-displacement curves for the (a) Ni/TiN/Si thin film and (b) Ni particles/TiN/Si.

(a)

2 um

(b)

2 um

(c)

2 um

(*continue*)

112
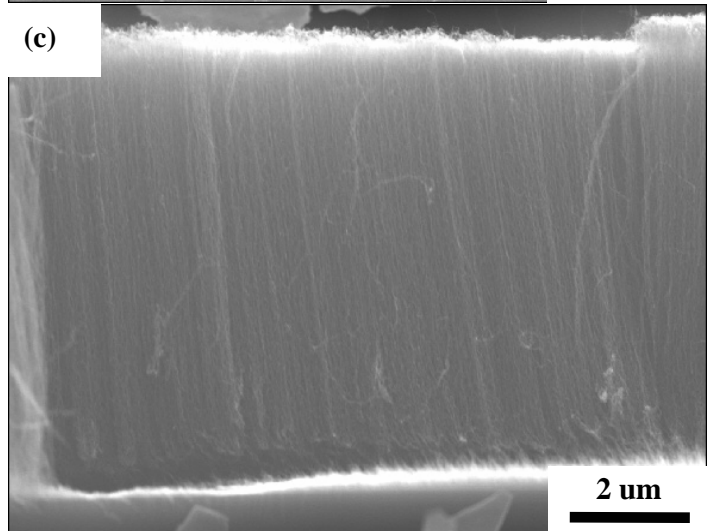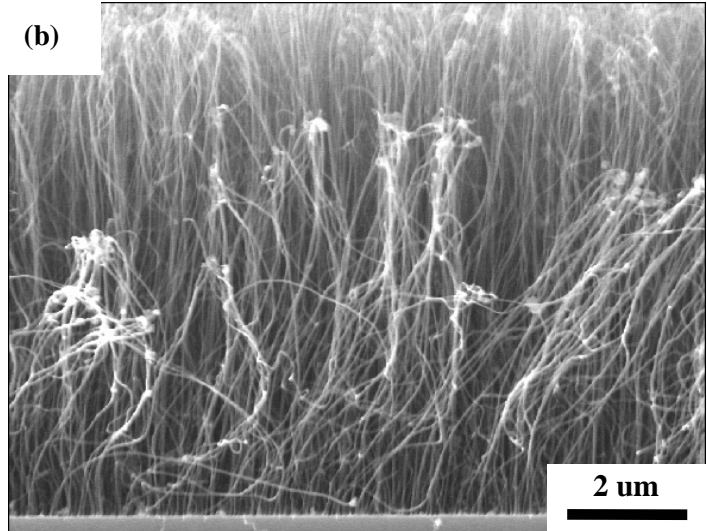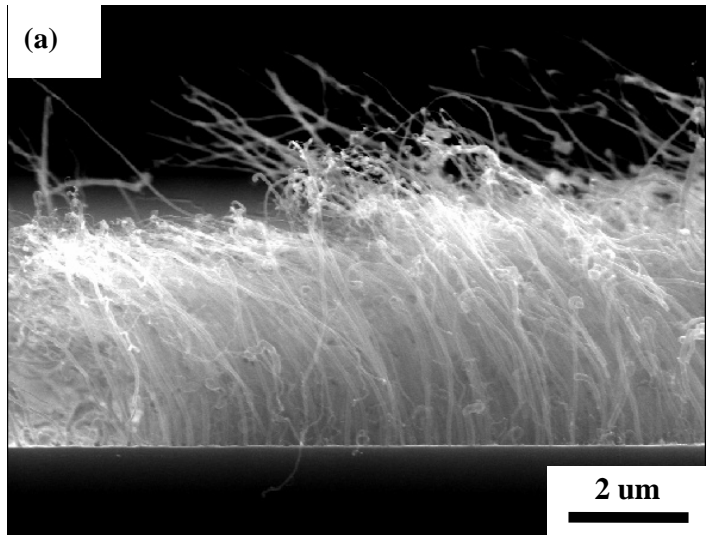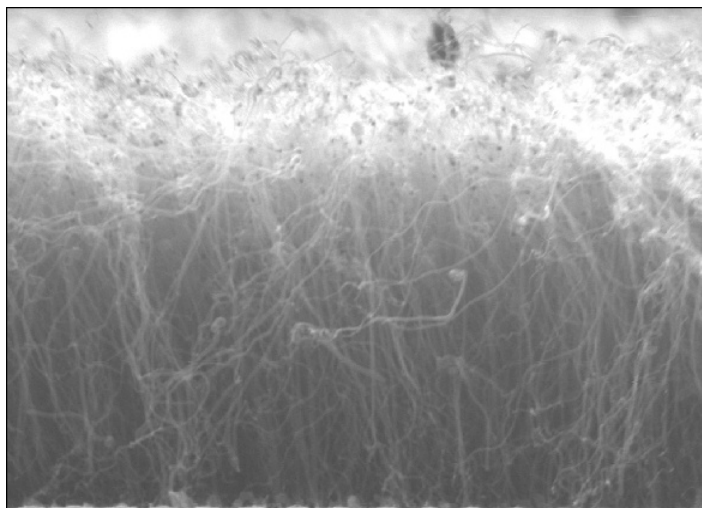
Fig. 4.7 The cross-sectional SEM images of the CNTs grown at the synthesis flow rates 200 sccm. It can be seen that amorphous carbon and carbonaceous particles were decreased and denser vertically-aligned CNTs were displayed at various pretreatment time (a) 3, (b) 5, (c) 10, and (d) 15 minutes. The diameter distribution of nickel catalysts is good indication of nanotube growth through island-like catalyst particles.
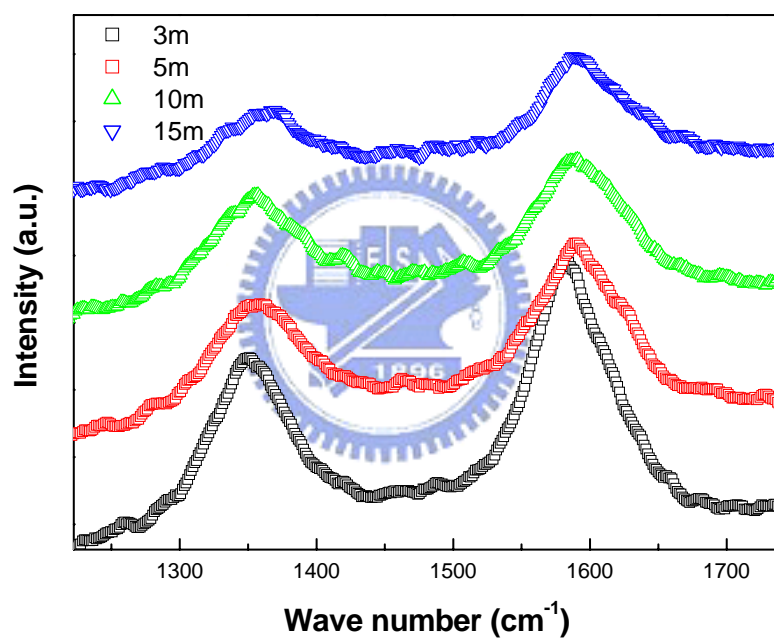
Fig. 4.8 The Raman spectra of CNTs were grown on the Ni/TiN systems. The Raman spectra of all samples show D-band peak and G-band peak around 1300 cm^{-1}, 1550 cm^{-1} respectively. The intensity increases according to increasing pretreatment time.
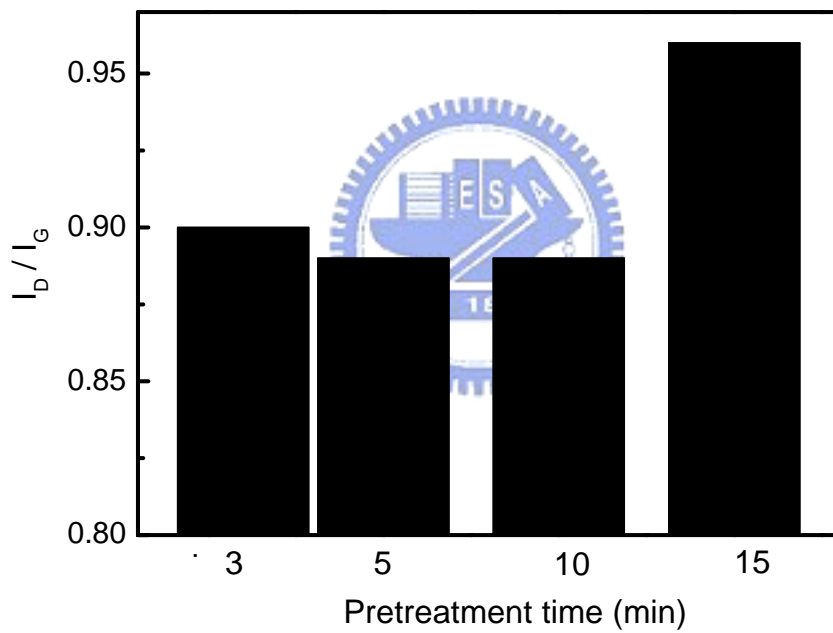
Fig. 4.9 The ratio of the intensities of the D-band and G-bands (I_D/I_G) was summarized. The ratio decrease according to pretreatment time, the I_D/I_G ratio is 0.90, 0.89, 0.86, and 0.96 respectively.
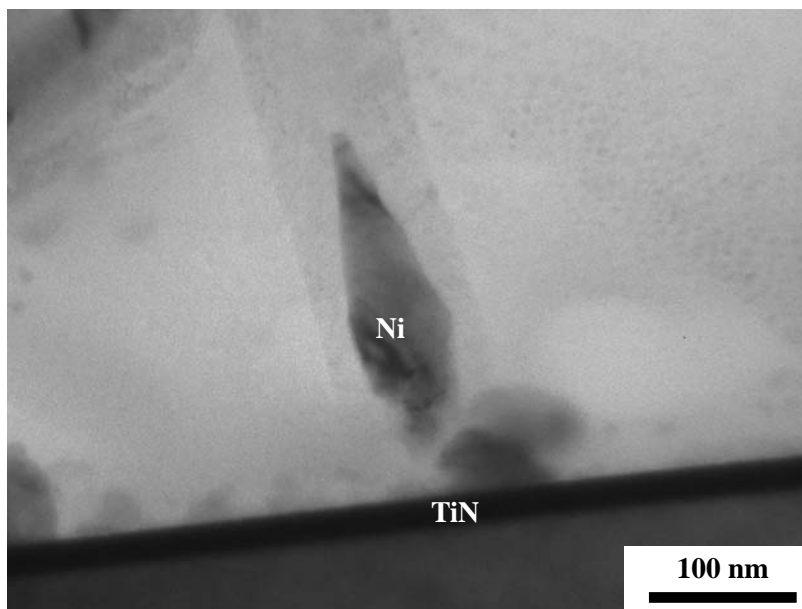
Fig. 4.10 The typical TEM image of the CNTs synthesized after hydrogen plasma pretreatment. TEM investigations reveal that the CNTs are not very straight at their root, their walls being corrugated.
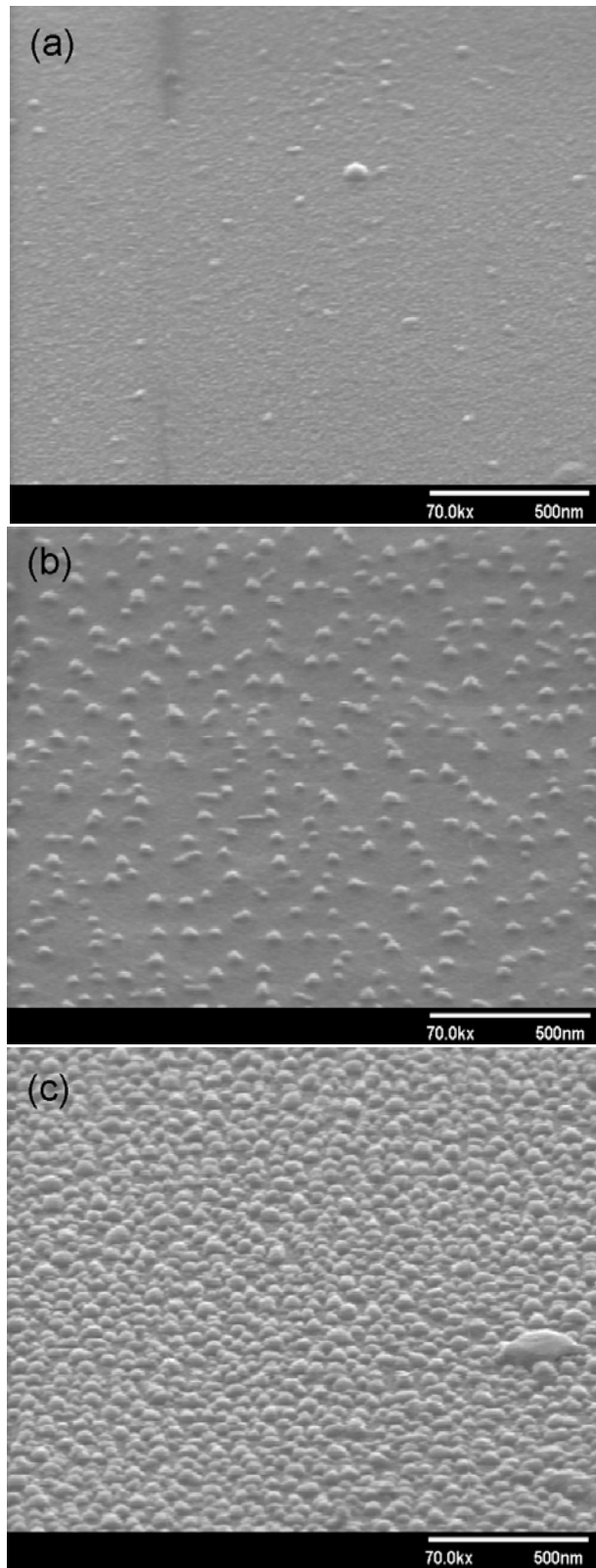
Fig.4.11 SEM images of Ni catalyst nanoparticles at various H_2 plasma pretreatment flow rates of (a) 100, (b) 200 and (c) 300 sccm.

(a) Ni nanoparticle · TaN · Si · 10 nm

(b) Ni nanoparticle · TaN · Si · 10 nm
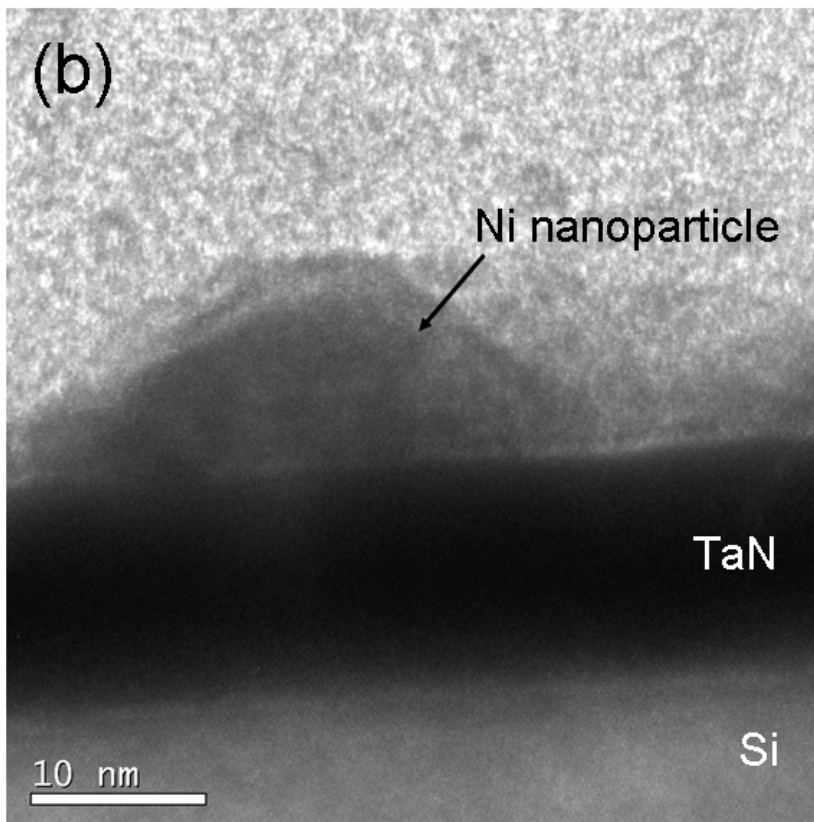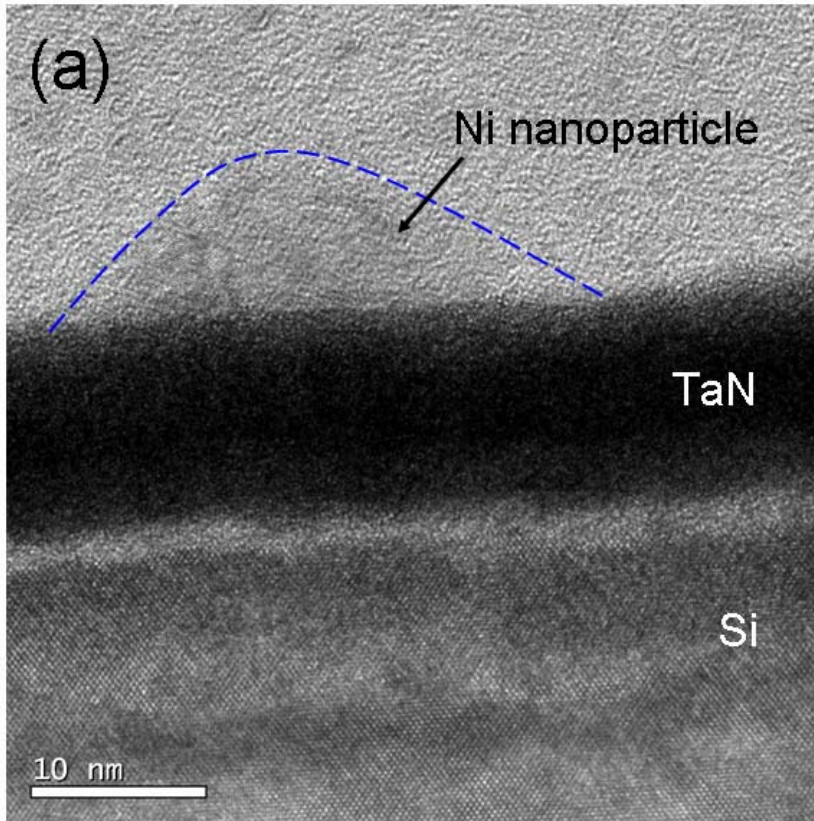
(*continue*)
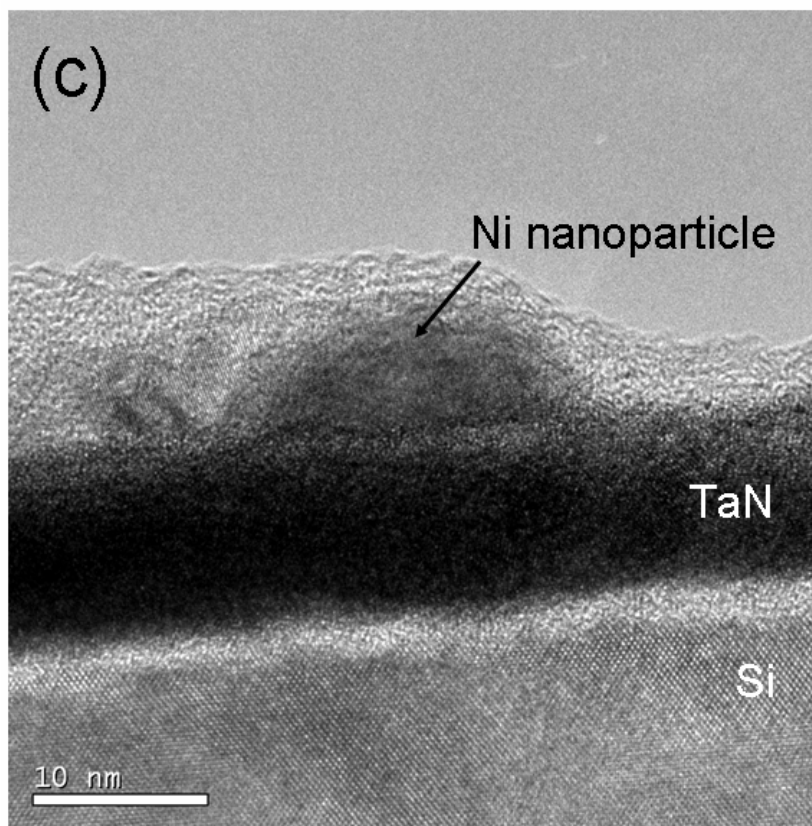
Fig.4.12 TEM images of Ni catalyst nanoparticles with the various H_2 plasma pretreatment flow rates of (a) 100, (b) 200 and (c) 300 sccm.
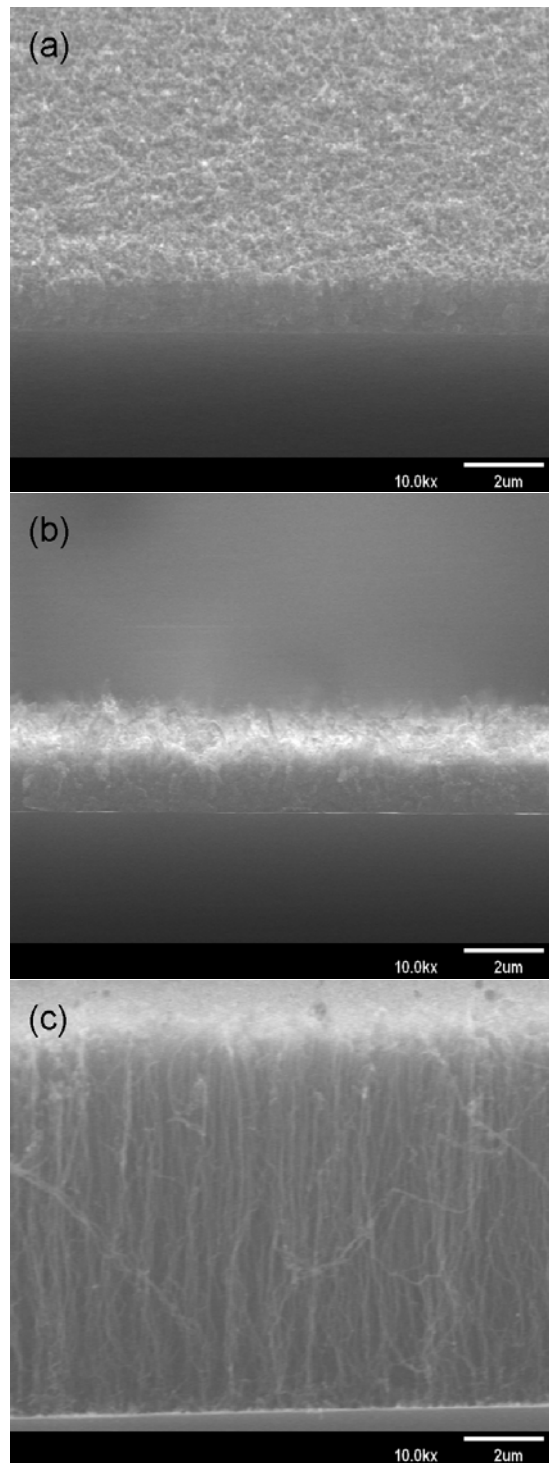
Fig.4.13 SEM images of CNTs with the various H_2 plasma pretreatment flow rates of (a) 100, (b) 200 and (c) 300 sccm.
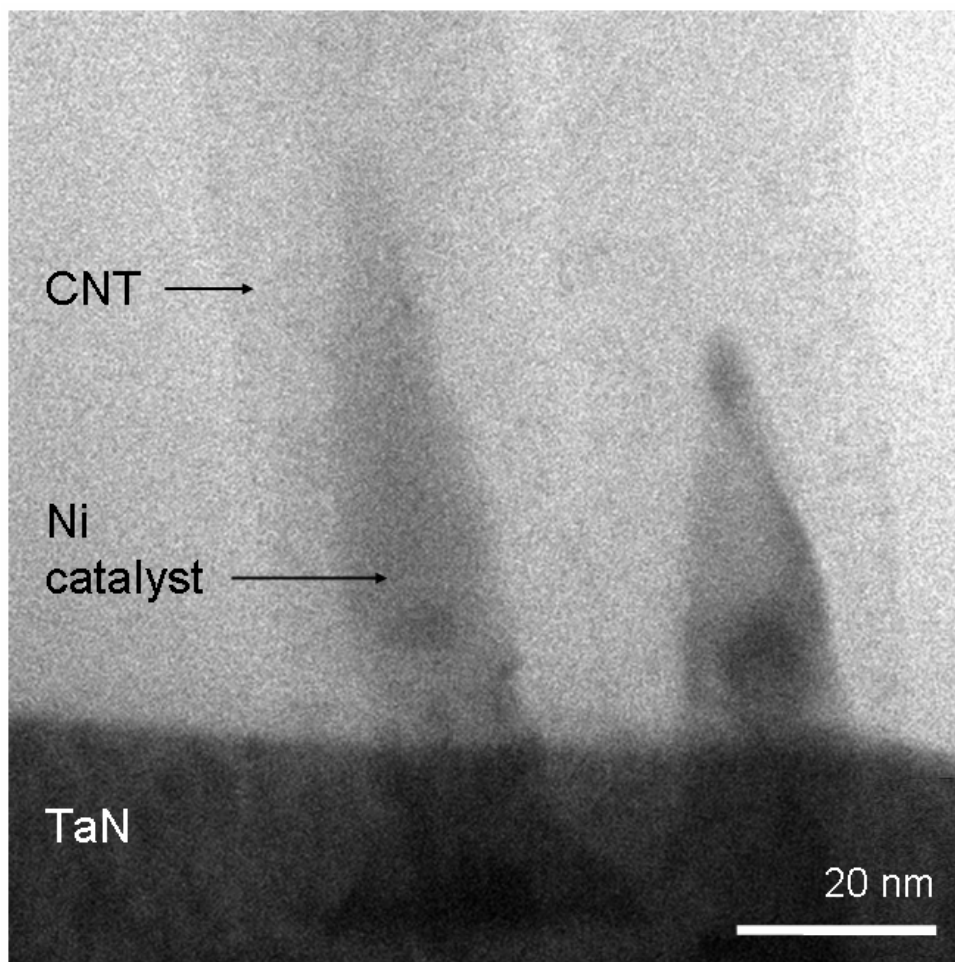
Fig.4.14 TEM image of CNT synthesized with the H_2 plasma pretreatment flow rate of 300 sccm.
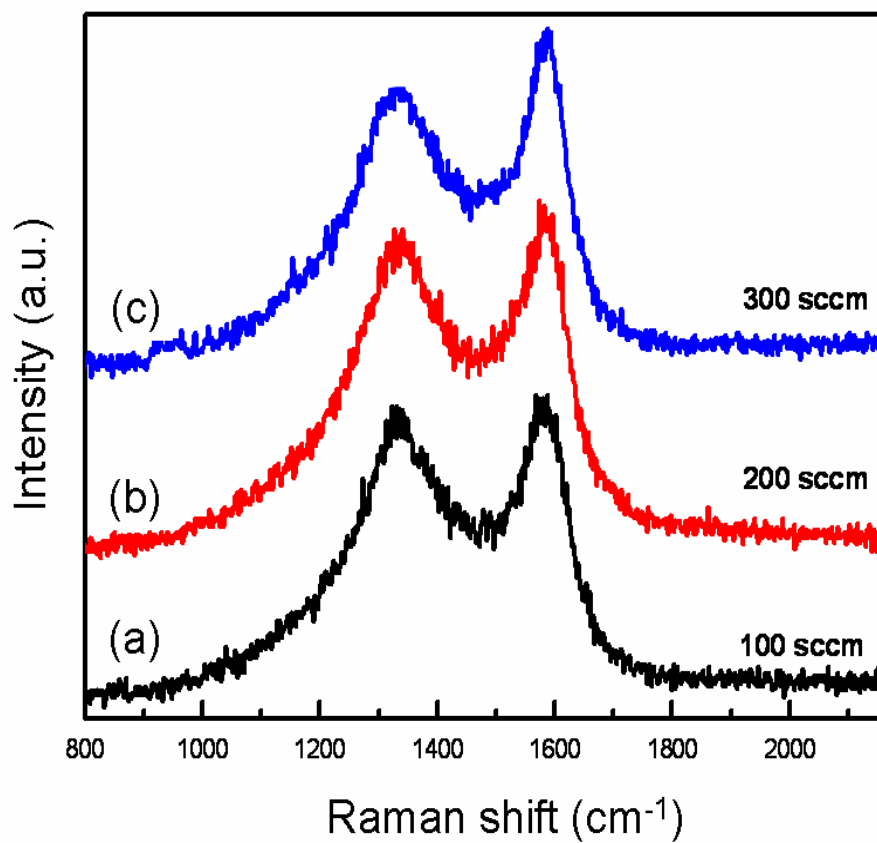
Fig.4.15 Raman spectra of CNTs with the various H_2 plasma pretreatment flow rates. The Raman spectra of all samples show D-band and G-band around 1330 cm^{-1} and 1580 cm^{-1}, respectively.
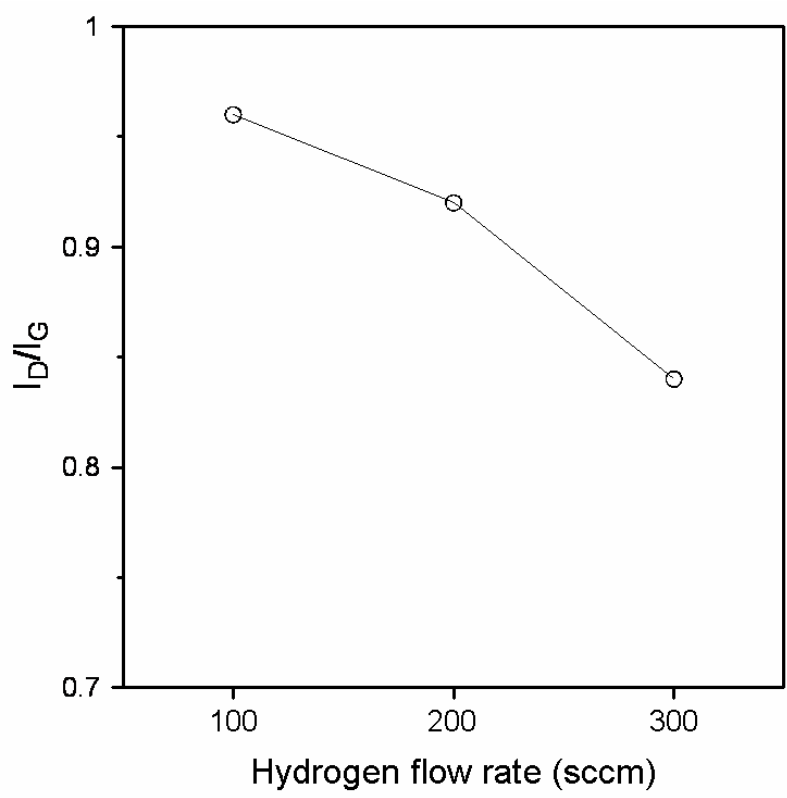
Fig.4.16 I_D/I_G rations of CNTs as a function of H_2 plasma pretreatment flow rates.
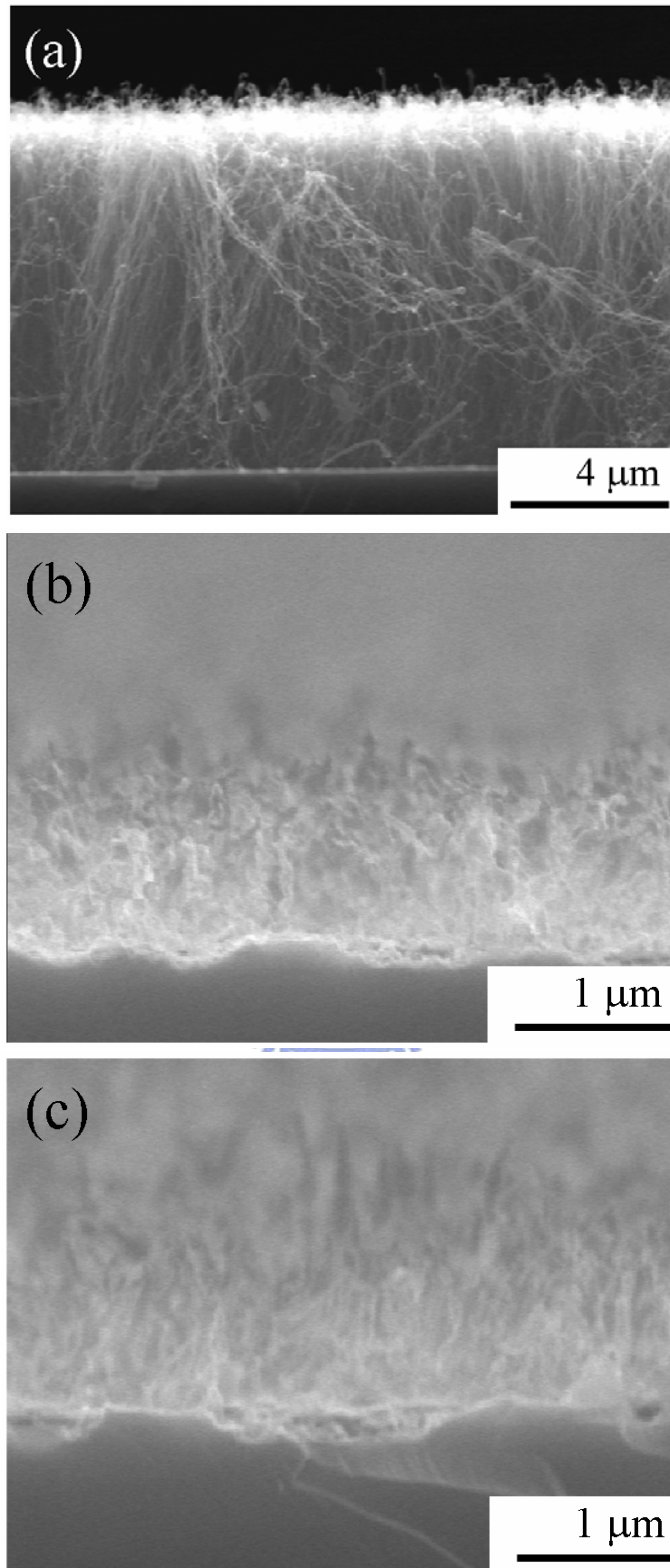
Fig. 4.17 SEM images of as-grown CNTs and, at various CF_4/O_2 plasma post-treatment times of (b) 2 and (c) 10 mins for CNTs.
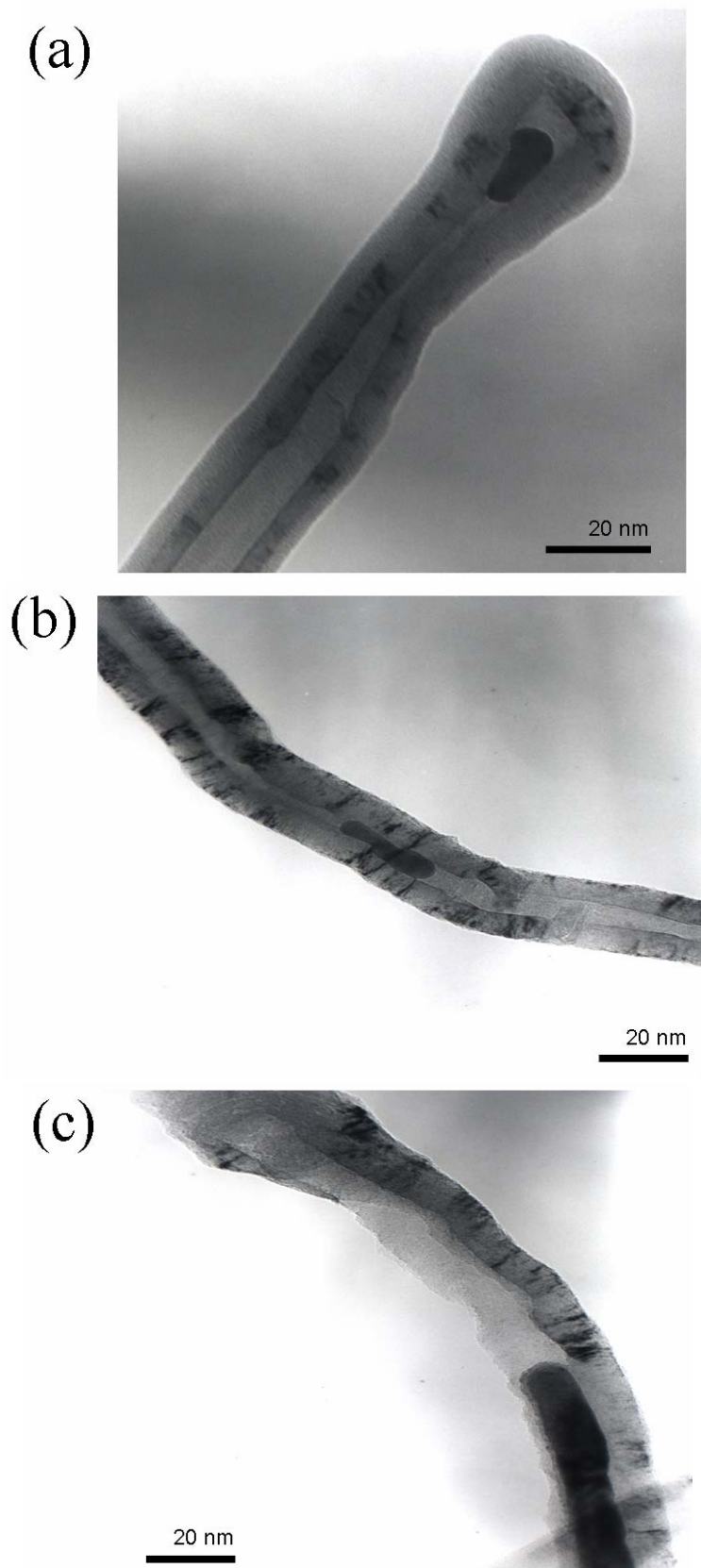
Fig. 4.18 TEM image of (a) as-grown CNTs and, with the various CF_4/O_2 plasma post-treatment times

of (b) 2 and (c) 10 mins for CNTs.
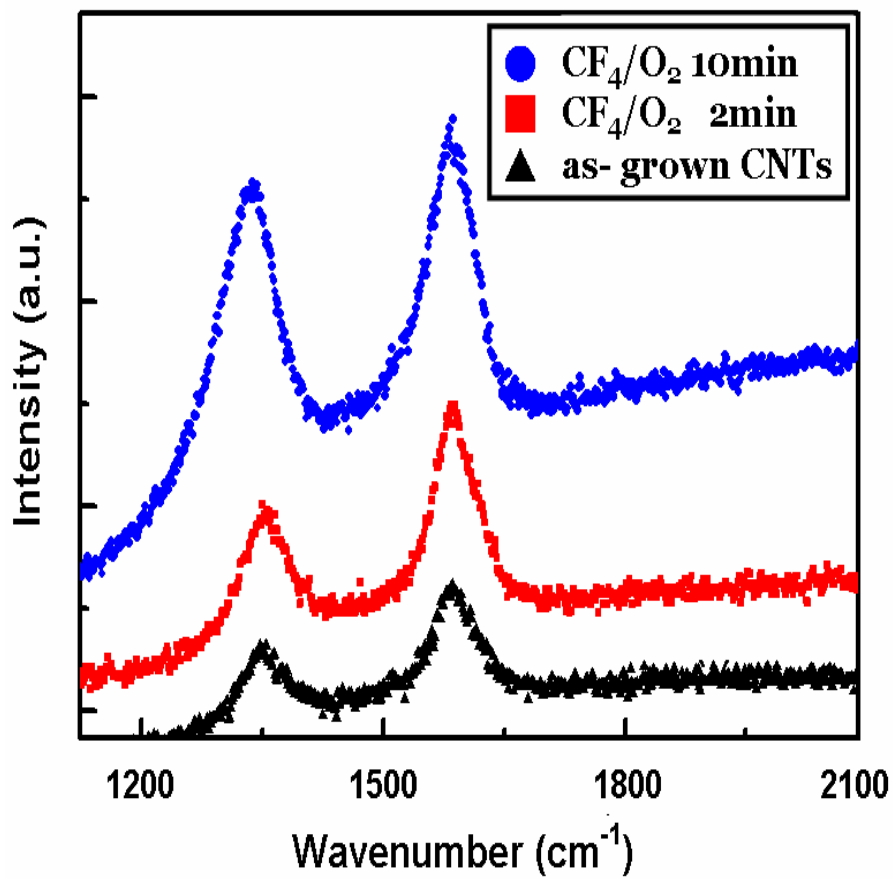
Fig. 4.19 Raman spectra of (a) as-grown CNTs and, with the various CF_4/O_2 plasma post-treatment times of (b) 2 and (c) 10 mins for CNTs.
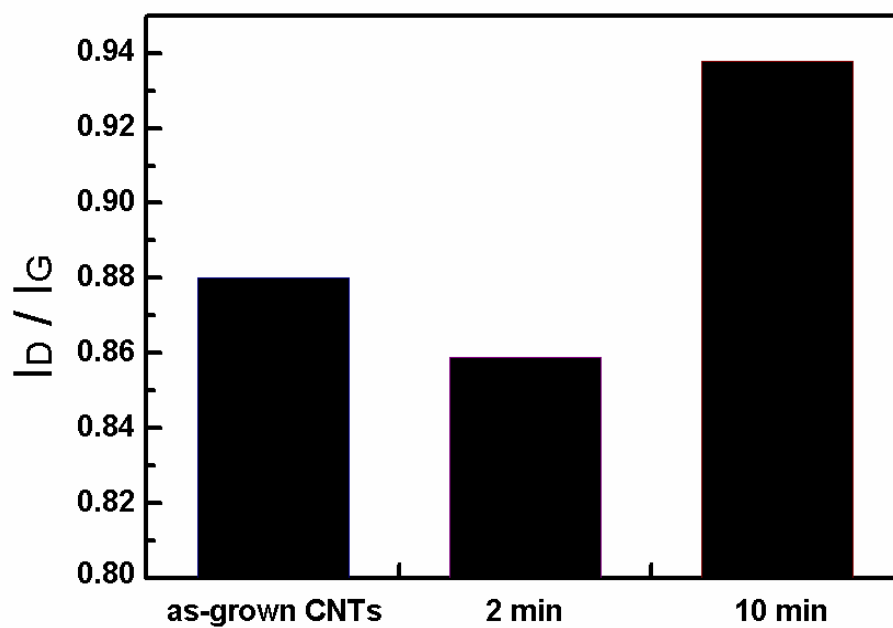
Fig. 4.20 The plots of intensity ratio (I_D/I_G) with (a) as-grown CNTs and, with the various CF_4/O_2 plasma post-treatment times of (b) 2 and (c) 10 mins for CNTs.
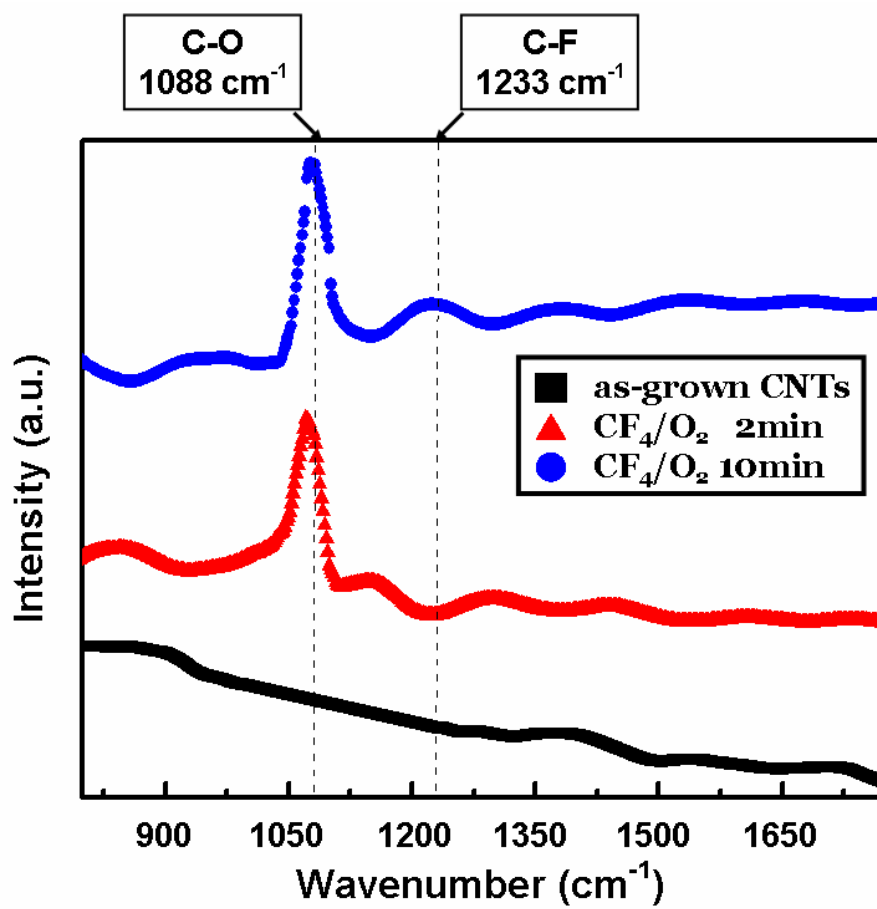
Fig. 4.21 FTIR absorption spectra (a) as-grown CNTs and, with the various CF_4/O_2 plasma post-treatment times of (b) 2 and (c) 10 mins for CNTs.
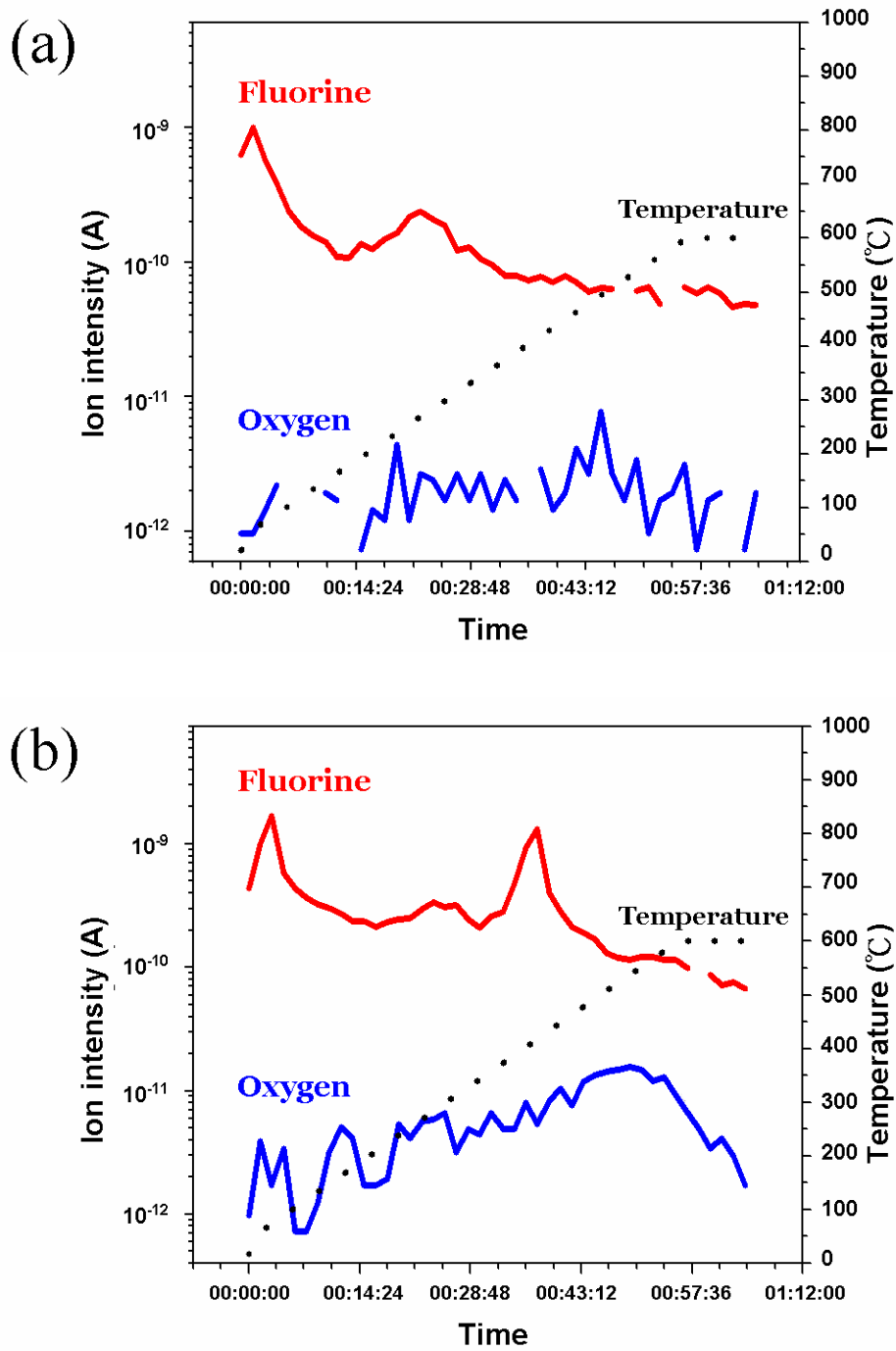
Fig. 4.22 The TDS analysis of CF_4/O_2 plasma post-treatment times of (a) 2 and (b) 10 mins for CNTs.
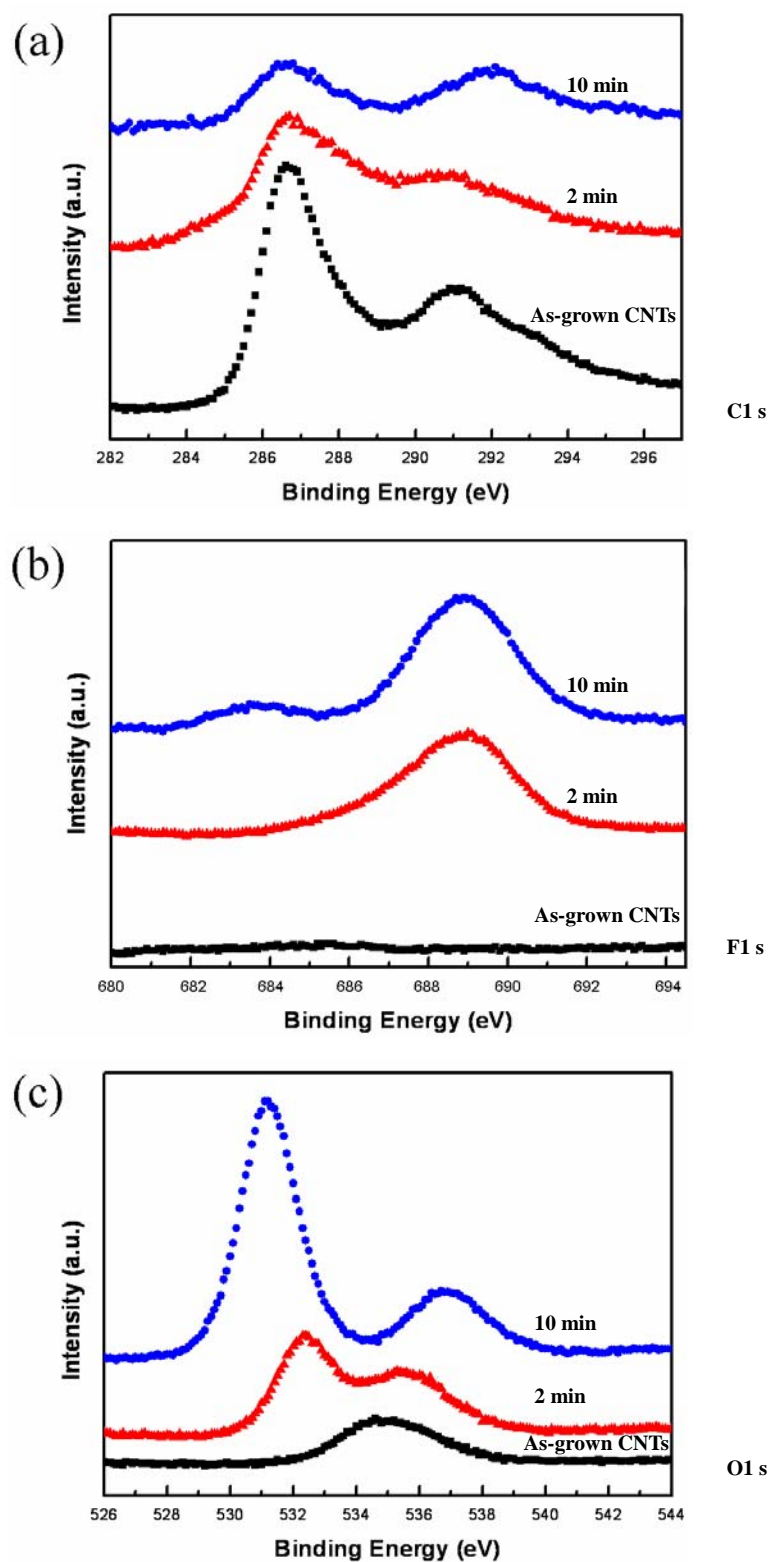
Fig. 4.23 (a) C 1s, (b) F 1s and (c) O 1s XPS spectra for the as-grown CNTs and, with the various CF$_4$/O$_2$ plasma post-treatment times of 2 and 10 mins for CNTs.
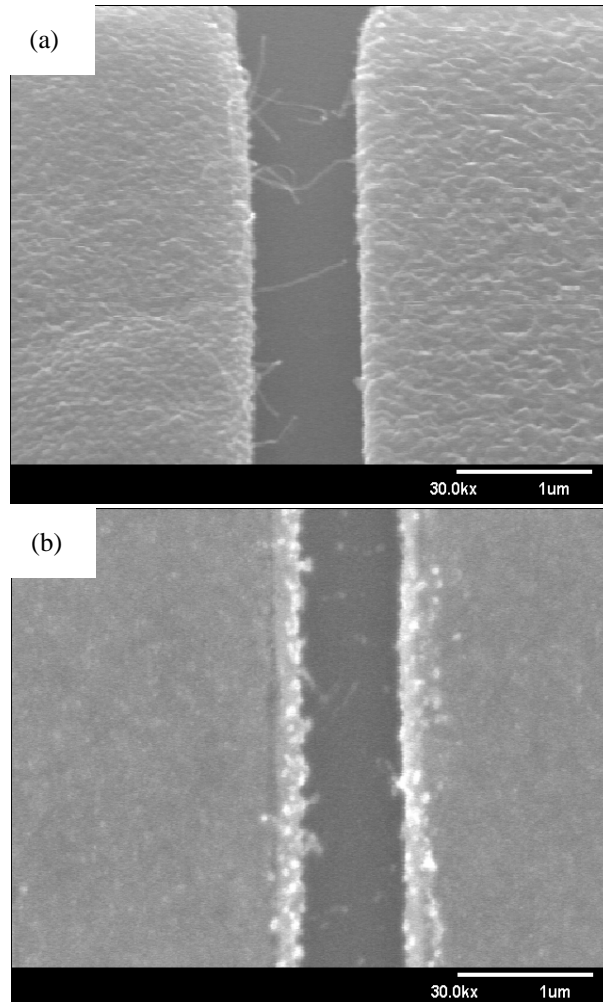
Fig. 4.24 (a) CNT grown by thermal CVD has lateral form between both of the two metal-pads. (b)The lateral CNT treated by CF_4/O_2 plasma 20s have broken form between both of the two metal-pads.
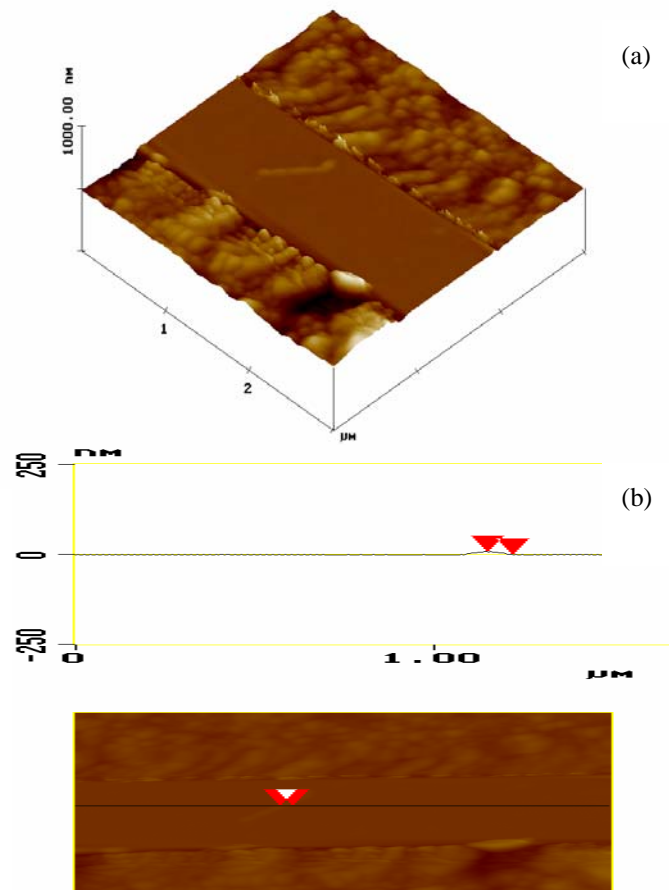
Fig. 4.25 (a) 3D AFM image (b) AFM section image of the lateral grown CNT have multiwalled graphite in the structure.
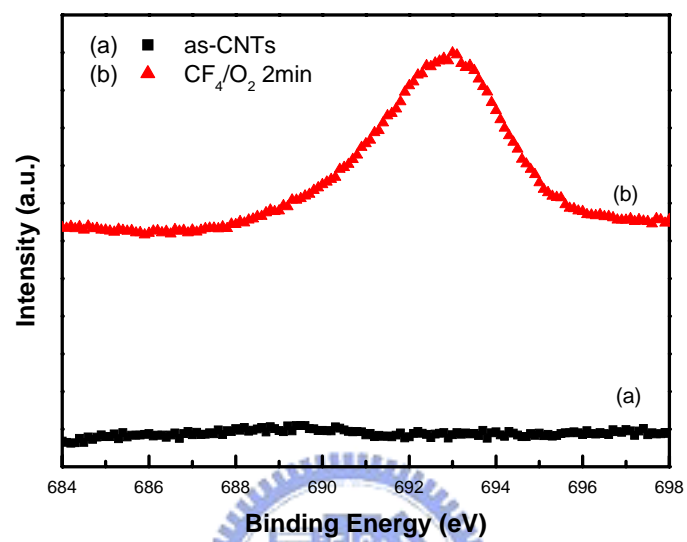
Fig. 4.26(a) and (b) correspond to the XPS spectrum curve of the as-CNT and the post-treated CNT sample.
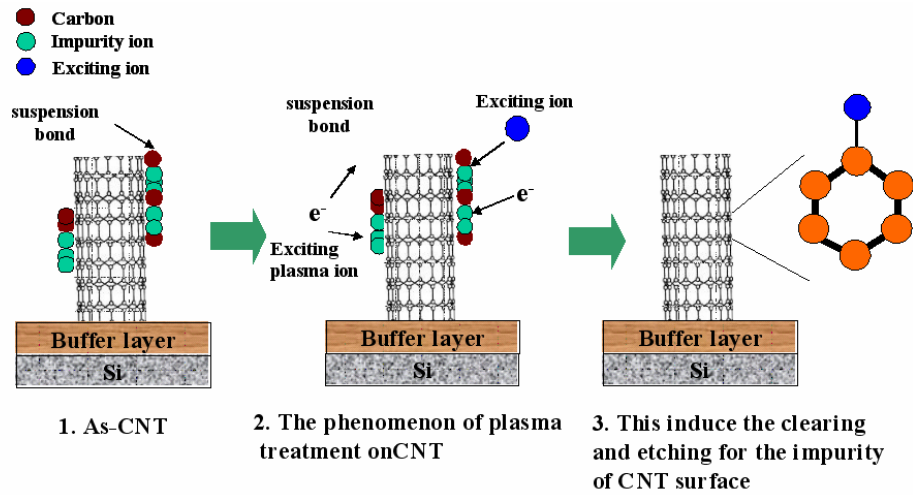
(a)
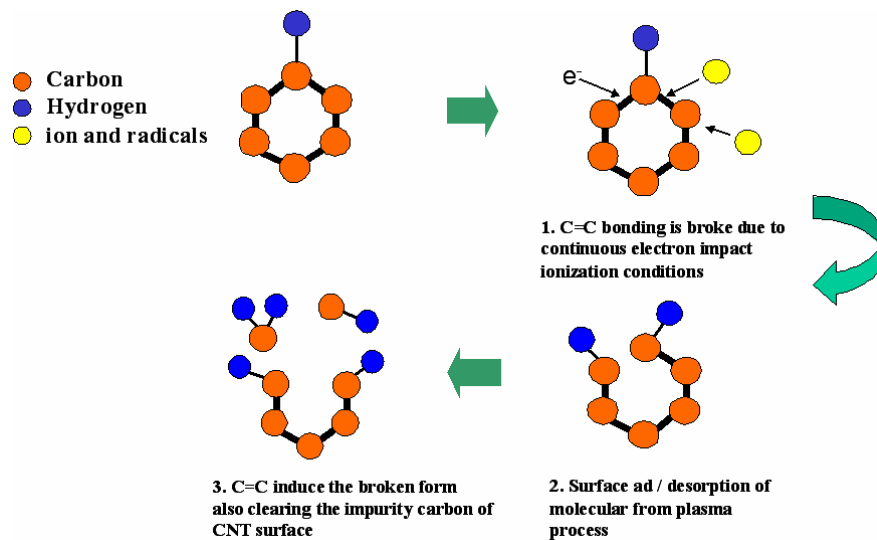
(b)

Fig. 4.27 (a) The fluorine are considered to react with the surface carbon layer of nanotubes if chemical bond formation. (b) As the plasma treated, the surface chemical bonding was occurred, and then the CNTs surface is etching by exciting ion.
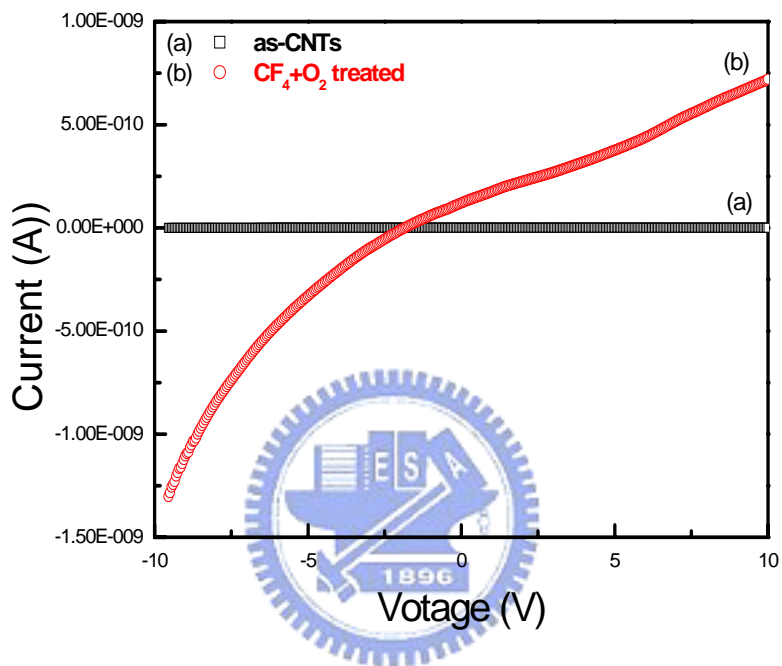
Fig. 4.28 The I-V characteristics for both (a) non-treated and (b) the post-treated CNT sample taken at room temperature. Compared the both of the current-voltage from -10 to 10 V with a step of 200 mV, it shows in overall a nonlinear I-V relations, signifying nonohmic contact between CNT on SiO_2. This is in agreement with the proposed statement that the bridges may behave a metal-semiconductor junction because of defects parts and cause nonlinear electron transport characteristics.
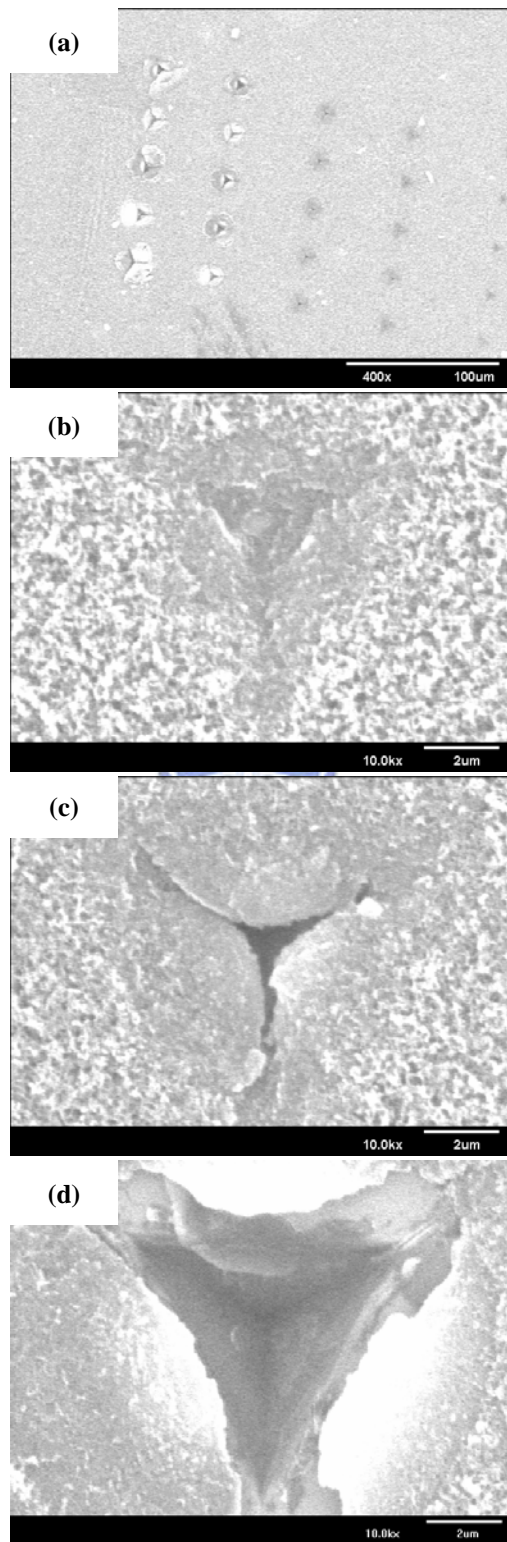
Fig. 4.29 The (a) CNTs/Si surface structure was induced cracks using a Nanoindenter with a Berkovitch indenter with various loads (b) 50, (c) 300, and (d) 500 mN.
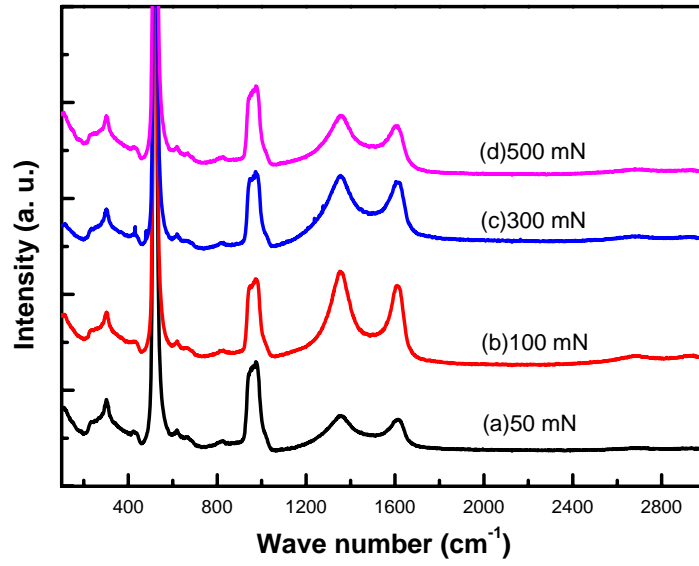
Fig. 4.30 The Raman spectrum analysis using a Nanoindenter with a Berkovitch indenter with various loads on the CNTs surface (a) 50, (b) 100, (c) 300, and (d) 500 mN.
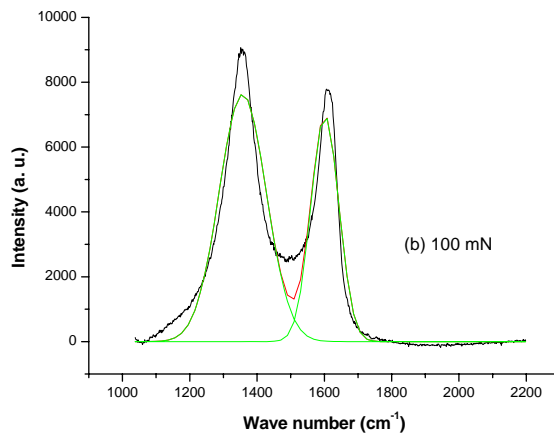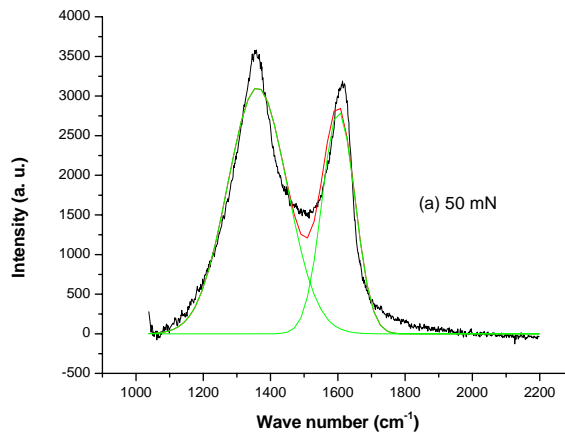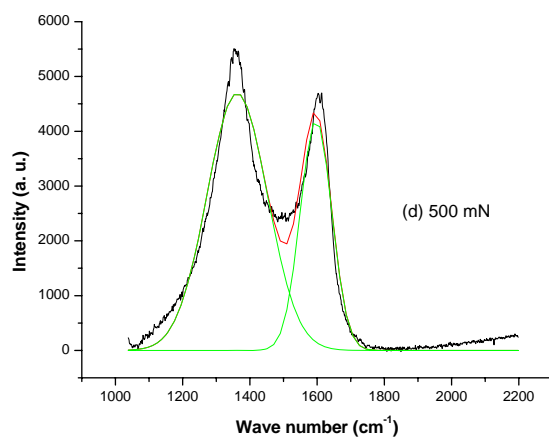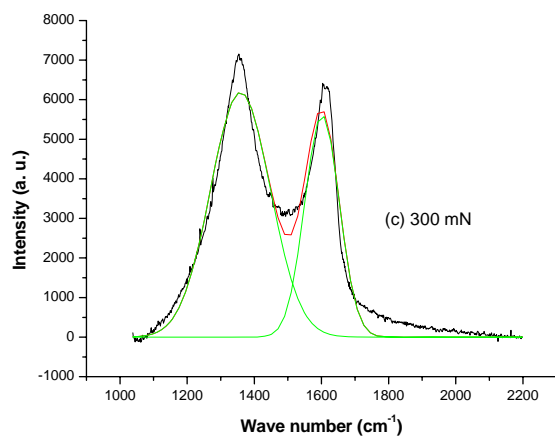
Fig. 4.31 The Raman spectrum analysis using a Nanoindenter with a Berkovitch indenter with various loads on the CNTs surface and the Gaussian curves fitting (a) 50, (b) 100, (c) 300, (d) 500 mN.
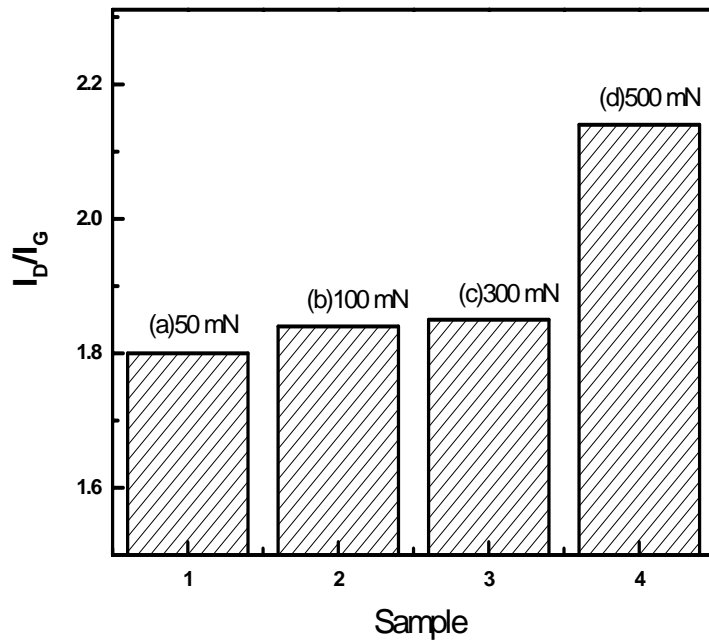
Fig. 4.32 The Raman spectrum analysis using a Nanoindenter with a Berkovitch indenter with various loads on the CNTs surface and the I_D/I_G ratios (a) 50, (b) 100, (c) 300, (d) 500 mN.

Chapter 5 Conclusions and future work

5-1 Conclusions

The physical, chemical, mechanical, and electronic characteristics of CNTs are discussed in this dissertation. Numerous important results are summarized and discussed.

Effect of pretreatment on the increasing time from the SEM image of Ni catalyst layer was described. By the nanoindentation technique, it is observed that the decreased in modulus (from 238.9±8.4 to 176.2±6.1GPa) and hardness (from 17.2±1.6 to 11±0.8 GPa) than those of the Ni film. Also, the density and alignment of CNTs could be controlled by nickel nanoparticles. Raman spectrum indicates that the pretreatment time decrease the disorder structures, which in turn yields the amounts of amorphous carbon and carbonaceous particles in the CNTs. TEM indicate that the crystalline graphite structure, depending on the H_2 plasma pretreatment flow rate. Surface performance of CNTs from CF_4/O_2 plasma post-treatment was investigated. The I_D/I_G ratios reveal that chemical treatment with CF_4/O_2 plasma for 2 min reduces the degree of disorder. After 10 min, however, the degree of disorder in CNTs is increased. FTIR absorption spectra include peaks that correspond to C-O and C-F stretching vibrations. The TDS results yield adsorption information. XPS datum reveals fluorination in CF_4/O_2 plasma-treated CNTs and the absence of a significant of physisorbtion on CNTs. This result shows that adding oxygen to the plasma increases the decomposition efficiency.

A CNT bridge on SiO_2 that is patterned photolithographically in an electronic device is described. The CNTs grow laterally to the substrate over a TiN vertical growth barrier and connect to the side of the electrode pad. The CF_4/O_2 post-treated has a higher current-voltage curve than the surface-modified. The typical Schottky contact characteristics at room temperature are discussed. The surface of the CNT interacts with

the surrounding plasma, breaking C-C bonds and creating active sites to bond the functional groups. Therefore, C-F binding in the amorphous carbon can be reduced by modifying the CNTs. A CNT film was studied using nanoindentation equipment (Berkovitch indenter) by varying the loading force. CNT films exhibit features that are associated with toughening against cracks caused by indentation. The quantitative indentation force is utilized to determine the CNTs axial modulus, depending on the Raman shift. The I_D/I_G ratios of the CNTs films are associated with an increase in the force. Such features follow in part from the fact that CNTs films generally contain some disordered regions.

5-2 Future work

The following issues warrant further research.

(a) The buffer layer study involves some interesting candidate materials, including thin Ti, Ta, Hf and HfN films on Si substrates. Sputtering (PVD) or electron beam evaporation (E-GUN) were used to,

(i) Strengthen the adhesion between Si substrates and catalyst thin films.

(ii) Elucidate the relationship between the buffer layer and the catalysts.

(iii) Improve the properties of CNTs for use in interconnection and metallization.

(b) The effect of plasma treatment on CNT thin films or a single CNT should be studied. The effects of different plasma treatments (H_2, NH_3, O_2 etc.) on CNTs should also be compared.

(c) The tensile properties of the composite upon addition of MWCNTs to the polymer matrix are of interest.

Reference

[1] Alexander Hellemans, "IBM Researchers Devise Nanotube ICs",IEEE Spectrum (2001) 26.

[2] A. Maiti, A. Svizhenko, M. P. Anantram, "Electronic Transport through Carbon Nanotubes: Effects of Structural Deformation and Tube Chirality", Physical Review Letters, 88 (2002) 25.

[3] C.T. White, J.W. Mintmire, "Density of states reflects diameter in nanotubes" Nature 394 (1998) 29.

[4] T. Hertel, R. E. Walkup, P. Avouris, "Deformation of carbon nanotubes by surface van der Waals forces", Physical Review B 58 (1998) 15.

[5] Y.G. Yoon, M.S.C. Mazzoni, H.J. Choi, J. Ihm, S.G. Louie, "Structural Deformation and Intertube Conductance of Crossed Carbon Nanotube Junctions", Physical Review Letters, 86 (2001) 22.

[6] T. Hertel, R. Martel, P. Avouris, "Manipulation of Individual Carbon Nanotubes and Their Interaction with Surfaces" J. Phys. Chem. B 102 (1998) 910.

[7] B.I. Yakobson, C. J. Brabec, J. Bernbolc, "Nanomechanics of carbon tubes:Instabilities beyond the linear response", Physical Review Letters 76 (1996) 2511.

[8] V.H. Crespi, "Local Temperature during the Growth of Multiwalled Carbon Nanotube", Applied Physics Letters 82 (1998) 5.

[9] M.S. Dresselhaus, "New tricks with nanotubes", Nature 391(1998) 1.

[10] C. Berger, P. Poncharal, Y. Yi, W. de Heer, "Ballistic conduction in multiwalled carbon nanotubes", Journal of Nanoscience and Nanotechnology 3 (2003) 171.

[11] S. Iijima, "Helical microtubules of graphitic carbon", Nature 354 (1991) 56.

[12] P. Delaney, H. J. Choi, J. Ihm, S. G. Louie, M. L. Cohen, "Broken symmetry and pseudogaps in ropes of carbon nanotubes", Nature 391(1998) 29.

[13] T.W. Odom, J.L. Huang, P. Kim, C. M. Lieber, "Atomic structure and electronic properties of single-walled carbon nanotubes", Nature 391 (1998) 1.

[14] L.F. Sun, S.S. Xie, W. Liu, W.Y. Zhou, Z.Q. Liu, D.S. Tang, G. Wang, L.X. Qian, "Creating the narrowest carbon nanotubes", Nature 403 (2000) 27.

[15] R.H. Baughman, A. A. Zakhidov, Walt A. de Heer, "Carbon Nanotubes-the route toward applications", Science 297 (2002) 2.

[16] M.S. Dresselhaus, "New tricks with nanotubes", Nature 391(1998) 1.

[17] J.W.G. Wildo¨er, L. Venema, A.G. Rinzler, R.E. Smalley, C. Dekker, "Electronic structure of atomically resolved carbon nanotubes", Nature 391(1998) 1.

[18] P. Calvert, "A recipe for strength", Nature 399 (1999) 20.

[19] J.H. Hafner, C.L. Cheung, C.M. Lieber, "Growth of nanotubes for probe microscopy tips", Nature 398 (1999) 29.

[20] L.C. Qin, X. Zhao, K. Hirahara, Y. Miyamoto, Y. Ando, S. Iijima, "The smallest carbon nanotube", Nature 408 (2000) 2.

[21] D. Gabel, Carbon Bonds in Chemistry, A National Curriculum Project for High School Science Education, Indiana University, Bloomington.

[22] S. Paulson, A. Helser, M. Buongiorno Nardelli, R. M. Taylor II, M. Falvo, R. SuperÞne, S. Washburn, "Tunable Resistance of a Carbon Nanotube-Graphite Interface", Science 290 (2000) 1.

[23] G. G. David, G. G. Ilana, "Momentous period for nanotubes", Nature 412(2001) 9.

[24] M. Ouyang, J.L. Huang, C.L. Cheung, C.M. Lieber, "Energy Gaps in Metallic Single-Walled Carbon Nanotubes", Science 92 (2001) 27.

[25] B. Vigolo, A. Pénicaud, C. Coulon, C. Sauder, R. Pailler, C. Journet, P. Bernier, P. Poulin, "Macroscopic fibers and ribbons of oriented carbon nanotubes", Science 290 (2000)17.

[26] M.F. Yu, O. Lourie, M.J. Dyer, K. Moloni, T.F. Kelly, R.S. Ruoff, "Strength and breaking mechanism of multiwalled carbon nanotubes under tensile load", Science 287 (2000) 28.

[27] E.W. Wong, P.E. Sheehan, C.M. Lieber, "Nanobeam mechanics: elasticity, strength, and toughness of nanorods and nanotubes", Science 277 (1997) 26.

[28] T.W. Tombler, C. Zhou, L. Alexseyev, J. Kong, H. Dai, L. Liu, C. S. Jayanthi, M. Tang, S.Y. Wu, "Reversible electromechanical characteristics of carbon nanotubes under local-probe manipulation", Nature 405 (2000) 15.

[29] L. Duclaux, "Review of the doping of carbon nanotubes (multiwalled and single-walled)", Carbon 40 (2002)1751.

[30] P. Avouris, "Carbon nanotube electronics", Chemical Physics 281 (2002) 429.

[31] C.T. White, T. N. Todorov, "Nanotubes go ballistic", Nature 411 (2001) 7.

[32] L.C. Venema, J.W.G. Wildoer, S.J. Tans, J.W. Janssen, H. Temminck Tuinstra, L. P. Kouwenhoven, C. Dekker, "Imaging electron wave functions of quantized Energy Levels in Carbon Nanotubes", Science 283 (1999)1.

[33] Roberto Livi and Stefano Lepri, "Heat in one dimension", Nature 421(2003) 23.

[34] D.H. Cobden, "A nanotube laboratory, Nature", Nature 397 (1999) 25.

[35] N. de Jonge, Y. Lamy, K. Schoots, T.H. Oosterkamp, "High brightness electron beam from a multi-walled carbon nanotube", Nature 420 (2002) 28.

[36] K.A. Williams, P.T. M. Veenhuizen, B.G. de la Torre, R. Eritja, C. Dekker, "Carbon nanotubes with DNA recognition", Nature 420 (2002)19.

[37] E.T. Thostenson, Z. Ren, T.W. Chou, "Advances in the science and technology of carbon nanotubes and their composites: a review", Composites Science and Technology 61 (2001) 1899.

[38] O.A. Nerushev, M. Sveningsson, L.K.L. Falk, F. Rohmund, "Carbon nanotube films obtained by thermal chemical vapor Deposition", Journal of Material Chemical 11 (2001)1122.

[39] M. Pérez-Cabero, E. Romeo, C. Royo, A. Monzón, A. Guerrero-Ruíz, I. Rodríguez-Ramos, "Growing mechanism of CNTs: a kinetic approach", Journal of Catalysis 224 (2004) 197.

[40] S.B. Sinnott, R. Andrews, D. Qian, A.M. Rao, Z. Mao, E.C. Dickey, F. Derbyshie "Model of carbon nanotube growth through chemical vapor deposition", Chemical Physics Letters 315 (1999) 25.

[41] S. Iijima, "Helical Microtubules of Graphitic carbon", Nature (London), 354 (1991) 56.

[42] R. Martel, T. Schmidt, H.R. Shea, T. Hertel, Ph. Avouris, "Single- and multi-wall carbon nanotube field-effect transistors", Applied Physics Letters 73 (1998) 2447.

[43] B.H. Chen, H.C. Lin, T.Y. Huang, J.H. Wei, H.H. Wang, M.J. Tsai, T.S. Chao, "Complementary carbon nanotube-gated carbon nanotube thin-film transistor",J. Applied Physics Letters 88 (2006) 093502.

[44] Y.T. Jang, S.I. Moona, J.H. Ahnb, Y.H. Lee, B.K. Ju, "A simple approach in fabricating. chemical sensor using laterally grown multi-walled carbon nanotubes", Actuators B 99 (2004) 118.

[45] A.S. Teh, S.B. Lee, K.B.K. Teo, M. Chhowalla, W.I. Milne, D.G. Hasko, H. Ahmed, G.A.J. Amaratunga, "Lateral field emitters fabricated using carbon nanotubes",Microelectronic Engineering 67-68 (2003) 789.

[46] C.P. Juan, C.C. Tsai, K.H. Chen, L. C. Chen, H.C. Cheng, "Fabrication and characterization of lateral field emission device based on carbon nanotubes", Japan Journal Applied Physics Letters 44(4B) (2005) 2612.

[47] Y.H. Lee, Y. T. Jang, B. K. Ju, "In situ nanointerconnection for nanoelectronics

via direct auto-catalytic lateral growth", Applied Physics Letters 86 (2005) 173103.

[48] J.H. Yen, I.C. Leu, C.C. Lin, M. H. Hon, "Effect of catalyst pretreatment on the growth of carbon nanotubes", Diamond Relate Material 13 (2004) 1237.

[49] J.S. Gao, K. Umeda, K. Uchino, H. Nakashima, K. Muraoka, "Plasma breaking of thin films into nano-sized catalysts for carbon nanotube synthesis", Materials Science and Engineering A 352 (2003) 308.

[50] J.S. Gao, K. Umeda, K. Uchino, H. Nakashima, K. Muraoka, "Control of sizes and densities of nano catalysts for nanotube synthesis by plasma breaking method", Materials Science and Engineering B 107 (2004) 113.

[51] H.F. Cheng, Y. Chou, K.S. Liu, C.H. Tsai, I.N. Lin, "Pretreatment of $Fe(C_5H_7COO)_3$ Metal-organics for growing carbon nanotubes on silicon substrates", Physica B 323 (2002) 308.

[52] J.H. Choi, T.Y. Lee, S.H. Choi, J.H. Han, J.B. Yoo, C.Y. Park, T. Jung, S.G. Yu, W. Yi, I.T. Han, J.M. Kim, "Control of carbon nanotubes density through Ni nanoparticle formation using thermal and NH_3 plasma treatment", Diamond Relate Material 12 (2003) 794.

[53] J.H. Choi, T.Y. Lee, S.H. Choi, J.H. Han, J.B. Yoo, C.Y. Park, T. Jung, S.G. Yu, W. Yi, I. T. Han, J.M. Kim, "Density control of carbon nanotubes using NH_3 plasma treatment of Ni catalyst layer", Thin Solid Films 435 (2003) 318.

[54] T. de los Arcos, F. Vonau, M. G. Garnier, V. Thommen, H.G. Boyen P.O.M. Düggelin, D. Mathis, R. Guggenheim, "Silicide formation during the CVD growth of nanotubes onto Si wafers", Applied Physics Letters 80 (2002) 2383.

[55] T. de los Arcos, M.G. Garnier, P. Oelhafen, D. Mathys, J.W. Seo, C. Domingo, J.V. García-Ramos, S. Sánchez-Cortés, "Effect of different buffer layers in CNT growth and characteristics", Carbon 42 (2004) 187.

[56] T. de los Arcos, M.G. Garnier, J.W. Seo, P. Oelhafen, V. Thommen, D. Mathys, "Different layers induce different chemical changes in the catalyst", Journal Physics Chemical B 108 (2004) 7728.

[57] D. Ge, V. Domnich, Y. Gogotsi, "Thermal stability of metastable silicon phases produced by nanoindentation", Journal Applied Physics 95 (2004) 2725.

[58] N.J.M. Carvalho, J.Th.M. De Hosson, "Deformation mechanisms in TiN/(Ti,Al)N multilayers under depth-sensing indentation", Acta Materialia 54(7) (2006)1857.

[59].E. Le Bourhis, G Patriarche, "Room-temperature plasticity of InAs ", Physica Status Solidi (a) 179 (2000) 153.

[60] J.E. Bradby, J.S. Williams, J.W. Leung, M.V. Swain, P. Munroe, "Mechanical deformation of InP and GaAs by spherical indentation ", Journal Applied Physics Letters 78 (2001) 21.

[61] V.A. Coleman, J.E. Bradby, C. Jagadish, P. Munroe, Y.W. Heo, S.J. Pearton, D.P. Norton, M. Inoue M. Yano, "Mechanical properties of ZnO epitaxial layers grown on a- and c-axis sapphire", Journal Applied Physics Letters 86 (2005) 203105.

[62] Z. Xia, L. Riester, W.A. Curtin, H. Li, B.W. Sheldon, J. Liang, B. Chang, J.M. Xu, "Direct. observation of toughening mechanisms in carbon nanotube ceramic matrix composites", Acta Materialia 52 (2004) 931.

[63] J.F. Waters, P.R. Guduru, M. Jouzi, J.M. Xu, T. Hanlon, S. Suresh, "Degraded axial buckling strain of multiwalled carbon nanotubes due to interlayer slips", Journal Applied Physics Letters 87 (2005) 103109.

[64] Y. Raichman, M. Kazakevich, E. Rabkin, Y. Tsur, "Inter-nanoparticle bonds in agglomerates studied by nanoindentation", Advanced Materials 18 (2006) 2028.

[65] R.H. Baughman, A.A. Zakhidov, W.A. de Heer, "Carbon nanotubes-the route toward applications", Science 297 (2002) 787.

[66] H.W.C. Postma, T. Teepen, Z. Yao. M. Grifoni, C. Dekker, "Logic circuits with carbon nanotube transistors", Science 293 (2001) 76.

[67] J. Kong, N.R. Franklin, C. Zhon, M.G. Chapline, S. Peng, K. Cho, H. Dai, "Nanotube molecular wires as chemical sensors", Science 287(1) (2000) 622.

[68] B.H. Chen, H.C. Lin, T.Y. Huang, J.H. Wei, H.H. Wang, M.J. Tsai, T.S. Chao, "Complementary carbon nanotube-gated carbon nanotube thin-film transistor", Applied Physics Letters 88 (2006) 093502.

[69] Y.T. Jang, S.I. Moon, J.H. Ahn, Y.H. Lee, B.K. Ju, Sens, "A simple approach in fabricating chemical sensor using laterally grown multiwalled carbon nanotubes", Actuators B 99 (2004) 118.

[70] C.P. Juan, C.C. Tsai, K.H. Chen, L.C. Chen, H.C. Cheng, "Fabrication and characterization of lateral field emission device based on carbon nanotubes", Japan Journal Applied Physics Letters 44 (2005) 2612.

[71] Y.H. Lee, Y.T. Jang, B.K. Ju, "In situ nanointerconnection for nanoelectronics via direct auto-catalytic lateral growth", Applied Physics Letters 86 (2005) 173103.

[72] D.S. Bethune, C.H. Kiang, M.S. de Urief, G. Gorman, R. Savoy, J. Vazquez, R.

Beyers, "Cobalt catalyzed growth of carbon nanotubes with single atomic layer walls", Nature 363 (1993) 605.

[73] W.K. Maser, E. Muñoz, A.M. Benito, M.T. Martinez, G.F. de la Fuente, Y. Maniette, E. Anglaret, J.L. Sauvajol, "Production of high-density single-walled nanotube materials by a simple laser-ablation method", Chemical Physics Letters 292 (1998) 587.

[74] Z.F. Ren, Z.P. Huang, J.W. Xu, J.H. Wang, P. Bush, M.P. Siegel, P.N. Provencio, "Synthesis of large arrays of well-aligned carbon nanotubes on glass", Science 282 (1998) 1105.

[75] S. Gan, M.G. Chapline, N.R. Franklin, T.W. Tombler, A.M. Cassen, H. Dai, "Self-oriented regular arrays of carbon nanotubes and their field emission properties ", Science 283 (1999) 512.

[76] D.B. Geohegan, A.A. Puretzky, I.N. Ivanov, S. Jesse, G. Eres, "*In situ* growth rate measurements and length control during chemical vapor deposition of vertically aligned multiwall carbon nanotubes", Applied Physics Letters 83 (2003) 1851.

[77] Y.C. Choi, Y.M. Shin, Y.H. Lee, B.S. Lee, G.S. Park, W.B. Choi, N.S. Lee, J.M. Kim, "Controlling the diameter, growth rate, and density of vertically aligned carbon nanotubes synthesized by microwave plasma-enhanced chemical vapor deposition", Applied Physics Letters 76 (2000) 2367.

[78] X. Ma, E.G. Wang, "CNx/carbon nanotube junctions synthesized by microwave chemical vapor deposition", Applied Physics Letters 78 (2001) 978.

[79] C. Lautent, E. Flahaut, A. Peigney, A. Rousset, "Metal nanoparticles for the catalytic synthesis of carbon nanotubes", New Journal Chemical 22 (1998) 1229.

[80] Y.H. Wang, J. Lin, C.H.A. Huan, G.S. Chen, "Synthesis of large area aligned carbon nanotube arrays from C_2H_2-H_2 mixture by rf plasma-enhanced chemical vapor deposition", Applied Physics Letters 79 (2001) 680.

[81] Z. Y. Juang, J. P. Chien, J. F. Lai, T. S. Lai, C. H. Tsai, "The effects of ammonia on the growth of large-scale patterned aligned carbon nanotubes using thermal chemical vapor deposition method", Diamond Relate Material 13, (2004) 1203.

[82] A.C. Ferrari, J. Robertson, "Interpretation of Raman spectra of disordered and amorphous carbon", Physical Review B 61 (2000) 14095.

[83] P.M. Ajayan, "Nanotubes from carbon", Chemical Reviews 99 (1999) 1787.

[84] P. Poncharal, Z.L. Wang, D. Ugarte, W.A. de Heer, "Electrostatic deflections and electromechanical resonances of carbon nanotubes", Science 283 (1999) 5407.

[85] O. Lourie, D.M. Cox, H.D. Wagner, "Buckling and collapse of embedded carbon nanotubes", Physical Review Letters 81 (1997) 1638.

[86] K.M. Liew, C.H. Wong, X.Q. He, M.J. Tan, S.A. Meguid, "Nanomechanics of single and multiwalled carbon nanotubes", Physical Review B 69 (2004) 115429.

[87] T.W. Ebbesen, H.J. Lezec, H. Hiura, J.W. Bennett, H.F. Ghacmi, T. Thio, "Electrical conductivity of individual carbon nanotubes", Nature 382 (1996) 54.

[88] Y.X. Liang, Q.H. Li, T.H. Wang, "Current saturation in multiwalled carbon nanotubes by large bias", Applied Physics Letters 84 (17) (2004) 3379.

[89] M. Meyyappan, L. Delzeit, A. Cassell, D. Hash, "Carbon nanotube growth by PECVD: a review", Plasma Sources Science Technology 12 (2003) 205.

[90] M.S. Bell, R.G. Lacerda, K.B.K. Teo, N.L. Rupesinghe, G.A.J. Amaratunga, W.I. Milne, M. Chhowalla, "Plasma composition during plasma-enhanced chemical vapor deposition of carbon nanotubes", Applied Physics Letters 85 (2004) 1137.

[91] S.J. Kyung, Y.H. Lee, C. Kim, J.H. Lee, G.Y. Yeom, "Field emission properties of carbon nanotubes synthesized by capillary type atmospheric pressure plasma enhanced chemical vapor deposition at low temperature", Carbon 44 (2006) 1530.

[92] H.C. Wen, K. Yang, K.L. Ou, W.F. Wu, C.P. Chou, R.C. Luo, Y.M. Chang, "Effects of ammonia plasma treatment on the surface characteristics of carbon fibers", Surface Coating Technology 200 (2006) 3166.

[93] J.M. Bonard, N. Weiss, H. Kind, T. Stöckli, L. Forró, K. Kern, A. Châtelain, "Tuning the field emission properties of patterned carbon nanotube films", Advanced Materials 13 (2001) 184.

[94] Y.S. Jung, D.Y. Jeon, "Surface structure and field emission property of carbon nanotubes grown by radio frequency plasma enhanced chemical vapor deposition", Apply Surface Science 193 (2002) 129.

[95] M. Sveningaaon, R.E. Morjan, O.A. Nerushev, Y. Sato, J. Bäckström, E.E.B. Campbell, F. Rohmund, "Raman spectroscopy and field-emission properties of CVD-grown carbon-nanotube films", Applied Physics A 73 (2001) 409.

[96] S.H. Lai, K.P. Huang, Y.M. Pan, Y.L. Chen, L.H. Chan, P. Lin, H.C. Shih, "Electron field emission from fluorinated amorphous carbon nanoparticles on porous alumina ", Chemical Physics Letters 382 (5-6): (2003) 567.

[97] J. Hone, M. Whitney, C. Piskoti, A. Zettl, "Thermal conductivity of single-walled carbon nanotubes", Physical Review B 59 (1999) R2514.

[98] B. Q. Wei, R. Vajtai, P. M. Ajayan, "Reliability and current carrying capacity of

carbon nanotubes", Applied Physics Letters 79 (2001) 1172.

[99] Y.H. Lee, Y.T. Jang, C.H. Choi, E.K. Kim, B.K. Ju, D.H. Kim, C.W. Lee, and S.S. Yoon, "Direct nano-wiring carbon nanotube using growth barrier: A possible mechanism of selective lateral growth", Journal Applied Physics 91(9), (2002) 6044.

[100] Y.T. Jang, J.H. Ahn, B.K. Ju, Y.H. Lee, "Lateral growth of aligned muitiwalled carbon nanotubes under electric field", Solid State Communications 126 (2003) 305.

[101] S.J. Wind, R. Martel, Ph. Avouris, "Localized and directed lateral growth of carbon nanotubes from a porous template", Journal Vacuum Society Technology B 20(6) (2002) 2745.

[102] J. Li, Q. Ye, A. Cassell, H.T. Ng, R. Stevens, J.H., M. Meyyappan, "Bottom-up approach for carbon nanotube interconnects ", Applied Physics Letters 82 (2003) 2491.

[103] Y.S. Han, J.K. Shin, S.T. Kim, "Synthesis of carbon nanotube bridges on patterned silicon wafers by selective lateral growth", Journal Applied Physics 90 (2001) 11, 5731.

[104] Kinneret Keren, Rotem S. Berman,Evgeny Buchstab, Uri Sivan, Erez Braun, "DNA-templated carbon nanotube field-effect transistor", science 302 (2003) 1380.

[105] L. Valentini, J.M. Kennya, L. Lozzi, S. Santucci, "Formation of carbon nanotubes by plasma enhanced chemical vapor deposition: Role of nitrogen and catalyst layer thickness", Journal Applied Physics 92 (2002) 6188.

[106] M. Matsushima, H. Araki, K. Kamide, T. Sakata, H. Mori, K. Yoshino, "Field emission from bamboo-like. multiwalled carbon nanotube arrays enhanced by mild oxidation", Japan Journal Applied Physics 42(8B) (2003) L 1036.

[107] L.Y. Heng, A. Chou, J. Yu, Y. Chen, J.J. Gooding, "Paper plan bamboo versus SWNTs for electrochemical application", Electrochemistry Communications 7 (2005)1457.

[108] M.F. Yu, O. Lourie, M.J. Dyer, K. Molor, T.F. Kelly, R.S. Ruoff. "Strength and breaking mechanism of multiwalled carbon nanotubes under tensile load", Science 287 (2001) 637.

[109] H.D. Wagner, O. Lourie, Y. Feldman, R. Tenne, "Stress-induced fragmentation

of multiwall carbon nanotubes in a polymer matrix", Applied Physics Letters 72 (1998) 188.

[110] Dong-Li Shi, Xi-Qiao Feng, Yonggang Y. Huang, Keh-Chih Hwang, Huajian Gao, The effect of nanotube waviness and agglomeration on the elastic property of carbon nanotube-reinforced composites, Journal of Engineering Materials and Technology 126(3)(2004) 250.

[111] M.B. Nardelli, B.I. Yakobson, J. Bernholc, "Brittle and Ductile Behavior in Carbon Nanotubes", Physical Review Letters 81 (1998) 4656.

[112] T. Belytschko, S.P. Xiao, G.C. Schatz, R.S. Ruoff, "Superconductivity of metallic boron in MgB_2", Physical Review B 65 (2002) 235430.

[113] S.J. Tans, A.R.M. Verschueren, C. Dekker, "Room-temperature transistor based on a single carbon nanotube", Nature 393 (1998) 49.

[114] R.F. Service, "R F service superstrong nanotubes show they are smart, too.", Science 281 (1998) 940.

[115] B.Q.Wei, R. Vajtai, P. M. Ajayan, " Reliability and current carrying capacity of carbon nanotubes", Applied Physics Letters 79 (2001) 1172.

[116] S. Frank, P. Poncharal; Z. L.Wang, W.A. De Heer, "Carbon nanotube quantum resistors", Science 280 (1998) 1744.

[117] J.L. Bahr, J. Yang, D.V. Kosynkin, M.J. Bronikowski, R.E. Smalley, J.M. Tour, "Functionalization of carbon nanotubes by electrochemical reduction of aryl diazonium salts:A bucky paper electrode", Journal of American Chemical Society 123 (2001) 6536.

[118] W. de Heer, A. Châtelain, D. Ugarte, "Carbon nanotubes field-emission-electron Source", Science 270 (1995) 1179.

[119] W.B. Choi, D.S. Chung, J.H. Kang, H.Y. Kim, Y.W. Jin, I.T. Han, Y.H. Lee, J.E. Jung, N.S. Lee, G.S. Park, J.M. Kim, "Fully sealed, high-brightness carbon-nanotube field-emission display", Applied Physics Letters 75 (1999) 3129.

Publications List of Hua-Chiang Wen

A-接受之國際期刊論文 (SCI Journal)

A1. Microelectronic Engineering

Hua-Chiang Wen [*], Koho Yang, Keng-Liang Ou, Wen-Fa Wu, Jen-Tsung Luo, Chang-Pin Chou, "Carbon nanotubes grown using cobalt silicids as catalyst and hydrogen pre-treatment", Microelectronic Engineering, 2005, 82 (3-4), pp. 221-227, (SCI).

A2. Surface & Coatings Technology

Hua-Chiang Wen [*], Koho Yang, Keng-Liang Ou, Wen-Fa Wu, Chang-Pin Chou, Jen-Tsung Luo, Yu-Ming Chang," Effects of Ammonia Plasma Treatment on the Surface Characteristics of Carbon Nanofiber", Surface & Coatings Technology, 2005, 200 (10), pp. 3166-3169, (SCI).

A3. Journal of Physics: Conference Series

Hua-Chiang Wen*, Yao-Nan Lin, Sheng-Rui Jian, Shih-Chun Tseng, Ming-Xiang Weng, Yu-Pin Liu, Po-Te Lee, Pai-Yen Chen, Ray-Quan Hsu , Wen-Fa Wu, and Chang-Pin Chou, "Observation of Growth of Human Fibroblasts on Silver Nanoparticles", Journal of Physics: Conference Series, Accepted.

A 4. Jorrnal of Composite material

Jen-Tsung Luo *, **Hua-Chiang Wen**, Wen-Fa Wu, Ben-Zu Wan, Chang-Pin Chou," Porous silica reinforced by carbon nanotubes to enhance mechanical performance, Jorrnal of Composite material, 2006, Accepted.

A 5. Journal of Colloid and Interface Science

Jen-Tsung Luo *, **Hua-Chiang Wen**, Yu-Ming Chang, Wen-Fa Wu, Chang-Pin Chou, "Mesoporous silica reinforced by silica nanoparticle to enhance mechanical performance", Journal of Colloid and Interface Science, 2006, Accepted.

A 6. Journal of Colloid and Interface Science

Jen-Tsung Luo *, **Hua-Chiang Wen**, Wen-Fa Wu, Chang-Pin Chou, "mechanical research of carbon nanotube/PMMA composite films", Composite composite, 2007, Accepted.

A 7. Thin Solid Film

Jen-Tsung Luo*, Wen-Fa Wu, **Hua-ChiangWen**, Yu-Ming Chang, Chang-Pin Chou, Jun-Ming Chen, "The role of hydrophobic group on the surface of nanoporuous ultra low dielectric constant during thermal treatment", Thin Solid Film, 2006 , Accepted.

A 8. Applied Surface Science

Wen-Pin Wang, **Hua-ChiangWen**, J. C. Huang , Sheng-Rui Jian, Kuan-Ting Chen, Wen-Fa Wu, Chang-Pin Chou, Chien-Huang Tsai, "The effects of hydrogen plasma pretreatment on the formation of vertically aligned carbon nanotubes", Applied Surface Science, 2007 , Revise.

B-接受之台灣期刊論文 (Taiwan Journal)

B1. 奈米通訊

陳百彥*, **溫華強**, 王文彬, 鄭宗杰, "場發射平面顯示器技術", 奈米通訊. 第十三卷. 第.三. 期, pp. 75-80

B2.奈米尺度之接合技術

Ming-Xiang Weng, **Hua-ChiangWen**, H-Y Huang, Chang-Pin Chou*, "The technology of welding in nano-size, "Welding & Cutting, vol15:4 2005, pp.32-35.

D-國際研討會論文(International Conference Paper)

D1. Asian CVD III International conference

. **Hua-Chiang Wen***, Yu-Ming Chang, Chang-Pin Chou, Jen-Tsung Luo, Wen-Fa Wu, "Effects of Ammonia Plasma Treatment on the Surface Characteristics of Carbon Nanotubes", Asian CVD III International conference, Taipei, Taiwan Nov. 12-14, page 116-117, 2004. **(台灣)**

D 2. Materials for Advanced Metallization International conference

Hua-ChiangWen*, Koho Yang, Keng-Liang Ou, Wen-Fa Wu, Jen-Tsung Luo, Chang-Pin Chou, "Carbon nanotubes grown using cobalt silicids as catalyst and hydrogen pre-treatment", Materials for Advanced Metallization International conference, Dresden, Germany, Mar. 06-09,page 41-42, 2005.

(德國)

 D 3. 3rd International Conference on Materials for 9th International Conference on Advanced Technologies

Hua-Chiang Wen*, Tien-Yu Lin, Yu-Ming Chang , Jen-Tsung Luo, Wen-Fa Wu, Chang-Pin Chou , J-T Sheu,"Growth Mechanism of Carbon Nanotubes with Hydrogen Plasma Pretreatment on Nickel/Titanium Nitride System", 3rd International Conference on Materials for 9th International Conference on Advanced Technologies (ICMAT), Singapore, page 238, 2005. **(新加坡)**

 D 4. 3rd International Conference on Materials for 9th International Conference on Advanced Technologies

Hua-Chiang Wen*, Kuo-Shu Lin, Jen-Tsung Luo, Yu-Ming Chang , Wen-Fa Wu , Chang-Pin Chou ,Jung-Hsiung Shen , Koho Yang, "Carbon Nanotubes Grown on Nickel/Titanium Nitride/Silicon System at various Temperature and Pretreating",3rd International Conference on Materials for 9th International Conference on Advanced Technologies (ICMAT), Singapore, page 135, 2005. **(新加坡)**

 D 5. 3rd International Conference on Materials for 9th International Conference on Advanced Technologies

 Jung-Hsiung Shen*, Kai-Yun Yang, **Hua-Chiang Wen**, Ko-Ho Yang, Kuan-Zong Fung, and Chang-Pin Chou, "Formation of La$_2$Zr$_2$O$_7$ and SrZrO$_3$ on Cathode-Supported Solid Oxide Fuel Cells",3rd International Conference on Materials for 9th International Conference on Advanced Technologies (ICMAT), Singapore, page 156, 2005. **(新加坡)**

 D 6. The Electrochemical Society Conference

 Jung-Hsiung Shen* , Ko-Ho Yang, **Hua-Chiang Wen**, Kai-Yun Yang, Kuan-Zong Fung, Chang-Pin Chou, "The Influence of Conductive Polymer on Deposition and Morphology Study of Compositional LSM/YSZ Cathode Layer Using Electrophoretic Deposition " ,The Electrochemical Society, Inc. the society for solid-state and electrochemical science and technology. Quebec City, Canada 207th Meeting, 2005. **(加拿大)**

 D 7. Materials for Advanced Metallization International conference

 Jen-Tsung Luo*, Wen-Fa Wu, **Hua-ChiangWen**, Yu-Ming Chang, Chang-Pin Chou, Jun-Ming Chen, "The role hydrophobic group on the surface of nanoporuous ultra low dielectric constant during thermal treatment", Materials for Advanced Metallization International conference, Dresden,

Germany, Mar. 06-09, page 173-174, 2005. (德國)

D 8. 2005 Nano Bioengineering International Symposium

Yao-Nan Lin, **Hua-Chiang Wen***, Shih-Chun Tseng, Yu-Pin Liu, Po-Te Lee, Ray-Quan Hsu, Wen-Fa Wu, Chang-Pin Chou, "A Period Observation of Fibroblasts Grow on Silver Nanoparticles", Nano Bioengineering International Symposium (NBIS 2005),15th-16th December, Chung Yuan Christian University, Taiwan, R. O. C, 2005. (台灣)

D 9. 3rd International Conference on Materials for 9th International Conference on Advanced Technologies

Yu-Ming Chang*, Tien-Yu Lin, **Hua-Chiang Wen**, Wen-Fa Wu, Chang-Pin Chou, J-T Sheu , "Localized Lateral Growth of Single-Walled Carbon Nanotube from Nickel Catalyst by Thermal Chemical Vapor Deposition" , 3rd International Conference on Materials for 9th International Conference on Advanced Technologies (ICMAT 2005) (新加坡)

D 10. **International COE Conference**

Yu-Ming Chang*, Chang-Pin Chou, **Hua-Chiang Wen**, Wen-Fa Wu, "Localized Lateral Growth proerties of Micro-Wave Plasma system " International COE Conference on Nano Processes and Devices, and Their Applications (Nagoya University, Nagoya, JAPAN) (日本)

D 11. **Nanotechnology Conference (MNC 2006).**

Yu-Ming Chang* ,**Hua-Chiang Wen** ,Chang-Pin Chou , Wen-Fa Wu , "Synthesis of nanocrystalline diamond films in Ar/H2/CH4 microwave discharges" 19th International Microprocesses and Nanotechnology Conference (MNC 2006).

D 12. 2006 International Conference on Nanoscience and Technology

Hua-Chiang Wen*, Yao-Nan Lin, Shih-Chun Tseng, Ming-Xiang Weng, Yu-Pin Liu, Po-Te Lee, Pei-Yen Chen, Jen Tsung Luo, Ray-Quan Hsu, Wen-Fa Wu, Chang-Pin Chou, "The Interaction between of the Human Fibroblasts and Silver Nanopartices by a Period Observation", International Conference on Nanoscience and Technology,30th July- 4th August, Basel, Switzerland, 2006. (瑞士)

D 13. 2006 International Conference on Nanoscience and Technology

Hua-Chiang Wen*,Wen-Pin Wang, Jung-Hsiung Shen, Pei-Yen Chen, Huang-Chung Cheng, Wen-Fa Wu, Chang-Pin Chou, Chong-Sin Wu, "Improvement in Electron Emission from Needle-like Carbon Nanotube after Argon Plasma Treatment", International Conference on

Nanoscience and Technology,30th July- 4th August, Basel, Switzerland, 2006. (瑞士)

D 14. 2006 International Conference on Nanoscience and Technology

Hua-Chiang Wen*, Wen-Pin Wang, Pei-Yen Chen, Jen Tsung Luo, Jen Tsung Luo, Wen-Fa Wu, Chang-Pin Chou, "Surface Performance of Carbon Nanotubes Post-Treated by Fluorocarbon/Oxygen Plasma", International Conference on Nanoscience and Technology,30th July- 4th August, Basel, Switzerland, 2006. **(瑞士)**

D 15. 2006 International Conference on Nanoscience and Technology

Kai-Wen Cheng, Pai-Yen Chen, Wen-Pin Wang, **Hua-Chiang Wen**, Huang-Chung Cheng, Chong-Sin Wu, Chang-Pin Chou *, "Effect of Carbon Nanotubes Treated by Oxygen Plasma Post-Treatment on the Performance of Field Emission and Simulation", International Conference on Nanoscience and Technology,30th July- 4th August, Basel, Switzerland, 2006. **(瑞士)**

D 16. 2006 International Conference on Nanoscience and Technology

Jen-Tsung Luo*, **Hua-Chiang Wen**, Chun-Hu Cheng, Wen-Fa Wu, Chang-Pin Chou," Distribution and mechanical properties of polymer matrix composites reinforced by carbon nanotube", International Conference on Nanoscience and Technology,30th July- 4th August, Basel, Switzerland, 2006. **(瑞士)**

D 17. 2006 International Conference on Nanoscience and Technology

Ta-Chuan Liao*, Chun-Yu Wu, Feng-Tso Chien, **Hua-Chiang Wen**, Chung-Yuan Kung, and Huang-Chung Cheng," A Novel Poly-Si Thin Film Transistor Fabricated with in-situ vacuum encapsulation", International Conference on Nanoscience and Technology,30th July- 4th August, Basel, Switzerland, 2006. **(瑞士)**

D 18. 2006 International Symposium on Nano Science and Technology

P. Y. Chen*, K. W. Cheng, **H. C. Wen**, and C. A. Chen, "Development of Three-Dimensional Poisson's Equation Solver   with Adaptive   Mesh Refinement and its Application for Electrostatic Predication of CNT-FET ", 2006 International Symposium on Nano Science and Technology, Tainan, Taiwan, 9-10 November 2006. **(台灣)**

E-台灣-研討會論文(Taiwan Conference Paper)

E1.台灣鍍膜科技協會年會

Hua-Chiang Wen*, Yu-Ming Chang, Koho Yang Chang-Pin Chou ,Wen-Fa Wu and Tien-Yu Lin, "Effects of Ammonia Plasma Treatment on the Surface Characteristics of Carbon Nanotubes", The 2004 Annual Symposium of Taiwan Association for Coating and Thin Film Technology (TACT), 2004

E 2.台灣奈米元件技術研討會

Hua-Chiang Wen*, Tien-Yu Lin,Yu-Ming Chang, Wen-Fa Wu, Chang-Pin Chou, "Nickel catalysts etching from Carbon Nanotubes by nitric/hydrogen chloride and horizontal observation", Symposium on Nano Device Technology, May. 4-5, Hsinchu, Taiwan, 2005.

E 3.台灣材料年會

Hua-Chiang Wen*, Tien-Yu Lin, J-T Sheu, Yu-Ming Chang, Wen-Fa Wu, Chang-Pin Chou, "Lateral Growth of Multi-Walled Carbon Nanotube from Nickel Catalyst under Aluminum Buffer Layer", The 2005 Annual Conference of Chinese Society for Materials Science, 2005

E 4.台灣材料年會

Hua-Chiang Wen*, Tien-Yu Lin, J-T Sheu, Yu-Ming Chang, Wen-Fa Wu, Chang-Pin Chou, 2005, "Effect of Pretreatment from Lateral Growth of Signal-Walled Carbon Nanotube under Molybdenum Buffer Layer", The 2005 Annual Conference of Chinese Society for Materials Science, 2005

E 5.台灣奈米元件技術研討會

Wen-Pin Wang*, **Hua-Chiang Wen**, Pei-Yen Chen , Jen-Tsung Luo , Chuan-Ping Juan, Huang-Chung Cheng, Wen-Fa Wu, Chang-Pin Chou ,"Characteristics of Field Emission on Carbon Nanotubes Using Various RF Bias of Oxygen Plasma Post-Treatment", Symposium on Nano Device Technology, April. 26-28, Hsinchu, Taiwan, 2006.

E 6 台灣奈米元件技術研討會

Wen-Pin Wang*, **Hua-Chiang Wen** , Pei-Yen Chen , Jen-Tsung Luo, Chuan-Ping Juan, Huang-Chung Cheng, Wen-Fa Wu, Chang-Pin Chou , "Characteristics of Field Emission on Various Lengths of Carbon Nanotubes and Pretreatment", Symposium on Nano Device Technology, April. 26-28, Hsinchu, Taiwan, 2006.

E7 台灣奈米元件技術研討會

Hua-Chiang Wen*, Wen-Pin Wang, Ming-Xiang Weng, Jen-Tsung Luo, Wen-Fa Wu, Chang-Pin Chou, "Effect of Various Quantity of Hydrogen Gas for Grown Carbon Nanotubes by Plasma Pretreated on Thin Nickel Catalyst", Symposium on Nano Device Technology, April. 26-28, Hsinchu, Taiwan, 2006.

E8 台灣奈米元件技術研討會

Hua-Chiang Wen*, Wen-Pin Wang, Ming-Xiang Weng, Wei-Che Chang [c], Jen-Tsung Luo, Wen-Fa Wu, Chang-Pin Chou, "Carbon Nanotubes Post-Treatment Using Fluorocarbon/Oxygen Plasma and Surface Performance", Symposium on Nano Device Technology, April. 26-28, Hsinchu, Taiwan, 2006.

E 9.台灣材料年會

Ming-Xiang Weng , *Kuan Ting Chen, Sheng-Rui Jian, **Hua-Chiang Wen**, Yuan-Te Chang, Wen-Fa Wu, and Chang-Pin Chou, "The Formation of Nickel Layer as Nanosize Particles by Hydrogen Plasma Treatment", The 2006 Annual Conference of Chinese Society for Materials Science, Tainan, Taiwan, 2006.

E 10.台灣材料年會

Ming-Xiang Weng, *Kuan Ting Chen, Sheng-Rui Jian, **Hua-Chiang Wen**, Yao-Tsung Yeh, Wen-Fa Wu, and Chang-Pin Chou, "The Growth of Carbon Nanotubes Using various Buffer Layers and Hydrogen Plasma Post-Treatment", The 2006 Annual Conference of Chinese Society for Materials Science, Tainan, Taiwan, 2006.

E 11.台灣材料年會

*Kuan Ting Chen, Ming-Xiang Weng, **Hua-Chiang Wen**, Jin-Shyong Lin, Chun-Hao Tu , Wen-Fa Wu, and Chang-Pin Chou, "Oxygen Plasma Post-Treatment of Carbon Nanotubes", The 2006 Annual Conference of Chinese Society for Materials Science, Tainan, Taiwan, 2006.

E 12.台灣材料年會

*Kuan Ting Chen, Ming-Xiang Weng, **Hua-Chiang Wen**, Shi-Zhang Chen, Jin-Shyong Lin, Wen-Fa Wu, and Chang-Pin Chou, "Ammonia Plasma Post-Treatment of Carbon Nanotubes", The 2006 Annual Conference of Chinese Society for Materials Science, Tainan, Taiwan, 2006.

E 13.台灣材料年會

Kuan Ting Chen, Ming-Xiang Weng, **Hua-Chiang Wen***, Wen-Fa Wu, and Chang-Pin Chou,

Fluorocarbon-oxygen Plasma Post-Treatment of Carbon Nanotubes, The 2006 Annual Conference of Chinese Society for Materials Science, Tainan, Taiwan, 2006.

E 14 台灣奈米元件技術研討會

Hua-Chiang Wen[*], Wen, Kuan Ting Chen, Wen-Fa Wu, Chang-Pin Chou, Zeng-Hung Wu, Koho Yang, and Chien-Huang Tsai, Characteristics of Indentation on Carbon Nanotubes Films, Symposium on Nano Device Technology Hsinchu, Taiwan, 2007.

E 15 台灣奈米元件技術研討會

Kuan Ting Chen, Chun-Hao Tu, **Hua-Chiang Wen**[*], Wen-Fa Wu, Chang-Pin Chou, Wu Zeng Hung, Koho Yang, and Chien-Huang Tsai, Surface Adsorption of Carbon Nanotubes Treated by Fluorocarbon/Oxygen Plasma, Symposium on Nano Device Technology Hsinchu, Taiwan, 2007.

E 16 台灣奈米元件技術研討會

Kuan Ting Chen, **Hua-Chiang Wen**[*], Wen-Fa Wu, Chang-Pin Chou, Zeng-Hung Wu, Koho Yang, and Mu-Sheng Chiang, Carbon Nanotubes Grown from Plug Structure and Pretreatment, Symposium on Nano Device Technology Hsinchu, Taiwan, 2007.

E 17 台灣奈米元件技術研討會

Kuan Ting Chen, **Hua-Chiang Wen**[*], Wen-Fa Wu, Chang-Pin Chou, Wu Zeng Hung, Koho Yang, and Mu-Sheng Chiang, Coating Characteristic of Copper Metal/Carbon Nanotubes, Symposium on Nano Device Technology Hsinchu, Taiwan, 2007.

E 18 台灣奈米元件技術研討會

Kuan Ting Chen, Chun-Hao Tu, **Hua-Chiang Wen**[*], Wen-Fa Wu, Chang-Pin Chou, Wu Zeng Hung, Koho Yang, and Mu-Sheng Chiang, Effect of Fluorocarbon/Oxygen Plasma Post-treatment on the Lateral Carbon Nanotubes, Symposium on Nano Device Technology Hsinchu, Taiwan, 2007.

E 19 台灣奈米元件技術研討會

Meng-Hung Lin, Wei-Ming Chiu, **Hua-Chiang Wen**[*], Jin-Shyong Lin, Tzu-Chin Chang, Chang-Pin Chou, Mechanical Properties of Carbon nanotube/ biodegradable Plastic Poly(lactic acid, PLA) Composites, Symposium on Nano Device Technology Hsinchu, Taiwan, 2007.